IntechOpen

BODIPY Dyes

A Privilege Molecular Scaffold with Tunable Properties

Edited by Jorge Bañuelos-Prieto and Rebeca Sola Llano

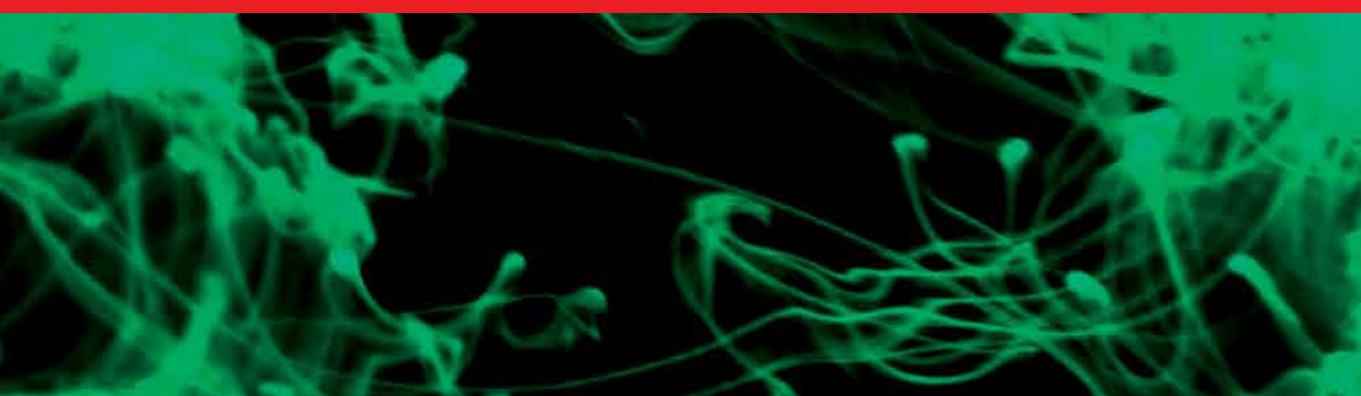

BODIPY DYES - A PRIVILEGE MOLECULAR SCAFFOLD WITH TUNABLE PROPERTIES

Edited by **Jorge Bañuelos-Prieto**
and **Rebeca Sola Llano**

BODIPY Dyes - A Privilege Molecular Scaffold with Tunable Properties
http://dx.doi.org/10.5772/intechopen.75220
Edited by Jorge Bañuelos-Prieto and Rebeca Sola Llano

Contributors

Yuriy Marfin, Evgeniy Rumyantsev, Sergey Usoltsev, Ana M. Costero, Margarita Parra, Salvador Gil, Pablo Gavina, Dokyoung Kim, Na Hee Kim, Zachariah Heiden, Brena Thompson, Jorge Bañuelos-Prieto, Rebeca Sola Llano

Notice

First published in London, United Kingdom, 2019 by IntechOpen
eBook (PDF) Published by IntechOpen, 2019
IntechOpen is the global imprint of INTECHOPEN LIMITED, registered in England and Wales, registration number: 11086078, The Shard, 25th floor, 32 London Bridge Street
London, SE19SG – United Kingdom
Printed in Croatia

British Library Cataloguing-in-Publication Data
A catalogue record for this book is available from the British Library

Additional hard and PDF copies can be obtained from orders@intechopen.com

BODIPY Dyes - A Privilege Molecular Scaffold with Tunable Properties
Edited by Jorge Bañuelos-Prieto and Rebeca Sola Llano

p. cm.

Print ISBN 978-1-78985-081-9

Online ISBN 978-1-78985-082-6

eBook (PDF) ISBN 978-1-83881-816-6

Meet the editors

Dr. Jorge Bañuelos Prieto is an associate professor at the Physical Chemistry Department of the Basque Country University (UPV/EHU). He was born in 1976 and received his PhD (2004) from the same university under the guidance of Professors Iñigo and Fernando López Arbeloa. From then to 2006 he was assistant lecturer, and after that a lecturer until 2011 when he attained his current position at UPV/EHU. In 2006 he did a postdoctoral stay with Professor Gion Calzaferri at Bern University (Switzerland). He belongs to the Molecular Spectroscopic Group at UPV/EHU and his main research topic is the computationally assisted design and photophysical characterization of organic fluorophores in solution, and solid hosts for photonic and biophotonic applications. He has published around 100 research articles in reputable and indexed scientific journals.

Dra. Rebeca Sola Llano is a postdoctoral researcher at the Physical Chemistry Department of the Basque Country University (UPV/EHU) and belongs to the Molecular Spectroscopy Group (UPV/EHU). She was born in 1989 and finished her degree in Chemistry in 2012 at UPV/EHU. After that, she completed an interuniversity Master´s degree in New Materials between UPV/EHU and Cantabria University in 2013. She finished her PhD in 2017 under the supervision of Professor Iñigo López Arbeloa and Dra. Virginia Martínez Martínez. Her research topics are focused on the hydrothermal synthesis of zeolitic materials and the photophysical characterization of organic dyes and photoactive materials, using spectroscopic techniques and confocal fluorescence microscopy. Her work has given rise to almost 10 publications in Q1 journals, two book chapters, and five oral presentations at international congresses.

Contents

Preface

Dye chemistry is nowadays becoming a booming area of research. Thanks to the advanced and available tools in organic synthesis, organic molecules displaying fluorescence emission are being intensively applied to hot topics of research related to photonics and biotechnology as a whole. As a result of the continuous search for molecular structures with improved photophysical and photochemical properties, at the beginning of the 1990s those dyes known as boron dipyrromethene (BODIPY) had a notable impact on and success among the scientific community, and these fluorophores have received a great deal of attention over the last few years. Indeed, currently they are at the forefront of applied multifunctional luminophores as reflected by the sustainable and unstoppable growth of publications dealing with this subject over the last few decades (around 1000 indexed articles per year). Their chromophoric core (based on dipyrrin) shows excellent stability against external factors and hard irradiation regimes, displays strong and sharp absorption and emission (both fluorescence and laser) bands in the visible spectral region, and is readily available to myriad synthetic avenues, which allow rich functionalization. Such a substitution pattern modulates the photophysical properties, allowing a tailor-made design of the chromophore to respond to the demands of a specific research topic. As a result, BODIPYs are successfully applied to a multitude of scientific and technological areas, from photonics to biomedicine. In fact, easy access to a fine modulation of photophysical properties of BODIPYs allows coverage of application fields demanding opposing and specific features of the chromophore. Thus, bright fluorophores can be designed for lasers and bioimaging, or, alternatively, dark dyes can be attained for singlet oxygen generation in the treatment of cancer or endowed with charge separation to activate semiconductors in solar cells.

This book was motivated by such popularity and optimal performance of BODIPY dyes as modern and functional fluorophores. In its chapters, we intend to show the state of the art dealing with BODIPYs, revisit their stability against irradiation and external factors, describe their tuneable photophysical and electrochemical properties by means of structural factors, and highlight their chemical versatility towards the design of photoactive molecules with specific and improved properties to be applied as fluorescence sensors and biomarkers, or in electrochemistry and light-driven reactions.

We hope that the launch of this book will be an inspiration for readers to design new BODIPY dyes tailored for a target issue or to incorporate them into their research scopes. We would like to acknowledge Ms. Manuela Gabric, Author Service Manager, for her kind assistance during the book project.

Jorge Bañuelos-Prieto and Rebeca Sola Llano
Basque Country University (UPV/EHU), Spain

Chapter 1

Introductory Chapter: BODIPY Dye, an All-in-One Molecular Scaffold for (Bio)Photonics

Rebeca Sola-Llano and Jorge Bañuelos

Additional information is available at the end of the chapter

http://dx.doi.org/10.5772/intechopen.82682

1. Introduction

Dye chemistry has witnessed a renewed interest in the last years. The reason of such impressive growth relies on the modern avenues in organic chemistry, which allow to develop new molecular structures, or decorate the backbone of an available chromophore with the desired substitution pattern, fulfilling the specific requirements of a given application field [1]. In this regard, those organic molecules able to emit fluorescence are receiving a great deal of attention owing to the recent technological advances in high-resolution spectroscopic techniques based on fluorescence. In fact, the Nobel Prize in 2014 was awarded to the development of super-resolution fluorescence microscopy (nanoscopy) [2–4]. Moreover, nowadays, bioimaging has become likely the most successful and widely used technique to monitor biochemical events at real time following the fluorescence emission of probes, sensors, and markers [5].

Actually, there is a wide chart of commercially available fluorophores spanning the whole ultraviolet-visible region of the electromagnetic spectrum and even reaching the near infrared (NIR). Nevertheless, the search for new organic fluorophores is an active task to find molecular structures with improved photophysical properties and photostability. These are key properties for any practical application (such as the aforementioned bioimaging) since they rule the sensitivity and efficiency, and the operative lifetime, respectively, of the detection process. Among them, definitely those chromophores known as borondipyrromethene (BODIPY) are in the forefront. A quick bibliographic search reveals that since their discovery (early 1990s) they have been intensively exploited (almost 1000 publications per year, **Figure 1**). The reason of their success is based on the chemical, photochemical and thermal stability of their boron-dipyrrin core, which provides strong absorption and fluorescence spectral bands [6–8]. Nevertheless, likely the main outstanding characteristic of BODIPYs is their chemical versatility, since their chromophoric core is amenable to a myriad of chemical reactions

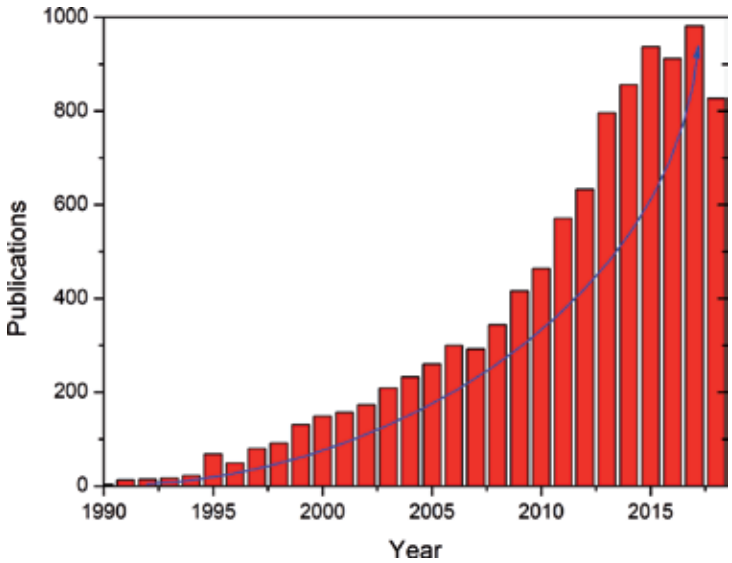

Figure 1. Evolution of the publications dealing with BODIPYs since their first reports (source: SciFinder, September 2018).

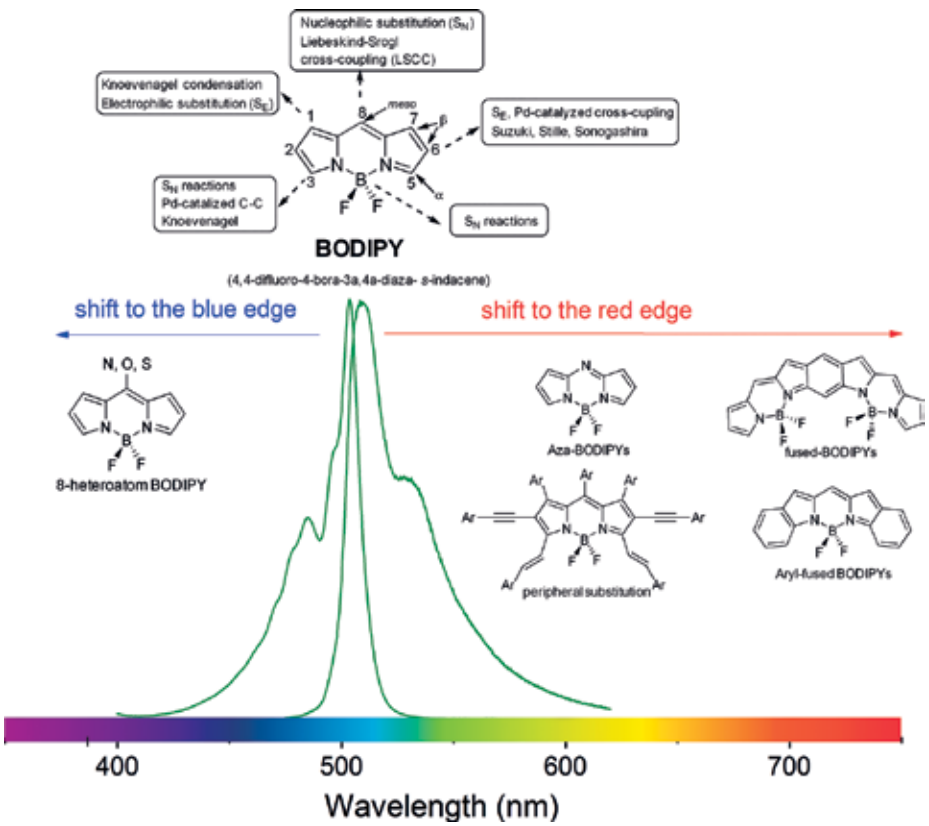

Figure 2. Molecular structure and main organic reactions applied to BODIPYs. The basic absorption and fluorescence bands of BODIPYs and some key structural modifications to achieve pronounced spectral shifts toward both edges of the visible are also included.

(all the chromophoric positions can be functionalized selectively, **Figure 2**) which allows an exhaustive and rich substitution pattern [9]. As a matter of fact, in the bibliography BODIPYs have been claimed as "El Dorado" for organic chemistry or "chameleons" to highlight their versatility [10]. Such functionalization enables the modulation of the photophysical properties or alternatively the induction of new photophysical phenomena. As a consequence, and upon a rational design, BODIPY dyes with absorption and emission along the whole visible region can be attained with improved photonic performance than the benchmark dyes in each spectral region 5 (**Figure 2**), or they can be tailor-made derived to match the requirements of plenty of application fields. All these facts explain and support the unstoppable growth and popularity of these dyes in these last decades (**Figure 1**).

2. Main application fields of BODIPYs

BODIPY dyes are applied in a multitude of diverse (bio)technological fields as photoactive media. Among them likely the most exploited are in organic lasers, biomedicine (probes and sensors for diagnosis by means of bioimaging and photosentitizers in photodynamic therapy of cancer), light harvesters (artificial antennae) and photovoltaic devices (photosensitizers of semiconductors) (**Figure 3**). Hereafter, the fundamentals of each application field with BODIPYs are briefly explained

2.1. Lasers

The high photostability and fluorescence response of BODIPYs make them suitable photoactive media for dye lasers (**Figure 3A**) [11, 12]. After amplification of the stimulated emission, a strong laser emission band can be achieved along the whole visible spectral region just

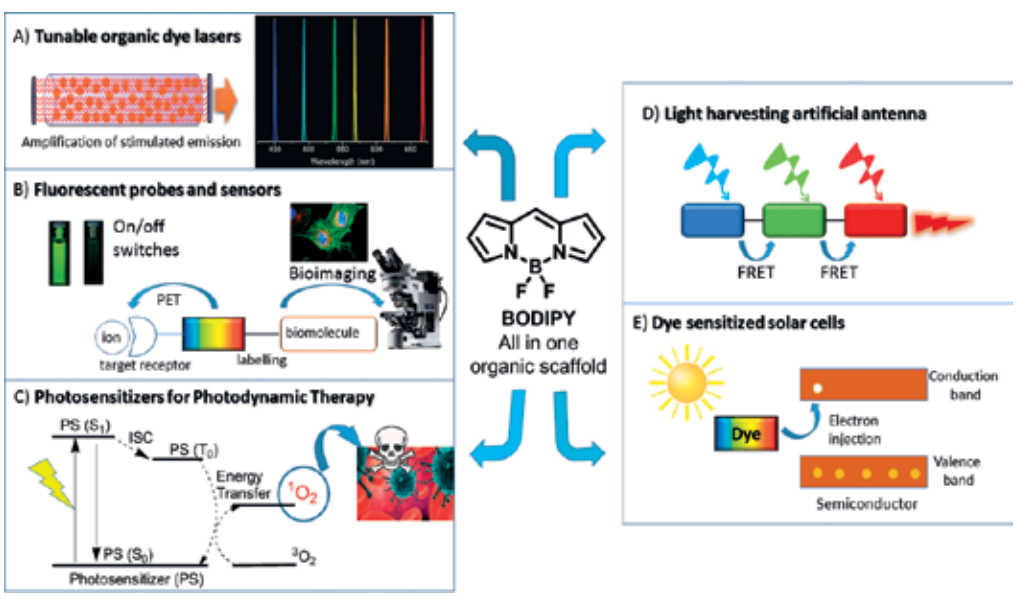

Figure 3. Scheme of the main application fields of BODIPYs.

changing the molecular structure thanks to the claimed chemical versatility of the chromophoric core. The achieved laser signal is highly efficient (even above 50%) and stable, since in some cases no sign of degradation is are detected even after prolonged and intense pumping (up to 100,000 pulses). Moreover, the tunable dye lasers based on BODIPYs, even in solid state, display better laser performance than the commercially available organic lasers considered hitherto as benchmarks in each spectral region.

2.2. Fluorescent probes and sensors

The vast number of synthetic protocols that can be applied in the chromophore of BODIPYs enables labeling of biomolecules with these fluorophores (**Figure 3B**). Thus, bright and stable fluorescent probes can be designed for bioimaging [13]. A high fluorescence response allows an easy and sensible detection of the biomarkers just monitoring the emission under a fluorescence microscope, being the signal also long-lasting owing to the high photostability of the BODIPY-tagged biomolecule.

As aforementioned, the substitution pattern of the chromophore can induce new photophysical processes (such as intramolecular charge transfer, ICT, or photoinduced electron transfer, PET) which are highly sensitive to specific environmental conditions (polarity, acidity) or the presence of certain analytes (ions, molecules) in the surrounding environments, respectively, and hence ideal to develop fluorescent sensors [14, 15]. There are plenty of designs of sensors based on BODIPYs to monitor different environmental properties and detect and quantify molecular species, but likely those called on/off switches show the best performance since the detection process is highly sensitive and can be clearly visualized by the naked eye (**Figure 3B**). Overall, they are based on the induction of a fluorescence-quenching PET process in the BODIPY upon binding a specific receptor (off state). After selective recognition of the target analyte, the PET is suppressed and the bright fluorescence from the chromophore is recovered (on state).

2.3. Photosensitizers in photodynamic therapy

The fluorescent probes are widely applied in biomedicine for diagnosis purposes. However, BODIPYs can be applied for treatment of diseases like cancer [16]. In photodynamic therapy (PDT), organic dyes are used as photosensitizers to generate singlet oxygen, a cytotoxic specie able to destroy tumoral cells. Comparing other alternative treatments of cancer, PDT shows advantages since it is noninvasive, with low side effects, the treatment is light-driven and in situ, and, upon absence of light, the photosensitizer is inert. Due to the said chemical versatility of the dipyrrin core, BODIPY dyes are able to generate singlet oxygen via the promotion of the population of their triplet state, and ulterior energy transfer to the ambient triplet oxygen can be designed (**Figure 3C**). Different approaches have been tested to enhance the intersystem crossing probability of BODIPYs in the bibliography, such as grafting heavy atoms (halogens, metals) and promoting ICT processes (orthogonal dimers). Moreover, a suitable balance between singlet oxygen generation and fluorescence response by molecular structural factors allows designing photosensitizers with dual functionality, thus suitable for theragnosis, which means that they are able to generate singlet oxygen and treat, but retaining high enough fluorescence signal for detection by bioimaging [17].

2.4. Artificial antennae

Artificial antennae are bioinspired in the photosynthesis, trying to mimic the efficient light harvesting of solar energy in natural organisms during its conversion into chemical energy [18]. The key process is the excitation energy transfer (EET) which is mediated usually through a Förster long-range mechanism (Förster Resonance Energy Transfer, FRET) [19]. At the molecular level, this can be attempted by the combination of chromophores working at different but complementary spectral regions and able to undergo FRET (spectral overlap to enable the through space dipole–dipole coupling). Moreover, their mutual covalent linkage imposes short distance between energy donor and acceptor boosting the FRET efficiency and eventually promoting other EET mechanism which further contributes to the whole energy transfer. Taking into account that there are BODIPYs available along the whole visible region, the scientific community has been tempted to link them to each other through suitable spacers to customize energy transfer cassettes. These molecular antennae outstand by their broadband absorption, spanning the whole visible, but selective red emission from the last energy acceptor after transport of the light via successive and efficient energy transfer hops from the energy donors (**Figure 3D**). This kind of molecular design is being applied in dye lasers, biomedicine and photovoltaic devices, as explained hereafter in Section 2.5.

2.5. Photosensitizers in solar cells

Photovoltaic devices usually feature inorganic semiconductors, where an electron is promoted from the valence band to the semiconductor band upon irradiation, thus converting sunlight into electricity. In this regard, one of the main drawbacks is their low absorption of the solar spectrum, which is limited to the NIR region, and low efficiency. One way to circumvent this limitation is by means of organic dyes since their light absorption ability is much better. Thus, the role of these photosensitizers is to absorb light and afterward inject an electron into the conduction band of the conductor (dye-sensitized solar cells, **Figure 3E**) [20, 21]. To this aim dyes should have a push-pull character (chromophore decorated with electron donors and acceptors) to enable an ulterior electron transfer upon excitation. Moreover, the antennae described in Section 2.4 are ideal for these devices since they ensure an efficient light harvesting of the sunlight (both in efficiency owing to the high absorption coefficient of BODIPYs and in spectral interval since all the incoming light from the UV–Vis–NIR can be absorbed simultaneously) and, after choosing a suitable red-emitting BODIPY subunit ables to promote electron transfer, activate the semiconductor with a better exploitation of the sunlight.

The aforementioned fields are the most tested ones with BODIPYs, but other areas of interest are tackled also successfully, such as materials science (self-assembly, or grafting the dye to nanoparticles, polymers, graphene, etc.) [22], electrochemistry (light-emitting diodes based on electroluminescence, photocatalyst and photochemical reactions overall) [23] or chirality (as optically active compounds able to absorb or emit selectively circularly polarized light of specific handedness) [24]. Even theoretical chemists have been attracted by the boom of BODIPYs, and many computational studies can be found in the bibliography to unravel their excited state dynamics [25].

Of course, BODIPYs have some drawbacks, mainly their low Stokes shift and poor water solubility. However, even those limitations can be easily overcome after suitable structural modifications. Indeed, BODIPYs endowed with high Stokes shift [26], and improved solubility [27] are now readily available to reduce the reabsorption/reemission effects at high optical densities and enable their solubility in the physiological media.

Therefore, BODIPYs can be described as an all-in-one scaffold where different functionalities can be added to the chomophore simultaneously and different non-interfering chromophoric positions, being the right choice for any application field or device demanding an organic dye.

This book aims to describe the state-of-art related to BODIPYs and provides an overview of their chemical versatility and tunable photophysical and electrochemical properties, and degradation mechanisms upon irradiation or external factors, to explore their performance as stable fluorescent sensors and biomarkers, or for electrochemical purposes. Costero et al. report the design of BODIPYs for chemosensing of anions, cations and neutral molecules in solution, gas phase and even in the solid state using nanoparticles. They also describe the ongoing mechanisms allowing the recognition of the target analyte. Related to this topic, Dokyoung et al. revisit the synthetic approaches to develop blue-emitting BODIPYs and their viability as fluorescent probes and sensors. They highlight the possibility of these fluorophores to label biomolecules (like proteins) or to detect metals, amino acids (like cysteine) or gases (like phosgene). Afterward, Heiden et al. report the electrochemical properties of BODIPY. They prove their ability to electrogenerate chemiluminescence and claim the key role of this chromophore in photochemistry and photocatalysis owing to their tunable redox activity. Finally, Yuriy et al. overview the degradation mechanisms and kinetics of BODIPYs in acid and basic media via spectroscopic techniques and computational simulations. They enlarge the study to dipyrrinates and bis-dipyrrinates, owing to their structural similarity with the dipyrrin core of BODIPYs. Indeed, BODIPY is named in the literature as the "little sister" of porphyrins.

Acknowledgements

Financial support from MICINN (MAT2017-83856-C3-3-P) and Gobierno Vasco (IT912-16) is acknowledged.

Author details

Rebeca Sola-Llano and Jorge Bañuelos*

*Address all correspondence to: jorge.banuelos@ehu.eus

Department of Physical Chemistry, University of the Basque Country (UPV/EHU), Bilbao, Spain

References

[1] Moliner F, Kielland N, Lavilla R, Vendrell M. Modern synthetic avenues for the preparation of functional fluorophore. Angewandte Chemie, International Edition. 2017;**56**: 3758-3769. DOI: 10.1002/anie.201609394

[2] Betzig E. Single molecules, cells, and super-resolution optics (nobel lecture). Angewandte Chemie, International Edition. 2015;**54**:8034-8053. DOI: 10.1002/anie.201501003

[3] Hell SW. Nanoscopy with focused light (nobel lecture). Angewandte Chemie, International Edition. 2015;**54**:8054-8066. DOI: 10.1002/anie.201504181

[4] Moerner WE. Single-molecule spectroscopy, imaging, and photocontrol: Foundations for super-resolution microscopy (nobel lecture). Angewandte Chemie, International Edition. 2015;**54**:8067-8093. DOI: 10.1002/anie.201501949

[5] Lovell JF, Liu TWB, Chen J, Zheng G. Activatable photosensitizers for imaging and therapy. Chemical Reviews. 2010;**110**:2839-2857. DOI: 10.1021/cr900236h

[6] Loudet A, Burgess K. BODIPY dyes and their derivatives: Synthesis and spectroscopic properties. Chemical Reviews. 2007;**107**:4891-4932. DOI: 10.1021/cr078381n

[7] Benstead M, Mehl GH, Boyle RW. 4,4′-difluoro-4-bora-3a,4a-diaza-*s*-indacenes (BODIPYs) as component of novel light active materials. Tetrahedron. 2011;**67**:3573-3601. DOI: 10.1016/j.tet.2011.03.028

[8] Bañuelos J. BODIPY dye, the most versatile fluorophore ever? Chemical Record. 2016;**16**: 335-348. DOI: 10.1002/tcr. 201500238

[9] Boens N, Verbelen B, Dehaen W. Postfunctionalization of the BODIPY core: Synthesis and spectroscopy. European Journal of Organic Chemistry. 2015;**30**:6577-6595. https://onlinelibrary.wiley.com. DOI/10.1002/ejoc.201500682

[10] Ziessel R, Ulrich G, Harriman A. The chemistry of BODIPY: A new El Dorado for fluorescence tools. New Journal of Chemistry. 2007;**31**:496-501. DOI: 10.1039/B617972J

[11] Costela A, García-Moreno I, Sastre R. Polymeric solid-state dye lasers: Recent developments. Physical Chemistry Chemical Physics. 2003;**5**:4745-4763. DOI: 10.1039/b307700b

[12] Kuehne AJC, Gather MC. Organic lasers: Recent developments on materials, device geometries, and fabrication techniques. Chemical Reviews. 2016;**116**:12823-12864. DOI: 10.1021/acs.chemrev.6b00172

[13] Kowada T, Maeda H, Kikuchi K. BODIPY-based probes for the fluorescence imaging of biomolecules in living cells. Chemical Society Reviews. 2015;**44**:4953-4972. DOI: 10.1039/c5cs00030k

[14] Boens N, Leen V, Dehaen W. Fluorescent indicators based on BODIPY. Chemical Society Reviews. 2012;**41**:1130-1172. DOI: 10.1039/c1cs15132k

[15] Wu D, Sedgwick AC, Gunnlaugsson T, Akkaya EU, Yoon J, James TD. Fluorescent chemosensors: The past, present and future. Chemical Society Reviews. 2017;**46**:7105-7123. DOI: 10.1039/c7cs00240h

[16] Kamkaew A, Lim SH, Lee HB, Kiew LV, Chung LY, Burgess K. BODIPY dyes in photodynamic therapy. Chemical Society Reviews. 2013;**42**:77-88. DOI: 10.1039/c2cs35216h

[17] Abrahamse H, Hamblin MR. New photosensitizers for photodynamic therapy. The Biochemical Journal. 2016;**473**:347-364. DOI: 10.1042/BJ20150942

[18] Ziessel R, Harriman A. Artificial light-harvesting antennae: Electronic energy transfer by way of molecular funnels. Chemical Communications. 2011;**47**:611-631. DOI: 10.1039/c0cc02687e

[19] Fan J, Hu M, Zhan P, Peng X. Energy transfer cassettes based on organic fluorophores: Construction and applications in ratiometric sensing. Chemical Society Reviews. 2013; **42**:29-43. DOI: 10.1039/c2cs35273g

[20] Singh SP, Gayathri T. Evolution of BODIPY dyes as potential sensitizers for dye-sensitized solar cells. European Journal of Organic Chemistry. 2014;**22**:4689-4707. https://onlinelibrary.wiley.com. DOI: 10.1002/ejoc.201400093

[21] Bessette A, Hanan GS. Design, synthesis and photophysical studies of dipyrromethene-based materials: Insights into their applications in organic photovoltaic devices. Chemical Society Reviews. 2014;**43**:3342-3405. DOI: 10.1039/c3cs60411j

[22] Solomonov AV, Marfin YS, Rumyantsev EV. Design and applications of dipyrrin-based fluorescent dyes and related organic luminophores: Form individual compounds to supramolecular self-assembled systems. Dyes and Pigments. 2019;**162**:517-542. DOI: 10.1016/j.dyepig.2018.10.042

[23] Nepomnyashchii AB, Bard AJ. Electrochemistry and electrogenerated chemiluminescence of BODIPY dyes. Accounts of Chemical Research. 2012;**45**:1844-1853. DOI: 10.1021/ar200278b

[24] Lu H, Mack J, Nyokong T, Kobayashi N, Shen Z. Optically active BODIPYs. Coordination Chemistry Reviews. 2016;**318**:1-15. DOI: 10.1016/j.ccr.2016.03.015

[25] Chibani S, Le Guennic B, Charaf-Eddin A, Laurent AD, Jacquemin D. Revisiting the optical signatures of BODIPY with ab initio tools. Chemical Science. 2013;**4**:1950-1963. DOI: 10.1039/c3sc22265a

[26] Chen Y, Zhao J, Guo H, Xie L. Geometry relaxation-induced large stokes shift in red-emitting borondipyrromethenes (BODIPY) and applications in fluorescent thiol probes. The Journal of Organic Chemistry. 2012;**77**:2192-2206

[27] Fan G, Chen Z. Water-soluble BODIPY and aza-BODIPY dyes: synthetic progress and applications. Frontiers of Chemical Science and Engineering. 2014;**8**:405-417. DOI: 10.1007/s11705-014-1445-7

Chapter 2

BODIPY Core as Signaling Unit in Chemosensor Design

Ana M. Costero, Margarita Parra, Salvador Gil and Pablo Gaviña

Additional information is available at the end of the chapter

http://dx.doi.org/10.5772/intechopen.79591

Abstract

BODIPY derivatives possess unique photophysical properties and for these reasons, they have been used in numerous fields. Among the different applications, they are used in designing chemosensors that has increased in the last years. Here, we report several strategies and examples for detecting analytes of different characteristics: cations, anions, and hazardous and pollutant neutral molecules using BODIPY core as signaling unit.

Keywords: chemosensor, fluorescence, anions, cations, neutral molecules

1. Introduction

Supramolecular chemistry has become a coherent and alive body of concepts which has recently incorporated new areas of research [1–4]. The "classical" supramolecular chemistry has developed basic tools and concepts such as coordination of specific substrates to receptor (recognition), chemical reactivity induced by the guests (transformation), and positional controlled changes of atoms or molecules (translocation). On the other hand, another promising area of investigation is the development of "programmed supramolecular systems," where the recognition process is coupled with a specific action.

Among these programmed systems of supramolecular background the so-called molecular chemical sensors, where the process of recognition is adapted to a process of detection, are of wide interest. The described behavior is achieved by means of the introduction in the ligand (or reactive site) of transducing units which are capable of transmitting information on the molecular recognition process through a change in its physical properties (e.g., optical or electrochemical).

There are three classical approaches for the development of chromogenic-fluorogenic sensors:

1. Binding site-signaling unit approach: In this approach, the receptor should contain two different subunits kept together by means of a covalent bond. One of such subunits is responsible for the complexation process, while the other transmits the molecular recognition process [5]. As it can be seen in **Figure 1**, the coordination of the guest induces a change of some properties of the signaling unit, that is, color (chromogenic chemosensors) or fluorescence (fluorescent chemosensors).

2. Displacement approach: This approach, as well as the former, implies the use of both, specific binding sites and signaling units. However, in this case, both subunits are not covalently linked, but forming a coordination ensemble [6]. In these systems, the addition of a given guest to the solution that contains this "molecular ensemble" favors the displacement reaction: the coordinating unit binds the guest, while the signaling unit is released toward the solution. If this unit shows different optical properties (color or fluorescence) depending on whether it is coordinated or in solution, its release causes a change of the signal. All these systems are based on the use of molecular receptors possessing coordination sites with size and charge distribution suitable to those of the guest (**Figure 2**).

3. Chemodosimeter approach: This approach involves the use of specific chemical reactions (generally irreversible) induced by the presence of certain guests that are coupled to a change of color or fluorescent emission [7, 8]. If the reaction is irreversible, the term sensor should not be strictly used, a more appropriate term should be a chromo or fluorogenic reagent or chemodosimeter. **Figure 3** shows a scheme of this approach. The ultimate idea is to take advantage of the selective reactivity that determined guests present. The use of reactions induced by determined chemical species has the advantage of presenting a high selectivity and a cumulative effect that is directly related to the concentration.

Depending on the physical property of the signaling unit that changes in the process of complexation, one can readily have systems of different types, that is, electrochemical, fluorescent, colorimetric, etc. Among the different possibilities, fluorescent and colorimetric systems are very interesting due to their high sensibility and the advantage of a possible detection of species of interest to the "naked eye."

Among the dyes or fluorophores that can be used as signaling unit, the BODIPY core presents several advantages due to its outstanding photophysical properties such as excitation/

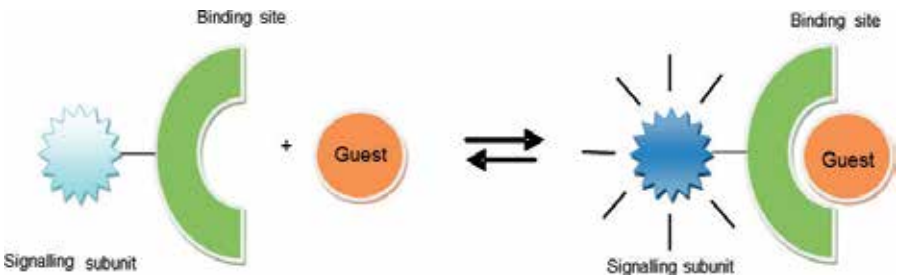

Figure 1. Scheme of the binding site-signaling unit approach.

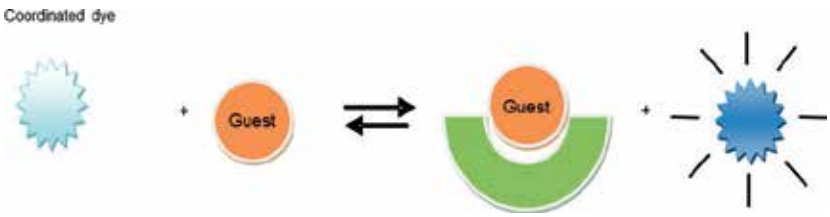

Figure 2. Schematic representation of displacement assays.

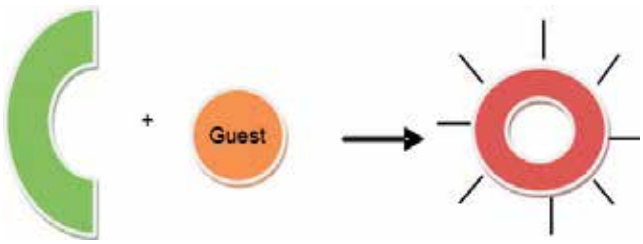

Figure 3. Scheme of the chemodosimeter.

emission wavelengths in the visible spectral region (≈500 nm), the relatively high molar absorption coefficients and fluorescence quantum yields, fluorescence lifetimes in the nanosecond range, and negligible triplet-state formation. On the other hand, they are relatively insensitive to pH and present good solubility, resistance toward self-aggregation in solution and robustness against light and chemicals [9, 10]. Moreover, the spectroscopic and photophysical profiles can be switched by introducing different electron releasing/withdrawing groups at the appropriate positions of the BODIPY core. Additionally, they usually show good biocompatibility that makes them useful for biological applications.

2. Fluoro- and chromogenic chemosensors and chemodosimeter based on the BODIPY derivatives

2.1. Sensors based on the binding site-signaling unit approach

Among the different substitutions in the BODIPY core, structures like these shown in **Figure 4** have been widely used in probe design. There are two main reasons for this selection: (a) the presence of the methyl substituents at 1 and 7 positions of the BODIPY core hinders the free rotation or the phenyl group at 8 which enhances the fluorescence emission and (b) the substitution at 5 or 6 in structure (II) and (III) enlarges electronic delocalization giving rise to possible color changes after the interaction with the analyte.

Many examples of fluorescent sensors based on this type of BODIPY structures were summarized in 2012 by Boens, Leen, Dehaen [11]. For this reason, in the present chapter, only more recent publications will be considered.

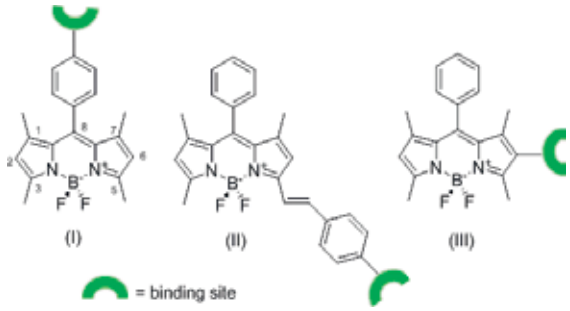

Figure 4. BODIPY structures widely used in sensor design.

In the field of alkaline cation sensors, compounds **1** and **2** are of interest [12] for two reasons: (a) they have been designed to act as cesium ion sensors and (b) they illustrate the influence that the position of the binding unit link to the BODIPY core has in the sensing response.

Complexation studies of **1** with potassium and cesium ions in CH_3CN and in a mixture of CH_3CN/CH_2Cl_2 9:1 were carried out. The obtained data showed a slight bathochromic shift both in the absorption and in the fluorescence spectrum and only a small increase in fluorescence quantum yield. However, complexation with sensor **2** induced a more pronounced hypsochromic shift of absorption and fluorescence spectra. In addition, a strong increase of the fluorescence quantum yield was also observed in the presence of the cation. The different behavior is related to the structural differences between both molecules. In **1**, the binding site is introduced at the meso position, while it is at the α position in compound **2**. In the first case, the conjugation between oxygen atoms of the crown-ether coordination site and the BODIPY chromophore is interrupted which can explain the very slight changes in the photophysical properties of this ligand in the presence of the cations. By contrast, in **2,** the BODIPY signaling unit is electronically conjugated with the oxygen system and this molecule presents a change. Therefore, important shifts in absorption and fluorescence spectra were observed in the presence of cations (**Figure 5**).

In relation to heavy metal cations, compound **3** is a selective sensor for Hg(II) *in vitro* and *in vivo* [13].

The sensing properties of **3** were studied using different metal ions (Li^+, Na^+, K^+, Ca^{2+}, Mg^{2+}, Mn^{2+}, Fe^{2+}, Co^{2+}, Ni^{2+}, Cu^{2+}, Zn^{2+}, Cd^{2+}, Hg^{2+}, Cr^{3+}, and Fe^{3+} as perchlorates) in CH_3CN/PBS solution. Visual color change (from pink to orange) of compound **3** solution was observed only in the presence of Cu(II) and Hg(II) (**Figure 6**). However, the change of color induced by Cu(II) was less intense than the observed in the presence of Hg(II). The selectivity of **3** toward Hg(II) was established by using both UV-visible (a blue shift > 50 nm) and fluorescence (a blue shift > 20 nm and a large enhancement of the fluorescence emission) spectroscopy.

Zinc and cadmium are both elements that play many important roles in our daily life. Zinc is the second most abundant transition metal in the human body, and it is vital for the functions of a large number of enzymes, the stabilization of DNA, gene expression, and neural signal transmission. By contrast, cadmium is a dangerous poison that harms human health and the

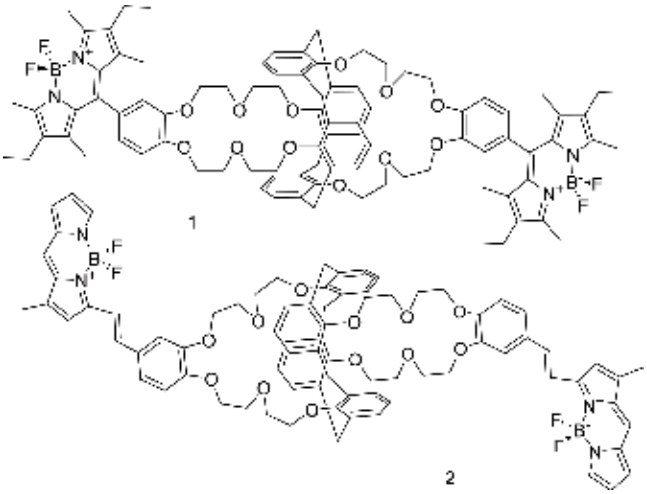

Figure 5. Sensors for detecting Cs^+.

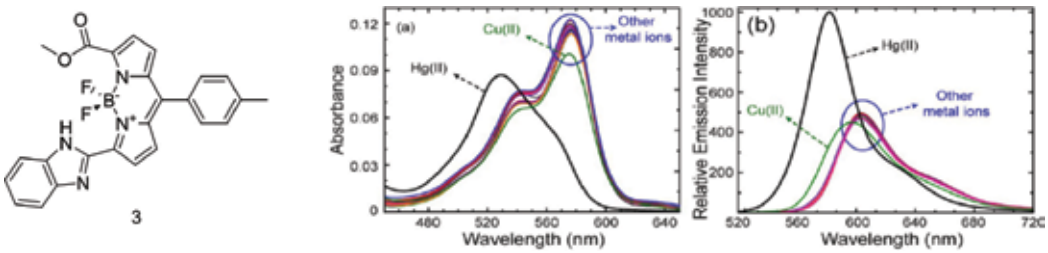

Figure 6. Left: Chemical structure of the sensor for Hg(II), Right: Absorption and emission spectra of BODIPY 3 (1 μM) upon the addition of different metal ions (20 μM) of (Li^+, Na^+, K^+, Ca^{2+}, Mg^{2+}, Mn^{2+}, Fe^{2+}, Co^{2+}, Ni^{2+}, Cu^{2+}, Zn^{2+}, Cd^{2+}, Hg^{2+}, Pb^{2+}, Cr^{3+}, and Fe^{3+}) in CH_3CN/PBS (7:3; v/v, pH 7.4) solution (reprinted with permission from Madhu et al. [13]. Copyright 2013 American Chemical Society).

environment. Two BODIPY-based sensors (**Figure 7**) able to differentiate these two cations have been described [14].

The photophysical properties of compound **4** showed strong changes in the presence of Zn^{2+} in acetonitrile solutions, whereas a large number of cations (Cd^{2+},Cu^{2+}, Pb^{2+}, Fe^{2+}, Co^{2+}, Ni^{2+}, Ag^+, Mg^{2+}, Ca^{2+}, Na^+, and K^+) induced small changes or no changes at all. Zn^{2+} induced the appearance of a new band in the UV spectrum and a strong enhancement of the fluorescence emission. On the other hand, compound **5** showed selectivity toward Cd^{2+} in phosphate buffered solution. Under these conditions, the absorption band showed a hypochromic effect upon the addition of Cd^{2+} ion. In addition, the weak emission at 570 nm of compound **5** in PBS was shifted hypsochromically by 5 nm, and its intensity was greatly enhanced (the fluorescence quantum yield increased about 15-fold).

Finally, chemosensors **6** and **7** (**Figure 8**) based on the BODIPY scaffold have been reported for selective sensing of trivalent cations [15].

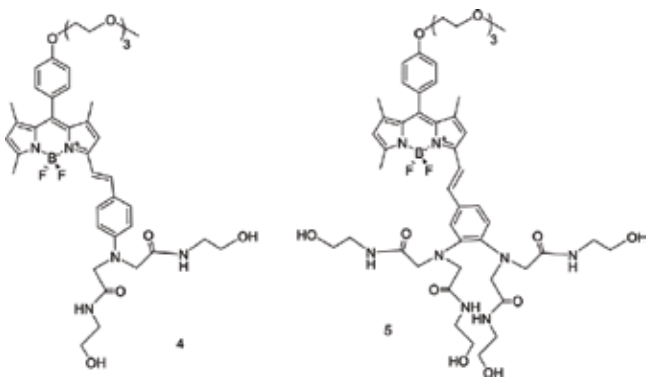

Figure 7. Selective sensors for Zn(II) and Cd(II).

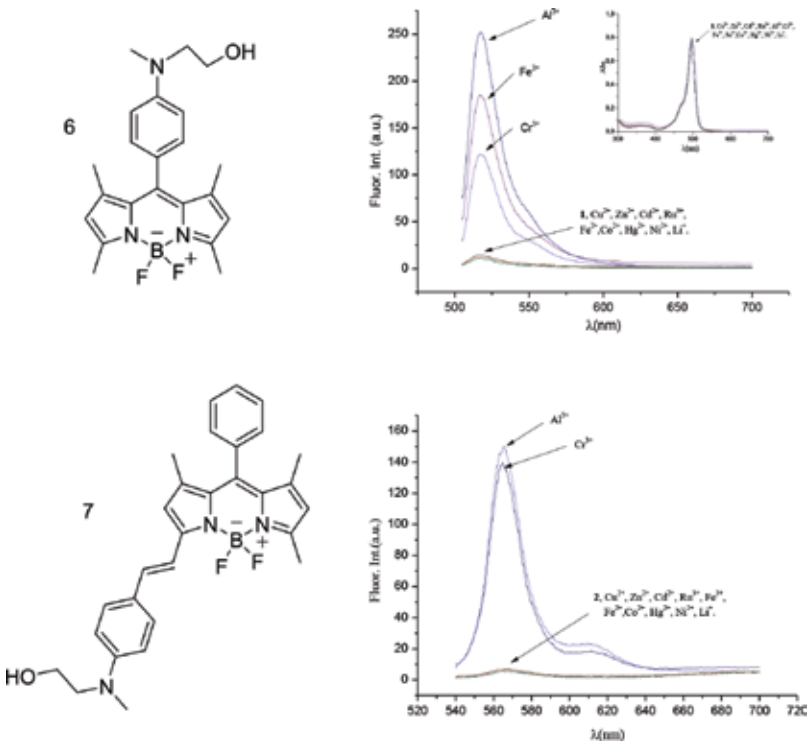

Figure 8. Sensors for selective detection of trivalent cations.

Chemosensor **6** showed, in water:CH_3CN (80:20 v/v), an intense absorption band at 490 nm, yet it was scarcely fluorescent. Addition of Fe^{2+}, Cu^{2+}, Zn^{2+}, Cd^{2+}, Co^{2+}, Ni^{2+}, Li^{+}, Hg^{2+}, and Ru^{3+} did not modify the emission of **6**, whereas trivalent cations Al^{3+}, Fe^{3+}, and Cr^{3+} led to a very remarkable enhancement of the fluorescence emission at 515 nm. Moreover, no color modulations in the presence of metal cations were found for **6**. This was an expected result bearing in mind the presence of methyl groups in the pyrrole units that most likely impose a

twist position of the phenyl ring that interrupts the conjugation between the N-methyl-N-(2-hydroxyethyl) coordination site and the signaling unit.

In contrast, the signaling unit and binding site in probe **7** are electronically connected, and therefore changes in both color and emission were found. In water:CH_3CN (40:60 v/v), **7** exhibited a strong absorbance with a maximum at 603 nm, and it was poorly fluorescent. Addition of Fe^{2+}, Zn^{2+}, Cd^{2+}, Co^{2+}, Ni^{2+}, Li^{+}, Cu^{2+}, Hg^{2+}, Ru^{3+} or Fe^{3+} to solutions of **7** in water:CH_3CN (40:60 v/v) did not induce any change neither in the UV-Vis nor in the fluorescence spectra. By contrast, in the presence of the trivalent cations Cr^{3+} and Al^{3+}, the color of the solutions changed dramatically from blue to pink due to the appearance of a new band at 560 nm. Probe **7** also shows some color change in the presence of Fe^{3+}, but only when CH_3CN alone or mixtures with a maximum of 8% water were used. Interestingly, probe **7** also displays a remarkable strong fluorescence emission at 563 nm in water:CH_3CN (40:60 v/v) upon the addition of the metal cations Cr^{3+} and Al^{3+}.

2.2. Sensors based on the displacement approach

Most of the sensors following the displacement approach are based on the complexes that in the presence of the analyte, undergoes a decomplexation process that induces strong changes in the optical properties of the system. In some cases, the fluorescence of BODIPY-based compounds is quenched when a complex with the appropriate metal ion is formed. Decomplexation induced by the analyte recovers the ligand fluorescence that can be observed. This approach allows preparing off-on fluorescent chemosensors.

In that sense, compound **8** (**Figure 9**) was prepared to detect nitrogen monoxide [16]. **8** in acetonitrile showed intense absorption band at 500.5 nm and an intense emission band at 520 nm. The fluorescence of the compound was quenched when Cu^{2+} (as nitrate salt) was added. This behavior agreed with the coordination of the cation to the bipyridine binding group. By contrast, Cu^{+} did not induce any change in the fluorescence of **8.** Detection mechanism was based on the known ability of NO to reduce Cu^{2+} to Cu^{+}. Thus, the analyte reduced the cation with the concomitant decomplexation and recovering of the ligand fluorescence.

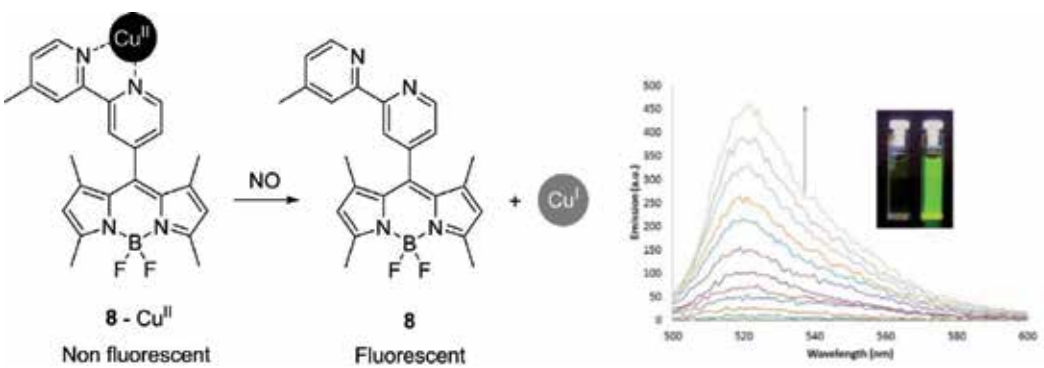

Figure 9. Sensor of NO based on the displacement approach.

The fluorogenic sensing ability of probe **8**-Cu^{2+} was also observed to the naked eye. In particular, bright-green emission was clearly seen when the solutions of **8**-Cu^{2+} exposed to NO were illuminated at 254 nm with a conventional UV lamp. From titration studies, limits of detection (LOD) of 3 ppm were calculated. In addition, **8**-Cu^{2+} was recovered after the oxidation of Cu^{+} to Cu^{2+} induced by atmospheric oxygen. In particular, the regeneration of the **8**-Cu^{2+} probe was achieved using NO-free air. This process was repeated at least 5 times with only minimal loss of fluorescence intensity. Supported sensor using polyethylene oxide was prepared, and the sensing properties were kept in the solid state. Finally, studies of detection of NO in cells were also successfully carried out.

Based also on Cu^{2+} complexes, compound **9** was prepared for detecting S^{2-} in CH_3CN:water [17]. In this example, decomplexation was induced by the formation of the corresponding CuS salt (**Figure 10**). The probe works in a reversible way by adding additional amounts of cation to the solution in each step and has been tested in cells with interesting results.

Based also on the displacement approach, two complexes able to detect the V-nerve agent mimic demeton-S have been described [18]. Acetonitrile solutions of **10** showed an intense absorption band in the visible centered at 600.5 nm responsible of its blue color. Besides, solutions of **10** were nearly nonemissive. This fact was attributed to an efficient ICT quenching of the excited state of the BODIPY fluorophore from the electron-donating aniline group. In contrast, **10**-Eu^{3+} and **10**-Au^{3+} were pink and presented strong emission bands (at 572 and 573 nm for **10**-Eu^{3+} and **10**-Au^{3+}, respectively) due to an inhibition of the quenching process, active in **10**, upon coordination with the metal cations (**Figure 11**).

The behavior of **10**-Eu^{3+} in the presence of demeton-S was tested in acetonitrile. Addition of increasing quantities of demeton-S induced a progressive and marked decrease of the absorption at 553 nm and the appearance of a new band at 600.5 nm with a color modulation from bright pink to blue easily detectable to the naked eye. Besides, a remarkable quenching of the emission band at 572 nm was also observed. A very similar behavior was observed upon the addition of demeton-S to acetonitrile solutions of complex **10**-Au^{3+}.

2.3. Sensors based on the chemodosimeter approach

Due to the selectivity showed by the probes designed following the chemodosimeter approach, there are a large number of applications for detecting different species.

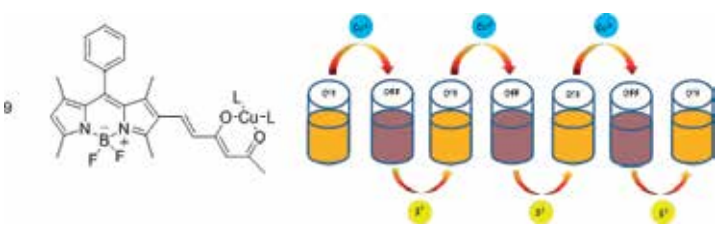

Figure 10. Sensor for detecting S^{2-}.

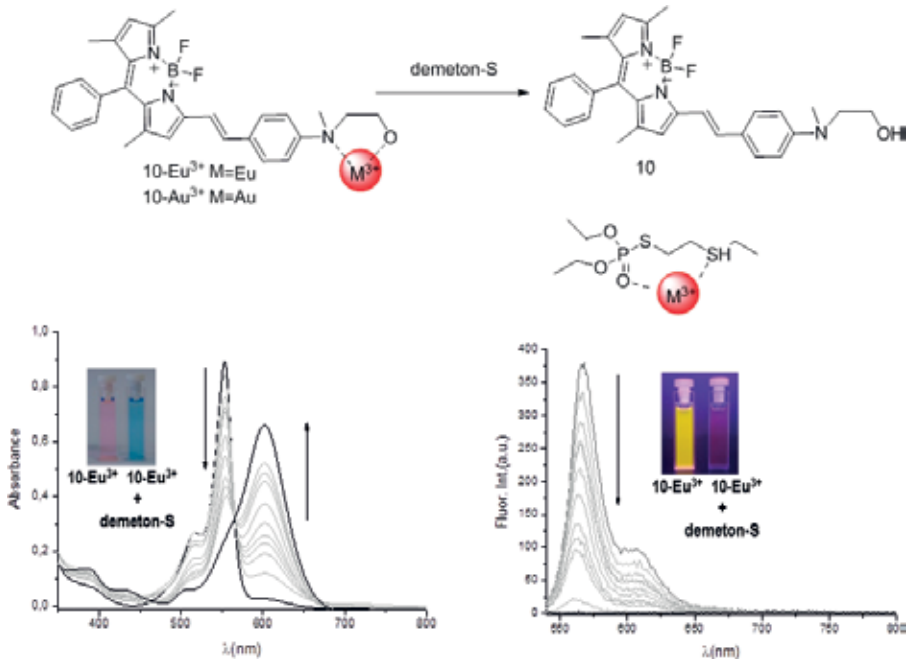

Figure 11. Sensors for detecting V-nerve agent mimic.

2.3.1. Detection of anions

Following an approach that combines the chemodosimeter and the displacement mechanism, compound **11** and its Cu^{2+} complex were prepared [19]. First, it was established that the loss of Cu^{2+} from **11**-Cu^{2+} led to fluorescence enhancement through the production of **11**. Due to the strong affinity of Cu^{2+} to thiols, the ability of **11**-Cu^{2+} to participate in the detection of various biological thiols was examined (**Figure 11**). Changes were displayed in the presence of thiol-containing amino acids and peptides (L-cysteine (L-Cys), homocysteine (Hcys), N-acetyl-L-cysteine (N-acetyl-L-Cys), methionine (Met), glutathione (GSH), and the remaining non-S-containing amino acids (Ala, Arg, Asn, Asp, Gln, Glu, Gly, His, Ile, Leu, Lys, Phe, Pro, Ser, Thr, Trp, Tyr, and Val) in aqueous solution (CH_3OH:HEPES buffer, 30:70, pH 6.5). Significant fluorescence enhancement was only observed upon the addition of Cys. The sensor selectively recognized cysteine over other biothiols (Hcys, N-acetyl-L-Cys, Met, and GSH). The limit of detection for Cys was determined as 6.0 μM (10 mM, CH_3OH:HEPES buffer, 30:70, pH 6.5) (**Figure 12**).

Also, in relation to detecting biothiol compound **12** was prepared [20]. BODIPY substituted with 8-phenylmecapto group was enabled to discriminate biothiols like GSH, Cys or Hcys through a thiol-induced SNAr substitution-rearrangement cascade reaction. Discrimination among different biothiols is related to the leaving group characteristic and steric hindrance in the reactive center. In CH_3CN/PBS buffer (3:7, v/v, 10 mM, pH 7.4) at 25°C, **12** showed a main

absorption at 528 nm and displayed a main absorption at 493 nm. The addition of 10 equiv. of Hcys or GSH gave rise to a slight hypsochromic shift in the absorption maxima in addition to a small increment of intensity. The emission behaviors of **12** showed an enhancement of the fluorescence emission of 20-fold enhancement for Hcys at 543 nm, and 80-fold for GSH at 547 nm when excited at 510 nm. By contrast, no enhancement was observed in the presence of Cys. However, Cys showed a strong emission band at 493 nm when excited at 440 nm. The enhancement was around 300-fold, whereas Hcys or GSH only induced small emission changes (**Figures 13**).

2.3.2. Detection of neutral molecules

There are a large number of neutral compounds whose detection has been developed using BODIPY-based chemodosimeters [21–28]. In this chapter, there are summarized some probes used in detecting dangerous or strongly pollutant analytes.

2.3.2.1. Explosives

3,5-Bis(acetal) BODIPY **13** was able to detect picric acid (PA) in a chloroform solution [29]. **13** showed a strong absorption band at 508 nm with a distinct shoulder at 478 nm. The emission spectra showed a maximum located at 514 nm and a quantum yield of 0.08. The fluorescent properties were similar when water-acetonitrile mixtures were used. The sensor response in the presence of several nitroaromatic explosives (picric acid (PA), 2,4,6- trinitrotoluene (TNT), 2,6-dinitrotoluene (DNT), 1,4-dinitrobenzene (DNB), 1,4-dinitrobenzoic acid (DNBA), 2,4-dinitrophenol (DNP), 1,4-benzoquinone (BQ), and 4-nitrophenol (NP)) was studied. The absorption spectrum of compound **13** showed a red shift of around 15 nm when PA was added. The other studied explosive did not induce any change. The absorption modification could be observed by naked-eye (from pale green to bright yellow-orange). In addition, the emission spectrum also was altered in the presence of PA, with a red-shift of the band (around 20 nm) and a simultaneous increase of the emission intensity (6-fold). The emission maxima remained unaltered in the presence of the other studied analytes (**Figures 14**).

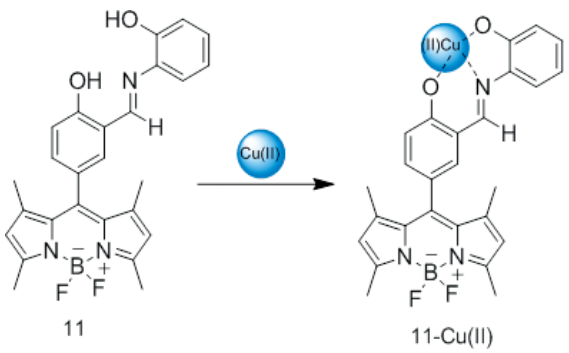

Figure 12. Sensor for detecting cysteine.

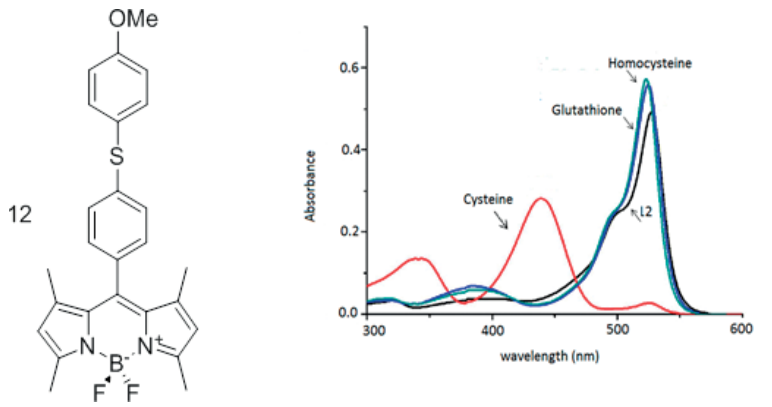

Figure 13. Sensor for biothiols.

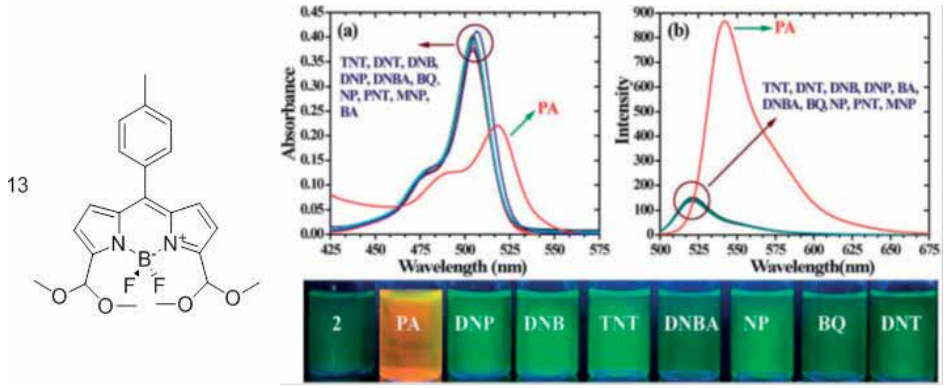

Figure 14. Left: Sensor for selective detection of picric acid, Right: Changes in absorption and emission intensity of BODIPY **13** (5 mM) upon addition of various nitro aromatics (50 equiv.) in a $CH_3CN:H_2O$ (9 : 1; v/v) solution. The color change induced after addition of various nitroaromatic com ounds to BODIPY **13** under a UV lamp detection of picric acid (reprinted with permission from Madhu et al. [29]. Copyright 2013 Royal Society of Chemistry).

2.3.2.2. Nerve agents

Several BODIPY derivatives have synthesized to recognize mimics and real nerve agents. In this sense, compounds **14-16** were prepared (**Figures 15** and **16**) [30, 31].

The sensing units in these compounds were based on the 2-(2-dimethylaminophenyl)ethanol moiety. This moiety has two nucleophilic groups, a dimethylamino group and a primary alcohol (**I**). The later, in the presence of some organophosphates and organophosphonates, attacks the electrophilic phosphorous atom of the nerve agent in a S_N2 phosphorylation reaction. Consequently, a phosphoester good leaving group is formed (**II**). Assisted by preorganization factors, the dimethylamino group attacks the carbon atom holding the phosphoester in an intramolecular cyclization reaction. This yields a cyclic quaternary ammonium salt (**III**) that has significantly different properties to those of the dimethylamino moiety (**Figure 17**).

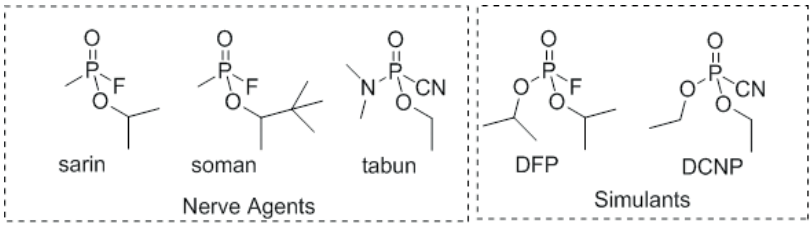

Figure 15. Nerve agent and their simulants.

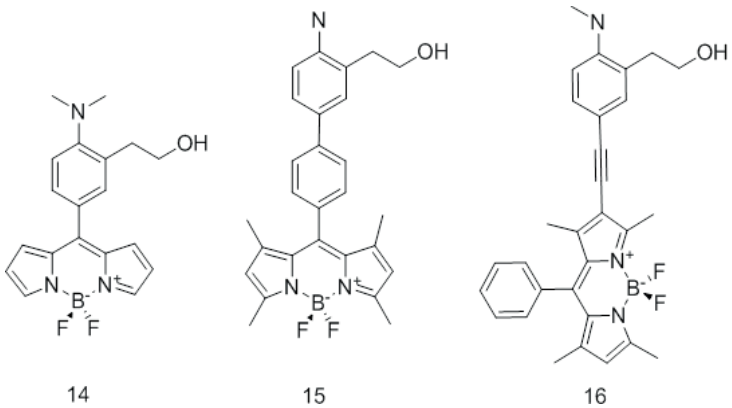

Figure 16. Sensors for detecting nerve agent simulants.

Acetonitrile solutions of **14** and **15** showed no fluorescence emission in the initial state, due to an ICT (from the dimethylamino moiety to the BODIPY core) in the excited state that efficiently deactivates the BODIPY fluorescence. Cyclization of the sensing unit after the detection reaction with the concomitant formation of the positive charge cancels the possibility of the electron pair of the dimethylamino group to travel to an ICT state. Thus, after excitation, the fastest relaxation path is *via* photon emission from the LE state. The orthogonal disposition of the phenyl group at the *meso*-position in compound **15** practically annuls the electronic conjugation between the sensing unit and the transducer. In consequence, no changes in absorption were observed for this compound. Comparative studies with other mimics (diethyl cyanomethylphosphonate (DECP), diethyl 1-phenylethyl phosphonate (DPDP), ethyl S-phenyl ethyl phosphonothiolthionate (diphonate), diethyl(methylthiomethyl)phosphonate (DMTP), malathion, diethyl(2-oxopropyl)phosphonate (DOPP), diethylchlorothiophosphate (DCTP), and compounds) present in real environments (gasoline and diesel) were studied (**Figure 18**).

On the other hand, the sensing unit of compound **16** was connected to the fluorophore by means of a rotation free triple bond that allows coplanarity between the two moieties. Thus, after cyclization, not only changes in emission but also a big hypsochromic shift of the main absorption band was observed (**Figure 19**).

Due to the probe structure, compounds **14–16** gave rise to positive false responses in the presence of acids. To overtake this problem, compound **17** was prepared [32]. This compound

http://dx.doi.org/10.5772/intechopen.79591

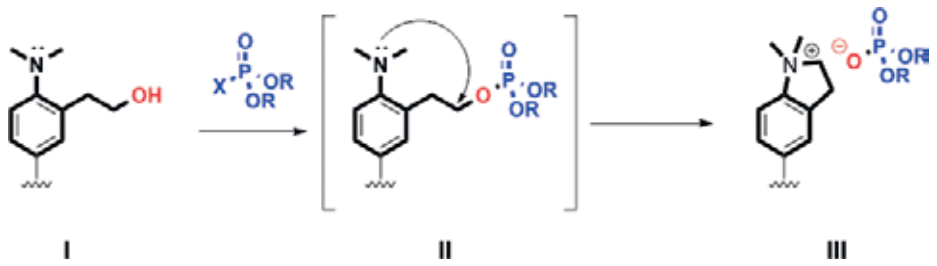

Figure 17. Sensing mechanism.

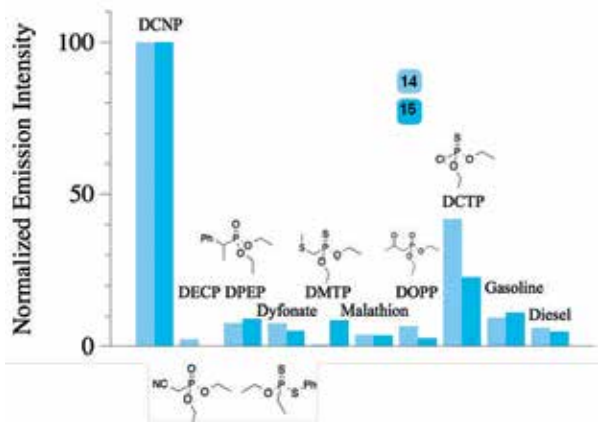

Figure 18. Selectivity of **14** and **15** toward DCNP (Tabun mimic).

possessed the necessary functionality to avoid false positives caused by adventitious acid contaminants. In fact, the pyridine moiety was more basic than the terminal amino group and was the first point of reaction in the presence of acid, thus triggering the characteristic signal response (i.e., little effect on the absorption profile but a significant change in fluorescence intensity). On the other hand, generation of the cyclic ammonium salt was the most favorable reaction in the presence of the nerve agent, thereby giving rise to the accompanying change of color. The system was designed in such a way that even in the presence of both species (i.e., nerve agent and acid), a response was reported (**Figure 20**).

On the other hand, compound **18** was prepared to respond differentially to Tabun and Sarin/Soman, in addition to being insensitive to acid interference (**Figure 21**) [33].

The chromogenic behavior of the acetonitrile solutions of probe **18** was tested in the presence of DFP and DCNP. Addition of DCNP to **18** induced a marked decrease in the band centered at 591 nm, and the appearance of new bands at 515 and 560 nm concomitantly with a clear color change from bright pink to orange. In contrast, a very different chromogenic response was observed when DFP reacted with **18**. In this case, a major bathochromic shift of the visible absorption band of **18** from 590 to 715 nm was observed. This bathochromic shift was reflected in a color modulation from bright pink to light blue.

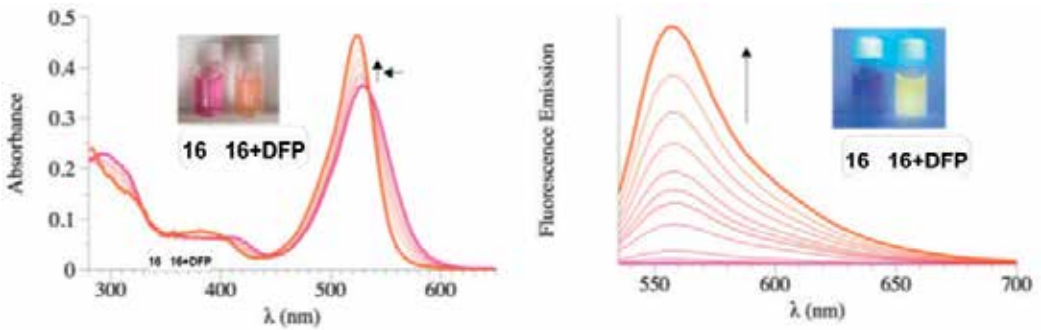

Figure 19. Response of compound **16** in front of DFP.

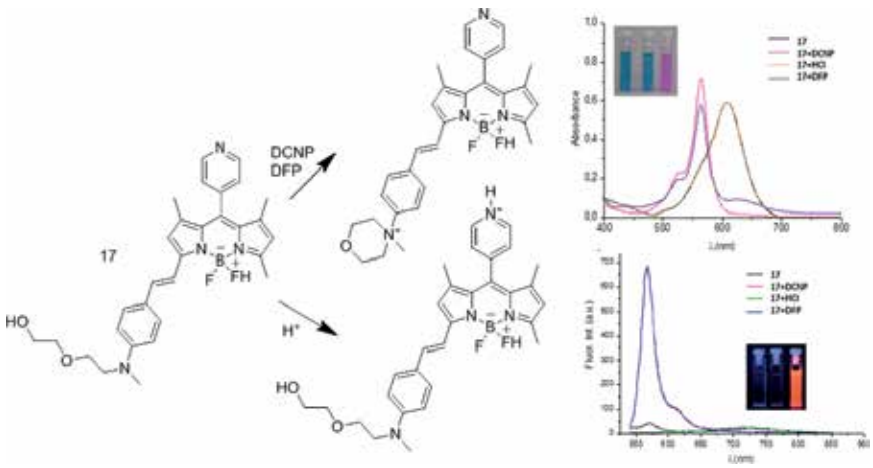

Figure 20. Sensor able to discriminate acids and nerve agent simulants.

The different chromogenic responses observed upon the addition of DCNP and DFP to **18** were related with the release of CN^- and F^- anions upon the phosphorylation of the phenol moiety. Cyanide (the unique by-product from the Tabun simulant DCNP) reacted with the carbonyl group at the 3-position of the BODIPY core of **18** to yield an electron-rich cyanohydrin moiety. Moreover, fluoride (the unique by-product from the Sarin and Soman simulant DFP) induced the hydrolysis of the triisopropylsilyl protective group. The deprotection reaction generated a strong intramolecular charge transfer (ICT) donor phenoxide ion in full conjugation with the BODIPY core, which would reduce the energy gap for the S_0-S_1 transition, and thus resulted in a large red shift in absorbance.

Oximates have been used from the beginning in designing chemosensors for detecting nerve agents and their simulants. Following this idea, compound **19** was prepared [34].

Emission spectrum of **19** ($2 \cdot 10^{-6}$ M in 0.1 mM, pH 7.4 HEPES buffer) showed a band at 508 nm. Fluorescence emission of **19** in the presence of diethylchlorophosphate (DCP) and

Figure 21. Discrimination between DCNP (Tabun simulant) and DFP (Sarin simulant).

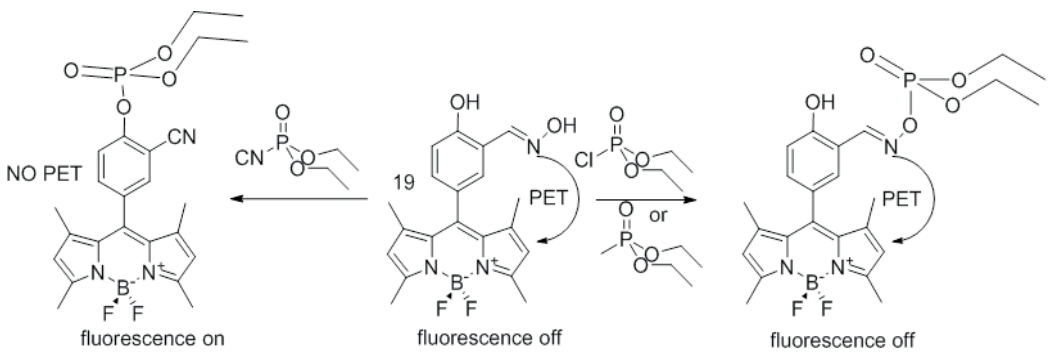

Figure 22. Discrimination between nerve agent simulants with compound **19**.

diethylmethylphosphonate (DEMP) decreased, but with diethylcyanophosphonate (DCNP), intensity increased. Possible mechanisms are described in **Figure 22**. The proposed mechanism was supported by the results obtained using model benzene derivatives bearing the same functional groups.

Compound **20** was prepared for detecting phosgene [35]. Fluorescent behavior of **20** in the presence of phosgene was investigated both in solution (acetonitrile, with 0.1% Et_3N) and supported on paper. In solution, compound **20** exhibited no emission because the PET-promoted quenching arising from the meso-amine moiety. However, upon the addition of triphosgene (1 equiv.), an intense emission band appeared at 511 nm. The PET inhibition was explained taking into account the chemical transformation of the amine group into the corresponding urea derivative. Paper supported probe was successfully used to detect the analyte by using a smart pone (**Figure 23**).

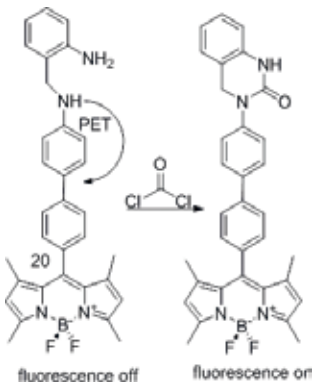

Figure 23. Detection of phosgene.

2.3.2.3. Pollutant gases

Nitrogen oxides are very dangerous contaminants source of severe environmental problems such as acid rain, smog formation, global warming, and ozone layer weakening. Among these compounds, NO_2 is one of the most prevalent and dangerous. Due to the ubiquitous presence of this gas and its health effects, the development of selective and sensitive methods for its detection and quantification has aroused a lot of interest. Thus, compounds **21** and **22** were designed to recognize this gas [36, 37]. The sensing mechanism was based on the carbonyl group regeneration in the analyte presence. In addition to the low limit of detection showed by these compounds, the simple synthesis pathway is an additional advantage (**Figure 24**).

Compound **22** silica nanoparticles-based material that worked following a similar protocol showed interesting chromogenic properties. In the presence of nitrogen dioxide, a change color from green to brown was observed (**Figure 25**).

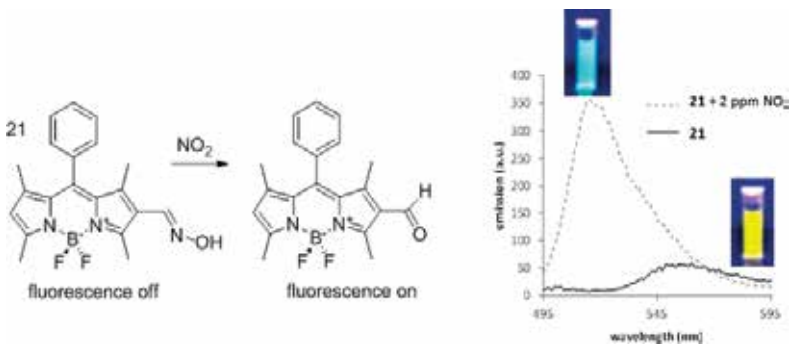

Figure 24. Sensor for detecting nitrogen dioxide in air.

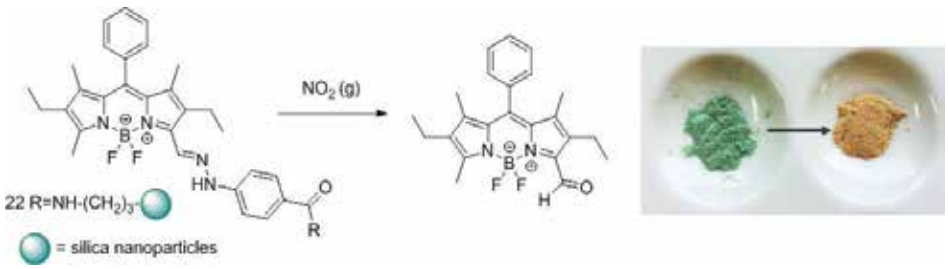

Figure 25. BODIPY functionalized silica nanoparticles for detecting NO_2.

3. Conclusions

The BODIPY core has been successfully used in the designing of chemosensors following the three more commonly used approaches: binding site-signaling unit, displacement, and chemodosimeter. Depending on the position of the reactive unit in the BODIPY core, chromogenic or fluorescent responses were achieved. In many cases, the analyte induced changes can be observed by the naked eye. Cations, anions, and neutral molecules can be detected in different media: organic or aqueous. The biocompatibility of many of these compounds allows their use in biological applications.

Author details

Ana M. Costero*, Margarita Parra, Salvador Gil and Pablo Gaviña

*Address all correspondence to: ana.costero@uv.es

Interuniversity Institute of Molecular Recognition and Technologic Development, University of Valencia-Polytechnic University of Valencia, Valencia, Spain

References

[1] Lörh H-G, Vogtle F. Chromo- and fluoroionophores. A new class of dye reagents. Accounts of Chemical Research. 1985;**18**:65-72. DOI: 10.1021/ar00111a001

[2] Izatt RM, Pawlak K, Bradshaw JS, Bruening RL. Thermodynamic and kinetic data for macrocycle interactions with cations and anions. Chemical Reviews. 1991;**91**:1721-2085. DOI: 10.1021/cr00008a003

[3] Bisel RA, de Silva AP, Gunaratne HQN, Lynch PL, Maguire GEM, Sandanayake KRAS. Molecular fluorescent signalling with 'fluor-spacer-receptor' systems: Approaches to sensing and switching devices *via* supramolecular photophysics. Chemical Society Reviews. 1992;**21**:187-195. DOI: 10.1039/CS9922100187

[4] An H, Bradshaw J, Izatt RM, Yan Z. Bis- and oligo(benzocrown ether)s. Chemical Reviews. 1994;**94**:939-391. DOI: 10.1021/cr00028a005

[5] Fabbrizzi L, Poggi A. Sensors and switches from supramolecular chemistry. Chemical Society Reviews. 1995;**22**:197-201. DOI: 10.1039/CS9952400197

[6] Wiskur SL, Aït-Haddou H, Lavigne JJ, Anslyn EV. Teaching old indicators new tricks. Accounts of Chemical Research. 2001;**34**:963-972. DOI: 10.1021/ar9600796

[7] Chae M-Y, Czarnik AW. Fluorometric chemodosimetry. Mercury(II) and silver(I) indication in water via enhanced fluorescence signaling. Journal of the American Chemical Society. 1992;**114**:9704-9705. DOI: 10.1021/ja00050a085

[8] Dujols V, Ford F, Czarnik AW. A long-wavelength fluorescent chemodosimeter selective for Cu(II) ion in water. Journal of the American Chemical Society. 1997;**119**:7386-7387. DOI: 10.1021/ja971221g

[9] Ziessel R, Ulrich G, Harriman A. The chemistry of bodipy: A new *El Dorado* for fluorescence tools. New Journal of Chemistry. 2007;**31**:496-501. DOI: 10.1039/B617972J

[10] Ulrich G, Ziessel R, Harriman A. The chemistry of fluorescent bodipy dyes: Versatility unsurpassed. Angewandte Chemie, International Edition. 2008;**47**:1184-1201. DOI: 10.1002/anie.200702070

[11] Boens N, Leen V, Dehaen W. Fluorescent indicators based on BODIPY. Chemical Society Reviews. 2012;**41**:1130-1172. DOI: 10.1039/C1CS15132K

[12] Depauw A, Kumar N, Ha-Thi M-H, Leray I. Calixarene-based fluorescent sensors for cesium cations containing BODIPY fluorophore. The Journal of Physical Chemistry. A. 2015;**119**:6065-6073. DOI: 10.1021/jp5120288

[13] Madhu S, Sharma DK, Basu SK, Jadhav S, Chowdhury A, Ravikanth M. Sensing Hg(II) *in vitro* and *in vivo* using a benzimidazole substituted BODIPY. Inorganic Chemistry. 2013;**52**:11136-11145. DOI: 10.1021/ic401365x

[14] He H, Ng DKP. Differential detection of Zn^{2+} and Cd^{2+} ions by BODIPY-based fluorescent sensors. Chemistry, an Asian Journal. 2013;**8**:1441-1446. DOI: org/10.1002/asia.201300183

[15] Barba-Bon A, Calabuig L, Costero AM, Gil S, Martínez-Máñez R, Sancenón F. Off–on BODIPY-based chemosensors for selective detection of Al^{3+} and Cr^{3+} *versus* Fe^{3+} in aqueous media. RSC Advances. 2014;**4**:8962-8965. DOI: 10.1039/C3RA46845C

[16] Juárez LA, Barba-Bon A, Costero AM, Martínez-Máñez R, Sancenón F, Parra M, Gaviña P, Terencio MC, Alcaraz MJ. A boron dipyrromethene (BODIPY)-based Cu^{II}-bipyridine complex for highly selective no detection. Chemistry–A European Journal. 2015;**21**:15486-15490. DOI: 10.1002/chem.201502191

[17] More AB, Mula S, Thakare S, Chakraborty S, Ray AK, Sekar N, Chattopadhyay S. An acac-BODIPY dye as a reversible "ON-OFF-ON" fluorescent sensor for Cu^{2+} and S^{2-} ions based on displacement approach. Journal of Luminescence. 2017;**190**:476-484. DOI: 10.1016/j.jlumin.2017.06.005

[18] Barba-Bon A, Costero AM, Gil S, Sancenón F, Martínez-Máñez R. Chromo-fluorogenic BODIPY-complexes for selective detection of V-type nerve agent surrogates. Chemical Communications. 2014;**50**:13289-13291. DOI: 10.1039/C4CC05945J

[19] Tsay OG, Lee KM, Churchill DG. Selective and competitive cysteine chemosensing: Resettable fluorescent "turn on" aqueous detection via Cu2+ displacement and salicylaldimine hydrolysis. New Journal of Chemistry. 2012;**36**:1949-1952. DOI: 10.1039/c2nj40387k

[20] Zhang J, Ji X, Ren H, Zhou J, Chen Z, Dong X, Zhao W. Meso-heteroaryl BODIPY dyes as dual-responsive fluorescent probes for discrimination of Cys from Hcy and GSH. Sensors and Actuators B: Chemical. 2018;**260**:861-869. DOI: org/10.1016/j.snb.2018.01.016

[21] Lin Q, Gurskos JJ, Buccella D. Bright, red emitting fluorescent sensor for intracellular imaging of Mg^{2+}. Organic & Biomolecular Chemistry. 2016;**14**:11381-11388. DOI: 10.1039/c6ob02177h

[22] Zhang C, Han Z, Wang M, Yang Z, Ran X, He W. A new BOPDUPY-derived ratiometric sensor with internal change transfer (ICT) effect: Colorimetric/fluorometric sensing of Ag^{+}. Dalton Transactions. 2018;**47**:2285-2291. DOI: 10.1039/c7dt04345g

[23] Üçüncü M, Karakus E, Emrullahoglu M. A BODIPY-based fluorescent probe for ratiometric detection of gold ions: Utilization of Z-enynol as the reactive unit. ChemComm. 2016;**52**:8247-8250. DOI: 10.1039/c6cc04100k

[24] Ashokkumar P, Weisshoff H, Kraus W, Rurack K. Test-strip-based fluorometric detection of fluoride in aqueous media with BODIPY-linked hydrogen-bonding receptor. Angewandte Chemie, International Edition. 2014;**53**:2225-2229. DOI: 10.1002/anie.201307848

[25] Ali F, Aute S, Sreedharan S, Nila HA, Saeed HK, Smythe CG, Thomas JA, Das A. Tracking HOCl concentrations across cellular organelles in real time using a super resolution microscopy probe. ChemComm. 2018;**54**:1849-1852. DOI: 10.1039/c7cc09433g

[26] Li B, He Z, Zhou H, Zhan H, Li W, Cheng T. Reaction based colorimetric fluorescence probes for selective detection of hydrazine. Dyes and Pigments. 2017;**146**:300-304. DOI: org/10.1016/j.dyepig.2017.07.023

[27] Sedgwick AC, Chepman RSL, Gardine JE, Peacock LR, Kim G, Yoon J, Bull SD, James TD. A bodipy based hydroxylamine sensor. ChemComm. 2017;**53**:10441-10445. DOI: 10.1039/c7cc05872a

[28] Purdey MS, McLennan HJ, Sutton-McDowall ML, Drumm DW, Zhang X, Capon PK, Heng S, Thompson JG, Abell AD. Biological hydrogen presoide detection with ary boronate and benzyl BODIPY-based fluorescent probes. Sensors and Actuators B: Chemical. 2019;**262**:750-757. DOI: org/10.1016/j.snb.2018.01.198

[29] Madhu S, Bandela S, Ravikanth M. BODIPY based fluorescent chemodosimeter for explosive picric acid in aqueous media and rapid detection in the solid state. RSC Advances. 2014;**4**:7120-7123. DOI: 10.1039/c3ra46565a

[30] Gotor R, Costero AM, Gaviña P, Gil S. Ratiometric double channel borondipyrromethene based chemodosimeter for the selective detection of nerve agent mimics. Dyes and Pigments. 2014;**108**:76-83. DOI: org/10.1016/j.dyepig.2014.04.011

[31] Gotor R, Gaviña P, Ochando LE, Chulvi K, Lorente A, Martínez-Máñez R, Costero AM. BODIPY dyes functionalized with 2-(2-dimethylaminophenyl)ethanol moieties as selective OFF–ON fluorescent chemodosimeters for the nerve agent mimics DCNP and DFP. RSC Advances. 2014;**4**:15975-15982. DOI: 10.1039/C4RA00710G

[32] Barba-Bon A, Costero AM, Gil S, Harriman A, Sancenon F. Highly selective detection of nerve-agent simulants with BODIPY dyes. Chemistry–A European Journal. 2014;**20**:6339-6634. DOI: org/10.1002/chem.201304475

[33] Barba-Bon A, Costero AM, Gil S, Martínez-Máñez R, Sancenón F. Selective chromo-fluorogenic detection of DFP (a Sarin and Soman mimic) and DCNP (a Tabun mimic) with a unique probe based on a boron dipyrromethene (BODIPY) dye. Organic & Biomolecular Chemistry. 2014;**12**:8745-8751. DOI: 10.1039/C4OB01299B

[34] Jang YJ, Tsay OG, Murale DP, Jeong JA, Segev A, Churchill DG. Novel and selective detection of Tabun mímics. ChemComm. 2014;**50**:7531-7534. DOI: 10.1039/c4cc02689f

[35] Sayar M, Karakus E, Gener T, Yildiz B, Yildiz UH, Emrullahoglu M. A BODIPY-Based fluorescent probe to visually detect phosgene: Toward the development of a handheld phosgene detector. Chemistry - A European Journal. 2018;**24**:3136-3140. DOI: 10.1002/chem.2017056 13

[36] Juárez LA, Costero AM, Sancenón F, Martínez-Máñez R, Parra M, Gaviña P. A new simple chromo-fluorogenic probe for NO_2 detection in air. Chemistry–A European Journal. 2015;**21**:8720-8722. DOI: 10.1002/chem.201500608

[37] Juárez LA, Costero AM, Parra M, Gil S, Martínez-Máñez R. A new chromo-fluorogenic probe based on BODIPY for NO_2 detection in air. Chemical Communications. 2015;**51**:1725-1727. DOI: 10.1039/C4CC08654F

Chapter 3

Blue-Emitting BODIPY Dyes

Na Hee Kim and Dokyoung Kim

Additional information is available at the end of the chapter

http://dx.doi.org/10.5772/intechopen.80349

Abstract

BODIPY which consists of a dipyrromethene complex with disubstituted boron has emerged as a superior fluorophore in various research fields. BODIPY typically shows high quantum yield with environment-insensitive fluorescence emission, sharp excitation and emission peaks, high water solubility and biocompatibility, and photostability. So far, various kinds of BODIPY derivatives have been developed and applied in not only academia such as chemistry, biochemistry, biomedical engineering, and medicine but also industries. BODIPY shows dramatic photophysical property changes upon substitution of functional groups or pi bond elongation on the main core structure. Among them, the blue-emitting BODIPY dyes with their synthesis and photophysical analysis were recently reported. In this chapter, the key information of the blue-emitting BODIPY dyes and their recent cutting-edge applications are summarized.

Keywords: BODIPY dyes, fluorophore, blue-emitting, bioimaging, probe

1. Introduction

4,4-Difluoro-4-bora-3a,4a-diaza-s-indacene (boron-dipyrromethene, abbreviated as BODIPY) is a small molecule that emits strong fluorescence with relatively environment-insensitive photophysical property and reasonably high stability in biological conditions (see their structure and numbering in **Figure 1**) [1, 2]. To date, many BODIPY-based fluorescence dyes, molecular probes, and protein-labeling reagents have been developed by tuning of their fluorescence character and functionality [3]. The emission wavelength is readily tunable by modification of the BODIPY framework (BDP, **Figure 1**) according to purpose. In progress, various kinds of the expanded or combined structure of BODIPY derivatives which show a fluorescence emission peak in the red- or near-infrared (NIR) region have been developed for bioimaging applications [4]. Recently, *in vitro* fluorescence study of specific analytes and its

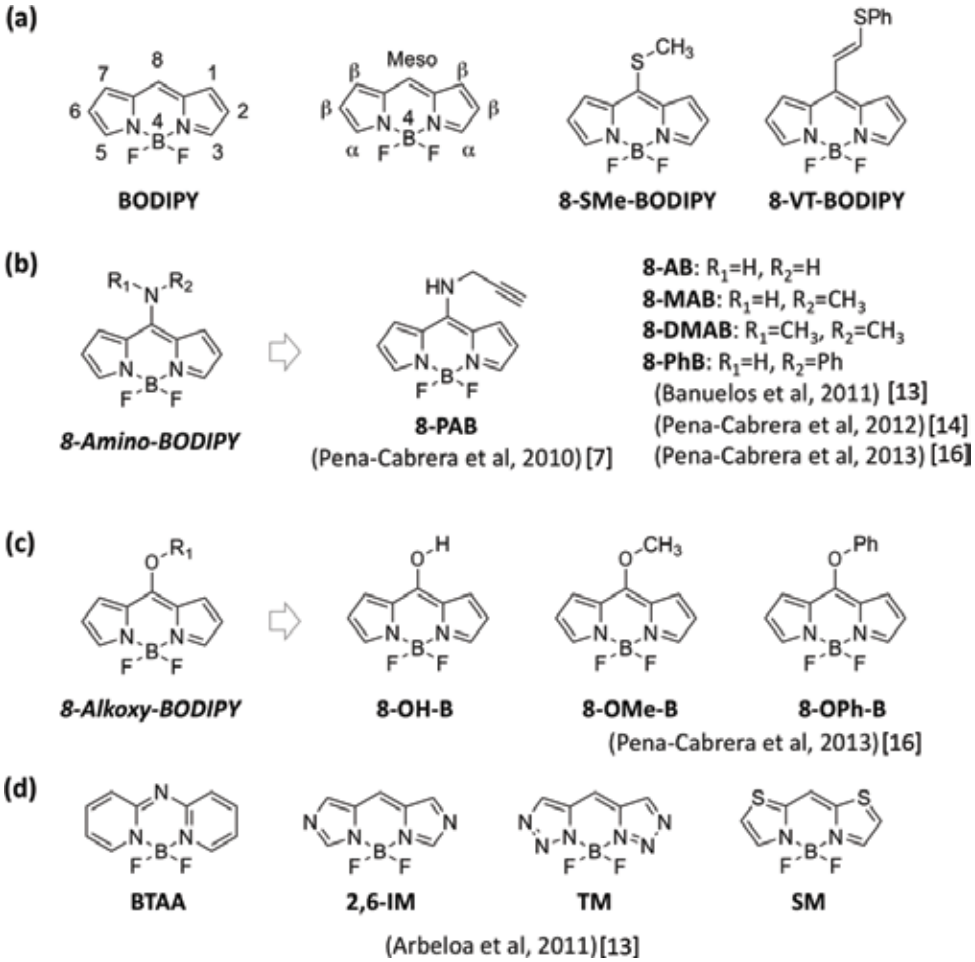

Figure 1. (a) Chemical structure and numbering of BODIPY core, and structure of 8-SMe-BODIPY, 8-VT-BODIPY. (b–d) Blue-emitting BODIPY derivatives.

bioimaging applications in the blue wavelength region also came into the highlight due to the multi-color analysis purpose [5]; thus, the preparation and photophysical property analysis of blue-emitting BODIPY derivatives received attention. In this chapter, a brief explanation of blue-emitting BODIPY derivatives with photophysical properties, their synthetic method, and recently reported applications such as fluorescent labeling and molecular probes for monitoring biologically important species are described.

2. Blue-emitting BODIPY dyes

Generally, BODIPY dyes show fluorescence emission in the green region (500–530 nm) [2]. The fluorescence emission wavelength of BODIPY can be exquisitely controlled by appropriate

substitution of chemical moieties such as aliphatic carbon, aromatic ring, pi-conjugation, halide element, and electron pushing-/donating-group. The pi-bond elongation on the alpha (α)- and beta (β)-positions of BODIPY core gives the red-shifted fluorescence emission wavelength, and the addition of nitrile (CN) moiety on the meso-position (8-position) also gives red-shifted emission [1]. In contrast, the preparation of blue-emitting BODIPY dyes is very limited to few approaches: (i) substitution of electron donating moiety (amine, alkoxy) on the meso-position of BODIPY (**Figure 1b, c**) and (ii) aza-/diaza-BODIPY (BTAA in **Figure 1d**), imidazole-/thiazole-based BODIPY (**Figure 1d**).

2.1 Photophysical properties of blue-emitting BODIPY dyes

2.1.1. 8-Amino-BODIPY

In 2007, Biellmann and co-workers reported the synthesis of 8-heteroatom-substituted BODIPY derivatives including 8-thiomethyl-BODIPY (8-SMe-BODIPY), 8-vinylic-thioether-BODIPY (8-VT-BODIPY), and 8-amino-BODIPY (**Figure 1a**) [6]. The thiomethyl group of 8-SMe-BODIPY displayed high reactivity for the nucleophilic substitution reaction. In the follow-up study, Peña-Cabrera and co-workers found that the substitution reaction of thiomethyl group and amine moiety proceed with high yield (>90%), and the resulting products showed bright blue fluorescence (**Figure 1b**, **Table 1**) [7, 8].

The primary-amine product, 8-AB, is characterized by maximum absorption and emission wavelengths at 399 and 437 nm with high-fluorescence quantum yield (0.92). Interestingly, the secondary-amine products, 8-PAB (propargyl amine substituted) and 8-MAB (monomethylamine substituted), show different photophysical properties each other, particularly quantum yield. Both emit fluorescence in the blue wavelength region, at 405 and 394 nm, upon excitation at 464 and 440 nm, respectively. However, 8-MAB gives lower quantum yield (0.1) than 8-PAB (0.52), because the higher electron-donating capacity of the amine group toward BODIPY core leads to a higher instability of the LUMO orbitals as well as enhancement of the non-radiative decay processes [7, 8]. For 8-PAB, the electron-deficient alkyne moiety decreases the electron-donating ability of amine; thus, 8-PAB keeps higher fluorescence quantum. The tertiary amine product, 8-DMAB, shows a similar photophysical property of 8-MAB. The aniline derivative, 8-PhB, shows less blue-shift of the absorption and emission wavelengths than aliphatic amine-substituted derivatives due to the less electron-donating ability of substituents, like 8-PAB.

2.1.2. 8-Alkoxy-BODIPY

Hydroxyl group-substituted 8-alkoxy-BODIPY, 8-OH-B, was identified by Ahn and co-workers in 2012 while developing a molecular probe for mercury ions using 8-SMe-BODIPY [9]. 8-OH-B showed the most blue-shifted absorption and emission wavelengths from the BODIPY core at 370 and 490 nm, respectively, but the quantum yield and other photophysical properties were not characterized due to its low stability. The other 8-alkoxy-BODIPY derivatives were reported by Peña-Cabrera, Boens, and co-workers in 2013 [10–12]. The significant blue shift of absorption and emission was not observed for these derivatives, probably due to the less electron-donating ability of their substituent.

Compound	λ_{abs} (nm)	λ_{emi} (nm)	Q.Y.	Solvent	Refs.
BDP	497.0	507.0	0.87	MeOH	[8, 11]
8-PAB	405.0	464.5	0.52	MeOH	[7, 8, 14]
8-AB	399.0	437.5	0.92	MeOH	[8]
8-MAB	394.5	440.0	0.10	MeOH	[8, 11]
8-DMAB	395.8	438.0	0.09	MeOH	[8]
8-PhB	403.5	461.0	0.16	MeOH	[10, 12]
8-OH-B	370.0	409.0	n.r.	Buffer/ACN	[9, 15]
8-OMe-B	441.0	484.0	0.85	MeOH	[11, 12, 16]
8-OPh-B	459.0	495.0	0.97	*c*-Hex	[16]
BTAA	384.0	398.4	0.43	MeOH	[13]
2,6-IM/TM/SM[a]	n.r.	400–430	n.r.	n.r.	[13]

The numbers indicate the highest-intensity wavelengths for the absorption and fluorescence emission spectra in the described solvent. Abbreviations: Q.Y.: quantum yield, n.r.: not reported, MeOH: methanol, c-Hex: cyclohexane, buffer: HEPES buffer (10 mM, pH 7.4), ACN: acetonitrile.
[a]Predicted blue-emitting BODIPY derivatives from quantum mechanical calculation.

Table 1. Photophysical properties of blue-emitting BODIPY dyes.

2.1.3. BTAA

Difluoro-boron-triaza-anthracene complex (BTAA) was reported by Arbeloa and co-workers in 2011 [13]. Newly synthesized diaza-BODIPY-type derivative, BTAA, showed an absorption and fluorescence emission peak at 384 and 398 nm, respectively, with high quantum yield (0.43). Their systematic analysis data represented the environment-insensitive photophysical property of BTAA. The properties of other derivatives (2,6-IM, TM, SM) were predicted by quantum mechanical calculation in their report, not by the experiments.

2.2. Synthesis of blue-emitting BODIPY dyes

Synthesis of blue-emitting BODIPY dyes follows established synthetic routes (**Figure 2**).

2.2.1. 8-Amino-BODIPY/8-alkyoxy-BODIPY

For the 8-amino-BODIPY derivatives or 8-alkoxy-BODIPY derivatives, 8-SMe-BODIPY has been used as a starting material (**Figure 2a**). 8-SMe-BODIPY can be prepared by three-step synthesis: (i) reaction of pyrrole with thiophosgene, (ii) methylation of the intermediate using methyl iodide, and (iii) boronation of methylated intermediate using boron trifluoride in the presence of organic base (triethylamine) [7, 9]. The thiomethyl (-SMe) moiety at the meso-position of 8-SMe-BODIPY acts as a good leaving group to prepare N– and O–based nucleophilic substitution reaction with excellent reactivity. Thus, 8-SMe-BODIPY can be converted in a S_NAr-like process by amines or alkoxy moieties to produce meso-amine-substituted

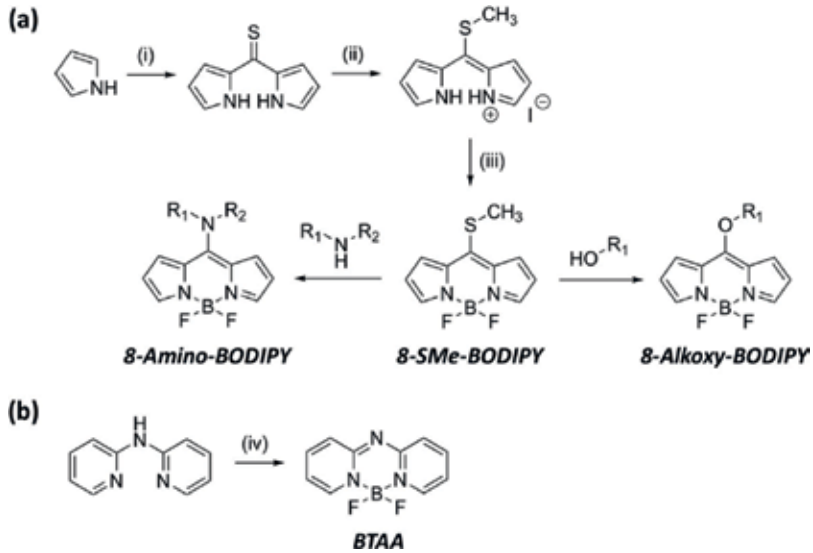

Figure 2. Synthetic routes for blue-emitting BODIPY derivatives: (a) 8-amino-BODIPY and 8-alkoxy-BODIPY, (b) BTAA. Regents: (i) thiophosgene, (ii) methyl iodide, (iii, iv) BF_3-Et_2O, triethylamine.

BODIPYs (8-amino-BODIPY) or meso-alkoxy-substituted BODIPYs (8-alkoxy-BODIPY) in mild reaction conditions with high yield [16, 17].

2.2.2. BTAA

In 2011, Arbeloa and co-workers reported the synthesis of BTAA dye. They successfully synthesized BTAA via boron complex formation of N-(2-pyridinyl)-2-pyridinamine with boron trifluoride in toluene solvent with organic base (triethylamine) with high yield (80%) (**Figure 2b**) [13].

3. Application of blue-emitting BODIPY dyes

Blue-emitting BODIPY derivatives have been used in various research areas. In particular, their unique photophysical property serves feasible application in biological study. Recently, a few examples of notable applications, such as fluorescent labeling and molecular sensing probes, were reported using blue-emitting BODIPY derivatives. As described above, fluorescence imaging in shorter wavelengths (blue-channel) is undoubtedly an essential and useful tool in biological study, because it can be used to avoid the interference of general fluorescent materials which have emission in green and red channels. Moreover, the high quantum yield with negligible solvent/media-dependence of BODIPY allows bioimaging of targeting substrate efficiently.

In this chapter, recently reported fluorescent labeling probes and molecular sensing probes based on blue-emitting BODIPY are summarized.

3.1. Labeling

Labeling of biomolecules with a signaling unit such as a fluorophore or radioisotope is an essential tool for studying molecular interactions in biological systems [18, 19]. In particular, a labeling technic based on fluorophore has received great attention because it enables researchers to monitor specific components in a complex biological environment [18].

A few blue-emitting dyes have been reported for biomolecule labeling, mainly based on coumarin backbone, which has drawbacks such as environment-sensitive fluorescence change. To overcome this issue, new labeling probes based on blue-emitting BODIPY have been recently reported.

In 2013, Peña-Cabrera and co-workers presented the fluorescent tagging of alcoholic and phenolic biomolecules using 8-SMe-BODIPY via a S_NAr-type reaction (**Figure 3**) [16]. They demonstrated the labeling of cholesterol (alcoholic) and estrone (phenolic) at the meso-position of BODIPY core in the presence of CuTC (Copper(I) thiophene-2-carboxylate) and sodium bicarbonate. Interestingly, the cholesterol-labeled product gives high blue fluorescence regardless of the media at 485 nm, but the estrone-labeled product gives poor fluorescence at 488 nm in polar solvents due to intramolecular charge transfer (ICT) [20] quenching.

For protein labeling, Kim and co-workers reported new approaches in 2017 (**Figure 3**). They found that 8-SMe-BODIPY could be useful for protein labeling in mild conditions via S_NAr-type reaction toward the lysine residues that have a secondary amine moiety [21]. As a model protein, a lysozyme (six lysine in the total 129 amino acid) undergo the substitution reaction, and the resulting product shows bright blue fluorescence, maximum absorption and emission at 375 and 409 nm, respectively. In the course of their ongoing research using 8-SMe-BODIPY, they developed a bio-conjugatable group containing blue-emitting 8-amino-BODIPY derivatives (BP-1–BP-4, **Figure 3**) [22]. They demonstrated the labeling of bovine serum albumin (BSA) using BP-2 by amide-bond formation and BP-3 by thiol-ene addition reaction. The labeling was successfully proceeded in a mild condition, and the resulting products showed bright blue fluorescence and absorption and emission maximums at 390–402 nm and 462–465 nm in deionized water, respectively.

In 2018, Chang and co-workers reported that 8-amino-BODIPY derivatives containing the azide and cyclooctyne moiety (AzA-1, COA-1, **Figure 3**) are applicable for copper-free click chemistry [23, 24]. The probes, namely "tame probes," show high biocompatibility with no background noise after labeling in live cells.

3.2. Fluorescent probes

3.2.1. Metal ions (mercury ions; Hg^{2+}, zinc ions; Zn^{2+})

Monitoring of metal ions in the biological system is very important to understand molecular interactions and processes [25]. So far, various kinds of monitoring techniques for metal ions have been developed which mostly depend on expensive instruments. Recently, new approaches based on fluorescence are highlighted for analyte sensing because of their ease of use, low cost, high efficiency, and biocompatibility [26–28].

http://dx.doi.org/10.5772/intechopen.80349

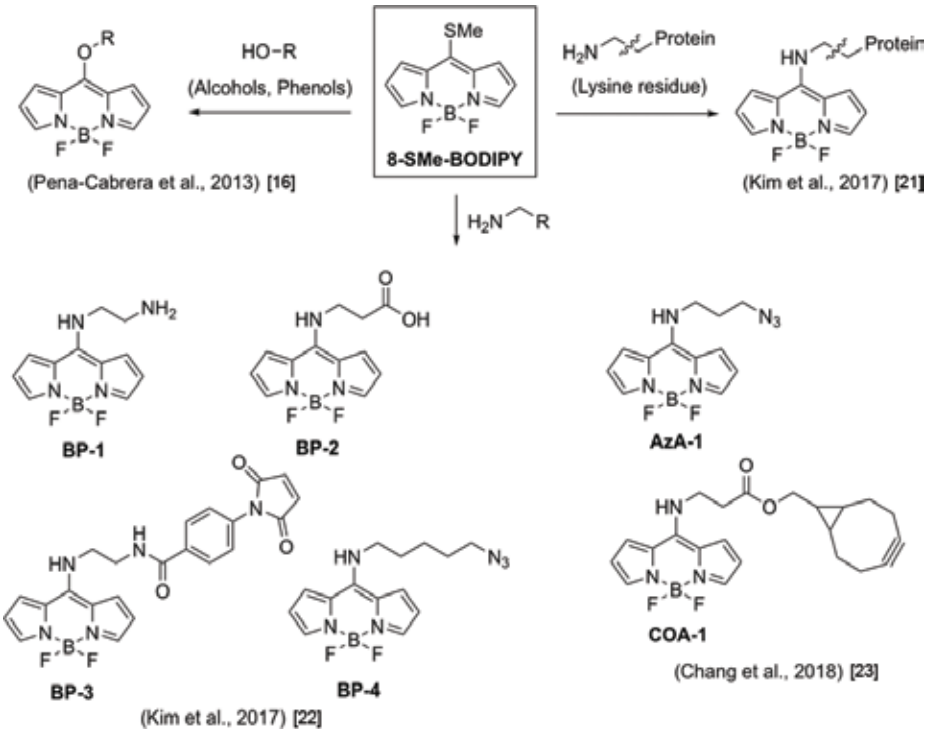

Figure 3. Reported blue-emitting BODIPY dyes for biomolecule labeling, prepared from 8-SMe-BODIPY (square box).

For toxic metal ion analysis, a few fluorescent probes based on blue-emitting BODIPY have been introduced, particularly for mercury ion. Mercury ion is one of the poisonous elements to environmental and biological systems. It can readily penetrate biological membranes and cause serious damage to the central nervous system (CNS) [29].

In 2012, Ahn and co-workers reported a new fluorescent probe for mercury ions based on 8-SMe-BODIPY which shows a ratiometric fluorescence behavior (**Figure 4**) [9]. The mercury ion promoted hydrolysis of thiomethyl (-SMe) at the meso-position of BODIPY core and generated 8-hydroxy-BODIPY (8-OH-B). In the sensing media of this work (HEPES buffer, 10% acetonitrile), 8-SMe-BODIPY shows an absorption maximum at 485 nm and an emission maximum at 525 nm, whereas the hydrolyzed product 8-OH-B shows blue-shifted absorption and emission peaks at 370 and 409 nm, respectively. Strong blue emission was only observed upon adding mercury ions among the other metal ions. However, the low chemical stability of 8-OH-B was observed in the NMR study.

Turn-on-type fluorescent probe based on blue-emitting BODIPY for mercury ion was also reported in 2016. Zhao and co-workers prepared an 8-amino-BODIPY linked to a thiourea unit which can be hydrolyzed via mercury ion-promoted cyclization (Hg Probe 1, **Figure 4**) [15]. Hg Probe 1 showed absorption and emission maximums at 400 and 465 nm in PBS buffer solution (0.5% DMSO) with very weak fluorescence. Upon adding mercury ions, a new

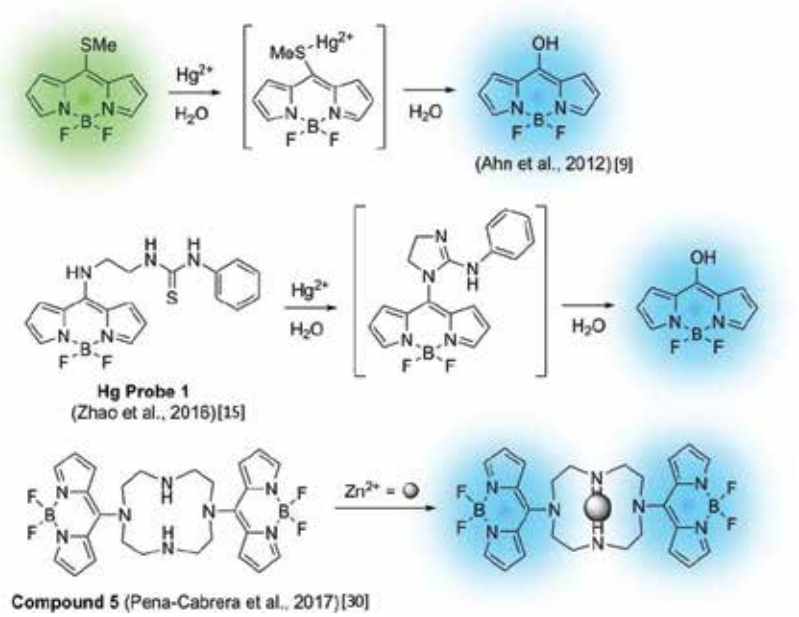

Figure 4. Reported blue-emitting 8-amino-BODIPY-based fluorescent probes for metal ions Hg^{2+} and Zn^{2+}.

absorption peak appeared at 370 nm, and fluorescence was dramatically increased with a new emission peak at 420 nm. The peak difference of 8-OH-B in Ahn's study and this work seems to be coming from the sensing media.

A coordination-based fluorescent probe using 8-amino-BODIPY for the zinc ion was reported by Peña-Cabrera and co-workers in 2017 [30]. In this study, they have synthesized several aza-crown 8-amino-BODIPY derivatives and analyzed their photophysical properties. Among them, the compound 5 gives the turn-on property toward zinc ions with emission maximum at 429 nm when excited at 330 nm (**Figure 4**).

3.2.2. Amino acid (cysteine; Cys, homocysteine; Hcy)

Biothiols such as cysteine (Cys) and homocysteine (Hcy) play crucial roles in the balance of biological system. The concentration of Cys and Hcy is associated with many diseases such as cancer, Alzheimer's disease (AD), Parkinson's disease (PD), osteoporosis, diabetes, and hematopoiesis decrease [31].

Recently, Ahn and co-workers reported a Cys/Hcy-selective probe (**Figure 5**, upper) [32] and a Cys-selective probe (**Figure 5**, bottom) [33], based on 8-amino-BODIPY.

For Cys/Hcy sensing, they used 8-SMe-BODIPY by mimicking the native chemical ligation strategy [32]. The methylthio group might be readily exchanged with thiol moiety in Cys/Hcy,

and the amine moiety in their amino acid backbone could further undergo intramolecular displacement to give the corresponding 8-amino-BODIPY (**Figure 5**). The original emission peak of 8-SMe-BODIPY at 524 nm disappeared upon adding Cys/Hcy, while a new peak in the shorter wavelength at 467 nm appeared which corresponded with 8-amino-BODIPY. After confirming selectivity and sensitivity, they applied the probe for the bioimaging of biothiols in living species, zebrafish. A brighter blue emission was observed from all the organs than the green emission, demonstrating the ratiometric fluorescence bioimaging application of blue-emitting BODIPY.

A fluorescence resonance energy transfer (FRET)-based ratiometric-type probe for Cys was also reported [33]. In the course of their ongoing research using 8-amino-BODIPY, they prepared a FRET couple between fluorescein (FITC, green emission) and 8-amino-BODIPY (P1, **Figure 5**). The FITC linked with diacrylate showed no fluorescence, thus P1 gives only blue fluorescence at 452 nm when excited at 400 nm. Upon treatment with Cys, the diacrylate moiety could be hydrolyzed in aqueous media and generate fluorescent FITC. A new emission band appeared at 520 nm when excited at 400 nm, indicating FRET. P1 has been applied for the analysis of Cys level in cell lines (B16F10, Rat1, N2A, HeLa, C6, and HT22) as well as human plasma.

3.2.3. Chemical warfare (phosgene gas)

Chemical warfare (CW) is the use of toxic chemical substances as weapons [34]. Among them, phosgene is a kind of colorless gas and a highly lethal chemical warfare. It reacts with the amine species and generates cross-linking by urea formation. This reaction can occur with proteins in the pulmonary alveoli, the site of gas exchange, and destroy the barrier of blood-air, causing suffocation [35]. Thus, a rapid and facile method for detecting phosgene is required. Fluorescence method possesses advantages in terms of high sensitivity with fast responsibility and real-time analysis for phosgene.

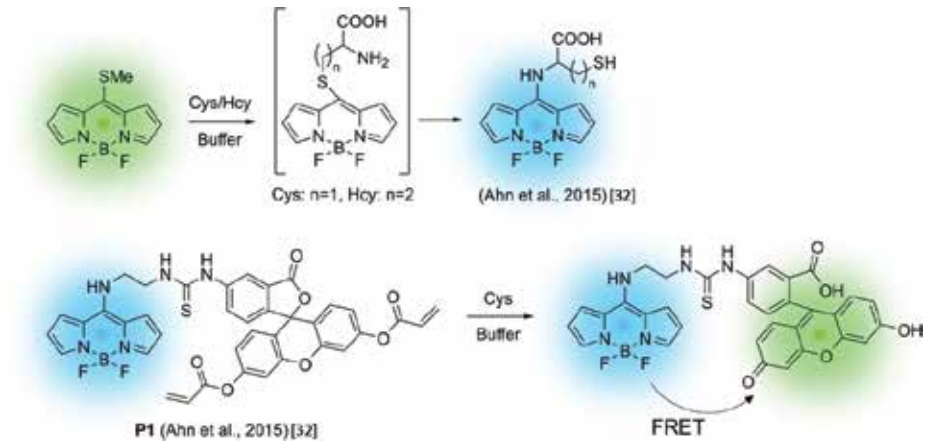

Figure 5. Reported 8-amino-BODIPY-based fluorescent probes for amino acid: cysteine (Cys), homocysteine (Hcy).

To date, various kinds of fluorescent probes for phosgene have been introduced [36]. In 2017, Tian and co-workers reported a phosgene probe based on 8-amino-BODIPY (8-EDAB, **Figure 6**) [37]. Phosgene reacts with primary amine moiety in 8-EDAB, which undergoes a fast intramolecular cyclization reaction (phosgene-mediated acidylation) to afford a urea-containing 8-amino-BODIPY. The 8-EDAB emitted blue fluorescence at 445 nm with low quantum yield (0.15) upon 390 nm excitation, probably due to the intramolecular charge transfer (ICT) quenching of secondary amine toward BODIPY core. Upon addition of phosgene, a new emission peak at 512 nm appeared upon 465 nm excitation with high quantum yield (0.65) and fast response (<1.5 sec) in sensing media (acetonitrile, 80 nM triethylamine). In addition, 8-EDAB showed sub-nanomolar detection limit (0.12 nM) for phosgene with high sensitivity.

In the same year, Song and co-workers reported a similar approach using ortho-phenylenediamine (OPD)-introduced BODIPY for phosgene sensing (o-Pab, **Figure 6**) [38]. Unlike the ethylenediamine-substituted fluorescent probe as described above (8-EDAB), o-Pab shows no fluorescence in sensing media (chloroform, 1% triethylamine) due to photoinduced electron transfer (PET) quenching [39] from OPD to the BODIPY core and rotational deactivation along the aryl-amine-aryl single bonds. Fluorescence spectra of o-Pab exhibit a turn-on response, with an emission peak at 530 nm upon 450 nm excitation. Although the OPD-substituted 8-amino-BODIPY does not show blue emission, their experimental data give information to understand the basic photophysical property of meso-substituted BODIPY derivatives.

3.2.4. Lipid membrane

Lipid membranes (mono-/bi-layers, vesicles, biological membranes) form a barrier around all cells and play important roles in almost all living organisms as well as viruses [40, 41]. To date,

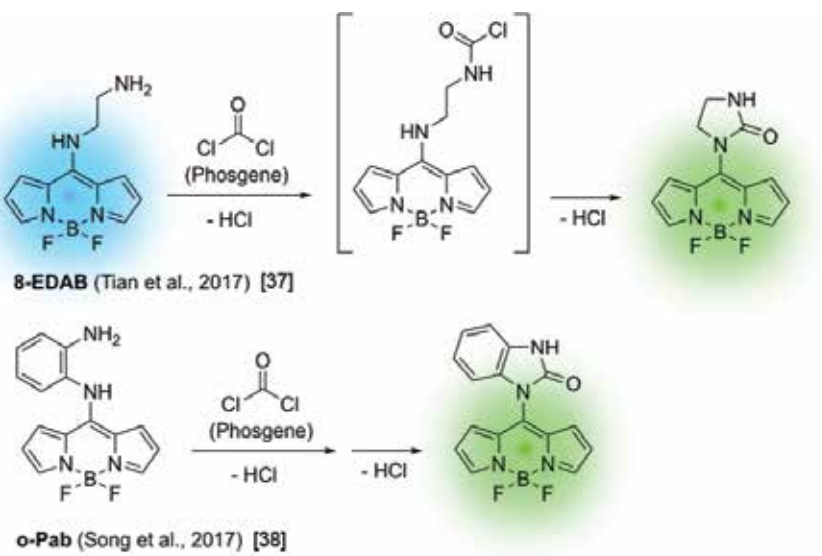

Figure 6. Reported 8-amino-BODIPY-based fluorescent probes for chemical warfare, phosgene gas.

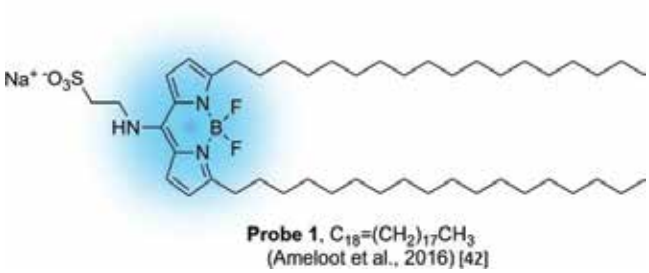

Figure 7. Reported 8-amino-BODIPY-based fluorescent probe for lipid membrane staining.

the staining of lipid membrane using fluorescence agents has been widely used for biological studies. Membrane targeting protein- or peptide-conjugated fluorophore and long aliphatic carbon chain-conjugated fluorophore are representative approaches. In the same vein, Ameloot and co-workers developed a new blue-emitting lipid membrane probe based on 8-amino-BODIPY linked with a long carbon chain (C_{18}-alkyl) at the 3,5-position and taurine substituent at the meso-position (Probe 1, **Figure 7**) [42]. Probe 1 shows blue fluorescence in the range between 480 and 494 nm with high quantum yield (0.38–0.93) upon excitation with 415–429 nm, in the various solvents. The lipid membrane-staining and fluorescence-imaging applications were successfully carried out for small unilamellar vesicles, giant unilamellar vesicles, and biological cells (OLN-93 cells) using one−/two-photon microscopy.

4. Summary and outlook

In this chapter, the basic photophysical property, synthetic method, and application of blue-emitting BODIPY derivatives are introduced. The amino- or alkoxy- moiety substitution at the meso-position of BODIPY core is expected to provide a shorter excitation and emission wavelength at the blue region with high quantum yield, and the systematic analysis results have given evidences. In addition, their superior photostability and chemical stability with facile functioning give many possibilities for developing fluorescent tagging reagents and molecular probes to monitor biologically important species. Most of the applications using blue-emitting BODIPYs were carried out very recently; therefore, we believe that this summary will be helpful for the beginner who wishes to study the fluorophore/fluorescent probe and will inspire scientists to develop many useful systems with practical applications.

Acknowledgements

This work was supported by the Bio & Medical Technology Development Program of the National Research Foundation (NRF) of Korea funded by the Ministry of Science & ICT (NRF-2018-M3A9H3021707). This research was also supported by Basic Science Research Program through the National Research Foundation (NRF) of Korea funded by the Ministry of Education (NRF-2018-R1A6A1A03025124, NRF-2018-R1D1A1B07043383).

Conflict of interest

The authors declare that there are no conflicts of interest.

Author details

Na Hee Kim[1] and Dokyoung Kim[1,2,3,4]*

*Address all correspondence to: dkim@khu.ac.kr

1 Department of Biomedical Science, Graduate School, Kyung Hee University, Seoul, Republic of Korea

2 Department of Anatomy and Neurobiology, College of Medicine, Kyung Hee University, Seoul, Republic of Korea

3 Center for Converging Humanities, Kyung Hee University, Seoul, Republic of Korea

4 Biomedical Science Institute, Kyung Hee University, Seoul, Republic of Korea

References

[1] Loudet A, Burgess K. BODIPY dyes and their derivatives: Syntheses and spectroscopic properties. Chemical Reviews. 2007;**107**:4891-4932. DOI: 10.1021/cr078381n

[2] Kowada T, Maeda H, Kikuchi K. BODIPY-based probes for the fluorescence imaging of biomolecules in living cells. Chemical Society Reviews. 2015;**44**:4953-4972. DOI: 10.1039/C5CS00030K

[3] Boens N, Leen V, Dehaen W. Fluorescent indicators based on BODIPY. Chemical Society Reviews. 2012;**41**:1130-1172. DOI: 10.1039/C1CS15132K

[4] Ni Y, Wu J. Far-red and near infrared BODIPY dyes: Synthesis and applications for fluorescent pH probes and bio-imaging. Organic & Biomolecular Chemistry. 2014;**12**: 3774-3791. DOI: 10.1039/C3OB42554A

[5] Mark B, Dempsey GT, Hao CK, Xiaowei Z. Multicolor super-resolution fluorescence imaging via multi-parameter fluorophore detection. Chemphyschem. 2012;**13**:99-107. DOI: 10.1002/cphc.201100735

[6] Goud TV, Tutar A, Biellmann J-F. Synthesis of 8-heteroatom-substituted 4,4-difluoro-4-bora-3a,4a-diaza-s-indacene dyes (BODIPY). Tetrahedron. 2006;**62**:5084-5091. DOI: 10.1016/j.tet.2006.03.036

[7] Gomez-Duran CFA, Garcia-Moreno I, Costela A, Martin V, Sastre R, Banuelos J, et al. 8-PropargylaminoBODIPY: Unprecedented blue-emitting pyrromethene dye. Synthesis,

photophysics and laser properties. Chemical Communications. 2010;**46**:5103-5105. DOI: 10.1039/C0CC00397B

[8] Jorge B, Virginia M, Azael G-DCF, Arroyo CIJ, Eduardo P-C, Inmaculada G-M, et al. New 8-Amino-BODIPY derivatives: Surpassing laser dyes at blue-edge wavelengths. Chemistry–A European Journal. 2011;**17**:7261-7270. DOI: 10.1002/chem.201003689

[9] Kim D, Yamamoto K, Ahn KH. A BODIPY-based reactive probe for ratiometric fluorescence sensing of mercury ions. Tetrahedron. 2012;**68**:5279-5282. DOI: 10.1016/j.tet.2012.01.091

[10] Ixone E, Arlette UB, Azael GDCF, Osorio-Martínez CA, Inmaculada GM, Angel C, et al. Reaction of amines with 8-MethylthioBODIPY: Dramatic optical and laser response to amine substitution. Chemistry, an Asian Journal. 2013;**8**:2691-2700. DOI: 10.1002/asia.201300760

[11] Ixone E, Ismael V-E, Gómez-Durán CFA, Arlette U-B, Betancourt-Mendiola ML, Iñigo L-A, et al. Blue-to-orange color-tunable laser emission from tailored boron-dipyrromethene dyes. Chemphyschem. 2013;**14**:4134-4142. DOI: 10.1002/cphc.201300818

[12] Boens N, Wang L, Leen V, Yuan P, Verbelen B, Dehaen W, et al. 8-HaloBODIPYs and their 8-(C, N, O, S) substituted analogues: Solvent dependent UV–Vis spectroscopy, variable temperature NMR, crystal structure determination, and quantum chemical calculations. The Journal of Physical Chemistry A. 2014;**118**:1576-1594. DOI: 10.1021/jp412132y

[13] Banuelos J, Arbeloa FL, Martinez V, Liras M, Costela A, Moreno IG, et al. Difluoro-boron-triaza-anthracene: A laser dye in the blue region. Theoretical simulation of alternative difluoro-boron-diaza-aromatic systems. Physical Chemistry Chemical Physics. 2011;**13**:3437-3445. DOI: 10.1039/C0CP01147A

[14] Osorio-Martínez CA, Urías-Benavides A, Gómez-Durán CFA, Bañuelos J, Esnal I, López Arbeloa I, et al. 8-AminoBODIPYs: Cyanines or hemicyanines? The effect of the coplanarity of the amino group on their optical properties. The Journal of Organic Chemistry. 2012;**77**:5434-5438. DOI: 10.1021/jo300724m

[15] Wang Y, Pan F, Zhang Y, Peng F, Huang Z, Zhang W, et al. A dual-mode turn-on fluorescent BODIPY-based probe for visualization of mercury ions in living cells. Analyst. 2016;**141**:4789-4795. DOI: 10.1039/C6AN00371K

[16] Flores-Rizo JO, Esnal I, Osorio-Martínez CA, Gómez-Durán CFA, Bañuelos J, López Arbeloa I, et al. 8-Alkoxy- and 8-Aryloxy-BODIPYs: Straightforward Fluorescent Tagging of Alcohols and Phenols. The Journal of Organic Chemistry. 2013;**78**:5867-5877. DOI: 10.1021/jo400417h

[17] Ravikanth M, Vellanki L, Sharma R. Functionalized boron-dipyrromethenes and their applications. Reports in Organic Chemistry. 2016;**6**:1-24. DOI: 10.2147/ROC.S60504

[18] Zhang G, Zheng S, Liu H, Chen PR. Illuminating biological processes through site-specific protein labeling. Chemical Society Reviews. 2015;**44**:3405-3417. DOI: 10.1039/C4CS00393D

[19] Kris G, Francis I, Bart G, Petra VD, Anja L, Joël V. Stable isotopic labeling in proteomics. Proteomics. 2008;**8**:4873-4885. DOI: 10.1002/pmic.200800421

[20] Grabowski ZR, Rotkiewicz K, Rettig W. Structural changes accompanying intramolecular electron transfer: Focus on twisted intramolecular charge-transfer states and structures. Chemical Reviews. 2003;**103**:3899-4032. DOI: 10.1021/cr940745l

[21] Kim D, Cho SW, Jun YW, Ahn KH. Fluorescent labeling of lysine residues in protein using 8-thiomethyl-BODIPY. Bulletin of the Korean Chemical Society. 2017;**38**:995-996. DOI: 10.1002/bkcs.11213

[22] Kim D, Ma D, Kim M, Jung Y, Kim NH, Lee C, et al. Fluorescent labeling of protein using blue-emitting 8-Amino-BODIPY derivatives. Journal of Fluorescence. 2017;**27**:2231-2238. DOI: 10.1007/s10895-017-2164-5

[23] Alamudi SH, Su D, Lee KJ, Lee JY, Belmonte-Vazquez JL, Park H-S, et al. A palette of background-free tame fluorescent probes for intracellular multi-color labelling in live cells. Chemical Science. 2018;**9**:2376-2383. DOI: 10.1039/C7SC04716A

[24] Jewett JC, Bertozzi CR. Cu-free click cycloaddition reactions in chemical biology. Chemical Society Reviews. 2010;**39**:1272-1279. DOI: 10.1039/B901970G

[25] Chan J, Dodani SC, Chang CJ. Reaction-based small-molecule fluorescent probes for chemoselective bioimaging. Nature Chemistry. 2012;**4**:973. DOI: 10.1038/nchem.1500

[26] Guo Z, Park S, Yoon J, Shin I. Recent progress in the development of near-infrared fluorescent probes for bioimaging applications. Chemical Society Reviews. 2014;**43**:16-29. DOI: 10.1039/C3CS60271K

[27] Gao M, Yu F, Lv C, Choo J, Chen L. Fluorescent chemical probes for accurate tumor diagnosis and targeting therapy. Chemical Society Reviews. 2017;**46**:2237-2271. DOI: 10.1039/C6CS00908E

[28] Wu D, Sedgwick AC, Gunnlaugsson T, Akkaya EU, Yoon J, James TD. Fluorescent chemosensors: The past, present and future. Chemical Society Reviews. 2017;**46**:7105-7123. DOI: 10.1039/C7CS00240H

[29] Kim HN, Ren WX, Kim JS, Yoon J. Fluorescent and colorimetric sensors for detection of lead, cadmium, and mercury ions. Chemical Society Reviews. 2012;**41**:3210-3244. DOI: 10.1039/C1CS15245A

[30] Costero AM, Betancourt-Mendiola ML, Gaviña P, Ochando LE, Gil S, Chulvi K, et al. Structure and conformational studies of Aza-Crown 8-Amino-BODIPY derivatives: Influence of steric hindrance on their photophysical properties. European Journal of Organic Chemistry. 2017;**42**:6283-6290. DOI: 10.1002/ejoc.201701016

[31] Jung HS, Chen X, Kim JS, Yoon J. Recent progress in luminescent and colorimetric chemosensors for detection of thiols. Chemical Society Reviews. 2013;**42**:6019-6031. DOI: 10.1039/C3CS60024F

[32] Ma DH, Kim D, Seo E, Lee S-J, Ahn KH. Ratiometric fluorescence detection of cysteine and homocysteine with a BODIPY dye by mimicking the native chemical ligation. Analyst. 2015;**140**:422-427. DOI: 10.1039/C4AN01791A

[33] Hee MD, Dokyoung K, Takuya A, Kyung-Ha L, Kyong-Tai K, Han AK. An FITC-BODIPY FRET couple: Application to selective, ratiometric detection and bioimaging of cysteine. Chemistry, an Asian Journal. 2015;**10**:894-902. DOI: 10.1002/asia.201403073

[34] Sambrook MR, Notman S. Supramolecular chemistry and chemical warfare agents: From fundamentals of recognition to catalysis and sensing. Chemical Society Reviews. 2013;**42**: 9251-9267. DOI: 10.1039/C3CS60230C

[35] Li W, Pauluhn J. Phosgene-induced acute lung injury (ALI): Differences from chlorine-induced ALI and attempts to translate toxicology to clinical medicine. Clinical and Translational Medicine. 2017;**6**:19. DOI: 10.1186/s40169-017-0149-2

[36] Jianhua C, Dongyang L, Shenghua L, Ying T, Jun Y. Recent advances in phosgene and nerve agents responsive fluorescent probes. Chinese Journal of Applied Chemistry. 2017; **34**:1413-1432. DOI: 10.11944/j.issn.1000-0518.2017.12.170309

[37] Zhang Y, Peng A, Jie X, Lv Y, Wang X, Tian Z. A BODIPY-based fluorescent probe for detection of subnanomolar phosgene with rapid response and high selectivity. ACS Applied Materials & Interfaces. 2017;**9**:13920-13927. DOI: 10.1021/acsami.7b02013

[38] Xia H-C, Xu X-H, Song Q-H. BODIPY-based fluorescent sensor for the recognization of phosgene in solutions and in gas phase. Analytical Chemistry. 2017;**89**:4192-4197. DOI: 10.1021/acs.analchem.7b00203

[39] Sören D, Hannes N, Markus S. Fluorescence quenching by photoinduced electron transfer: A reporter for conformational dynamics of macromolecules. Chemphyschem. 2009;**10**: 1389-1398. DOI: 10.1002/cphc.200900238

[40] Yang Z, Cao J, He Y, Yang JH, Kim T, Peng X, et al. Macro-/micro-environment-sensitive chemosensing and biological imaging. Chemical Society Reviews. 2014;**43**:4563-4601. DOI: 10.1039/C4CS00051J

[41] Demchenko AP, Mély Y, Duportail G, Klymchenko AS. Monitoring biophysical properties of lipid membranes by environment-sensitive fluorescent probes. Biophysical Journal. 2009;**96**:3461-3470. DOI: 10.1016/j.bpj.2009.02.012

[42] Bacalum M, Wang L, Boodts S, Yuan P, Leen V, Smisdom N, et al. A blue-light-emitting BODIPY probe for lipid membranes. Langmuir. 2016;**32**:3495-3505. DOI: 10.1021/acs.langmuir.6b00478

Chapter 4

Redox Chemistry of BODIPY Dyes

Brena L. Thompson and Zachariah Heiden

Additional information is available at the end of the chapter

http://dx.doi.org/10.5772/intechopen.79704

Abstract

The implementation of BODIPY dyes in electron transfer reactions is an exciting new frontier that expands the toolbox of the dye molecule that has primarily been implemented in biological and chemical sensing applications. BODIPY dyes are capable of reversible reductions at the average reduction potential of −1.53 V vs. ferrocene/ferrocenium, varying about 700 mV from this average value depending on the substitution of the BODIPY core. BODIPY dyes are also capable of reversible oxidations, exhibiting an average oxidation potential of 610 mV with the ability to manipulate the oxidation potential up to 600 mV from the average potential. The respective azaBODIPY dyes are on average about 600 mV easier to reduce (more positive potentials) and are oxidized at almost identical oxidation potentials to the respective BODIPY dyes. The oxidation and reduction potentials of BODIPY dyes are heavily dependent on substitution of the BODIPY core, which allows for a high degree of tunability in the redox potentials. This characteristic makes BODIPY dye molecules good candidates for use as photoredox catalysts, redox flow batteries, redox-active ligands, light harvesting antenna, and many other applications in materials science, biology, and chemical synthesis.

Keywords: BODIPY, redox, oxidation, reduction, chemiluminescence, photoredox, electron transfer, electrochemistry

1. Introduction

Electron transfer reactions, oxidations (removal of an electron) and reductions (addition of an electron), are involved in energy conversion processes, analytical methods, synthetic procedures, and even data processing systems. With the advent of new energy sources, the search for new chemical redox reagents is at the forefront of energy research. With many chemical

redox reagents consisting of metallocene or quinone fragments, the search for new redox platforms exhibiting unique redox characteristics and are amenable to tunable redox potentials is at the cutting edge of electron transfer research.

Fluorescent dyes have been widely utilized as chemical sensors, laser dyes, and in therapeutic applications, but exploitation of their redox-active nature in chemical and electron transfer reactions has remained mostly unexplored. Fluorescent dyes are attractive substrates for introducing redox capabilities, as their fluorescent nature demonstrates their capability of redox behavior [1]. Two dye molecules that have been of recent interest due to their electrochemical behavior is 4,4-difluoro-4-bora-3a,4a-diaza-s-indacene (BODIPY) and the related 4,4-difluoro-4-bora-3a,4a,8-triaza-s-indacene (azaBODIPY) (**Figure 1**) [2]. BODIPY and azaBODIPY molecules are attractive as redox fragments for the incorporation into molecular scaffolds, as the BODIPY and azaBODIPY cores can be readily synthesized and incorporated into molecular frameworks [3]. For example, diamines have been employed in many biological and catalytic applications, but the incorporation of additional functionality (e.g. redox behavior) into the diamine scaffold could open up additional chemical reactivity not previously accessible. One and two BODIPY fragments have been incorporated into a diamine scaffold, resulting in a complex that exhibits one and two redox events, respectively [4].

One of the appealing characteristics of BODIPY compounds is their tunable electrochemical properties. Substitution at different positions effects the electronic environment surrounding the BODIPY core (**Figure 1**), causing characteristic changes to the oxidation and reduction potentials [2]. Upon examination of the BODIPY and azaBODIPY scaffolds, a conjugated system is observed, suggesting some degree of aromatic character. Using a NICS(0) calculation to investigate the degree of aromaticity of the BODIPY and azaBODIPY core, the parent-BODIPY dye is seen to exhibit greater aromatic character than the parent-azaBODIPY dye. Given the aromatic nature of a BODIPY molecule, the BODIPY core can act as an electron-withdrawing substituent. Appending an amino group to the 8-position of the BODIPY core has been shown to result in an amine that is more electron deficient than if appended to a pentafluorophenyl or a tosyl group [4]. The electron deficient nature of BODIPY dyes suggest that the BODIPY core could be susceptible to the addition of electrons. In addition to BODIPY dyes being susceptible to reductions, BODIPY dyes are also capable of undergoing oxidation reactions. This chapter will discuss the recent advances of BODIPY dyes as chemical redox agents in reductions, oxidations, and photopromoted reactions. The ability to manipulate BODIPY dyes to tune the redox potential of these dye molecules will also be discussed. To simplify comparisons

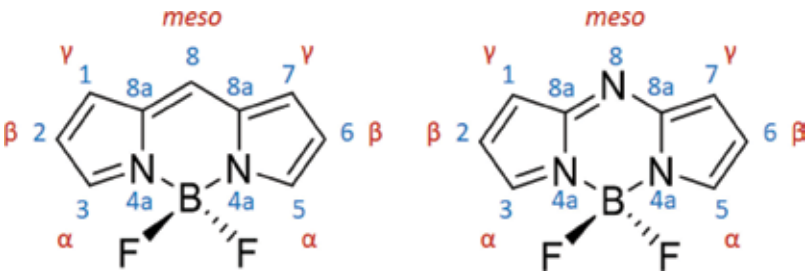

Figure 1. Numbering system for describing the substitution of (left) BODIPY and (right) azaBODIPY cores.

http://dx.doi.org/10.5772/intechopen.79704

between BODIPY molecules, all redox potentials described within are referenced to the ferrocene/ferrocenium couple (Cp_2Fe/Cp_2Fe^+, where Cp = η^5-cyclopentadienyl). To convert a redox potential described vs. Cp_2Fe/Cp_2Fe^+ to NHE (normal hydrogen electrode), SCE (saturated calomel electrode), Ag/Ag^+, or Pt/Pt^+ reference electrodes, +0.270 V, +0.424 V, +0.469 V, or + 1.069 V, respectively, can be added to the redox potential described vs. Cp_2Fe/Cp_2Fe^+.

2. Reduction of BODIPY and azaBODIPY dyes

The electron deficient nature of the BODIPY core makes the dye molecule an attractive electron acceptor in electron transfer reactions. The reduction potential of a BODIPY core can be manipulated by almost 1.40 V, ranging from a potential as reducing as −2.40 V to a potential as moderate as −0.35 V vs. Cp_2Fe/Cp_2Fe^+. Although the reduction potentials can span a large range, depending on the substitution of the BODIPY core, the average reduction potential of a BODIPY core resides at −1.53 V vs. Cp_2Fe/Cp_2Fe^+, with about 2/3 of the reported BODIPY molecules exhibiting a reduction potential within 460 mV of the average value.

Using unpaired spin density plots of the reduced parent-BODIPY and reduced parent-azaBODIPY molecules, the likely location of the added electron can be determined (**Figure 2**). Using the M06-2X/6-31G(d,p) level of theory, an unpaired spin density plot of a reduced parent-BODIPY molecule revealed 32% of the electron density resided in the 8-position, about 24% of the electron density resided in the 1,7-positions (12% each), and about 16% of the electron density resided in the 3,5-positions (8% each). Only about 2% of the unpaired spin density resided in each of the 2,6-positions of the BODIPY dye. About 3% of the unpaired spin density resided in each of the nitrogen centers, and about 7% resided in each of the carbon atoms in the 8a-position (between the 1,7-positions and the 8-position). Surprisingly, the most electronegative atoms, boron and fluorine, contained negligible spin density.

Although the 8-position of the reduced parent-azaBODIPY contained the largest unpaired spin density (**Figure 2**), the 8-position of the reduced azaBODIPY contained about 6% less unpaired spin density than the reduced parent-BODIPY molecule. Where there was a reduction in the spin density in the 8-position of the reduced parent-azaBODIPY molecule, when

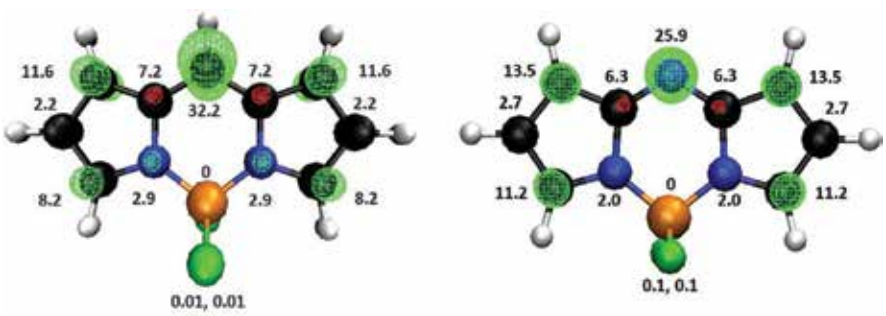

Figure 2. Unpaired spin density plots of the reduced (left) parent-BODIPY and (right) parent-azaBODIPY molecules. Isovalue = 0.01 e^-/a.u. The numbers indicate the percent of unpaired spin density present on each atom.

compared to the reduced parent-BODIPY dye, there was an increase of about 2 and 3% in the unpaired spin density at the 1,7- and 3,5-positions, respectively. As with the reduced parent-BODIPY dye, a negligible unpaired spin density resided on the boron and fluorine atoms.

Analysis of bond lengths and bond orders upon reduction of a BODIPY and azaBODIPY core revealed an increase in aromaticity of the BODIPY and azaBODIPY core (**Figure 3**). The increase in aromaticity was further verified by Wiberg bond index analysis, where bond orders of the BODIPY core become more alike in the reduced BODIPY and azaBODIPY dyes than in the parent compounds. Upon reduction, lengthening of the bonds between the 1,7- and 2,6-positions and the 3,5- and 4a-positions occurred. A contraction of the bonds between the 1,7- and 8a-positions and the 2,6 and 3,5-positions also resulted from the reduction of the parent-BODIPY dye. The greatest changes in bond distance occurred between the 8- and 8a-positions (+0.03 Å) and between the 2,6- and 3,5-postions (−0.03 Å). Analysis of the Mulliken charges of the reduced BODIPY core revealed that the carbon center residing in the 8-position contained most of the anionic charge. In contrast to the reduced BODIPY dye, the reduced azaBODIPY dye contained most of the negative charge on the carbon centers residing in the 8a positions (between the 1,7 and 8-position of the azaBODIPY core). The nitrogen atom in the 8-position of the reduced azaBODIPY actually exhibited less of a negative charge than the other two nitrogen atoms.

To analyze the influence of substitution on the unpaired spin density of a reduced BODIPY or azaBODIPY dye, the presence of methyl, phenyl, or chloride substituents on the reduction potential and unpaired spin density was investigated. Incorporation of a phenyl substituent in the 1- or 2-position of a BODIPY or azaBODIPY core resulted in a 2% lower spin density in the 5-position than in the 3-position. A phenyl substituent in the 1-position also resulted in a 3% decrease in spin density in the 8-position. Phenyl substitution in the 8-position of a BODIPY dye resulted in a 6% decrease in unpaired spin density in the 8-position. Methyl and chloride substitution had a minimal effect on the unpaired spin density of the BODIPY and azaBODIPY core, where no changes beyond a 1% difference occurred. The presence of a methyl substituent generated a BODIPY dye that was about 100–150 mV more difficult to reduce (more negative

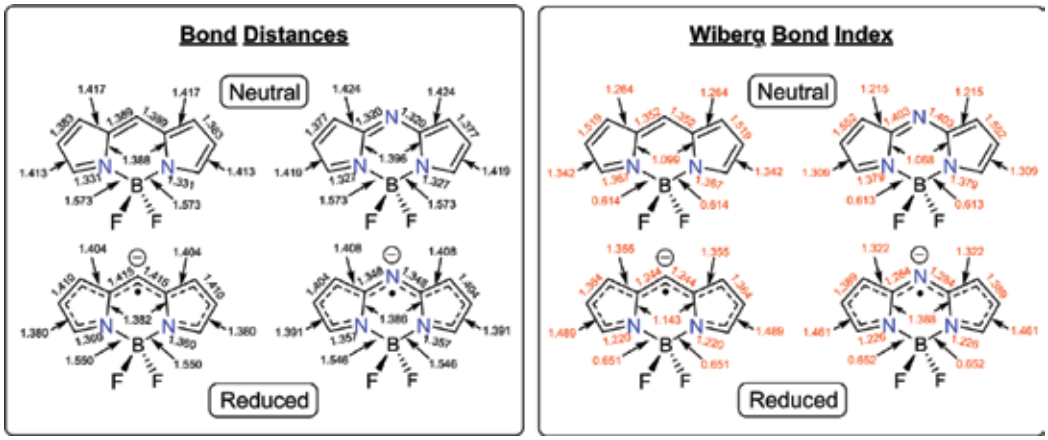

Figure 3. Lists of computed bond distances (black, Å) and Wiberg bond indices (red) for the (top) parent-BODIPY and parent-azaBODIPY cores and the (bottom) reduced parent-BODIPY and parent-azaBODIPYcore.

http://dx.doi.org/10.5772/intechopen.79704

potentials). Investigation of the influence of substitution on the reduction potential of a BODIPY dye, revealed that substitution in the 3-postion resulted in the most negative reduction potential, followed by the 8-position, 1-position, and the 2-position. Similar results were obtained for the reduction of a substituted azaBODIPY dye. The reverse trend is observed for the stabilization of the LUMO (easiest to reduce), where substitution in the 2-position resulted in the lowest energy LUMO, demonstrating a correlation between the LUMO energy and reduction potential. Substituents consisting of electron-withdrawing groups lower the LUMO energy of the BODIPY and azaBODIPY core, resulting in dye molecules that are reduced at milder (more positive) potentials. The opposite trend occurs for substitution of a BODIPY and azaBODIPY core with electron-donating groups.

Analysis of the reduction potentials of substituted azaBODIPY and BODIPY dyes revealed the reduction potential of azaBODIPY dyes were on average about 600 mV easier to reduce (more positive potentials) than the respective BODIPY dyes. The increased ability to reduce an azaBODIPY dye when compared to the respective BODIPY dye is attributed to the reduced azaBODIPY dye gaining a greater degree of aromaticity than a BODIPY dye upon reduction. Connecting the reduction potentials to the molecular orbitals of the parent BODIPY and azaBODIPY dyes revealed a linear correlation between the LUMO energy and the reduction potential. The milder reduction potentials for azaBODIPY dyes is also attributed to the energy of the LUMO which is about 12 kcal lower (easier to oxidize) in energy than the respective BODIPY dye.

From the computational analysis of the unpaired spin density plots, substitution at the 8-position would suggest the greatest influence in the reduction potential and stabilization of the reduced BODIPY dye. Electrochemical analysis of substitution of the parent-BODIPY dye with a phenyl, chloride, methanesulfide, amide, and diethylamide substituent in the 8-position resulted in an ability to shift the reduction potential by 600 mV (**Figure 4**). Substituted electron acceptors in the 8-position resulted in the greatest stabilization of the radical anion

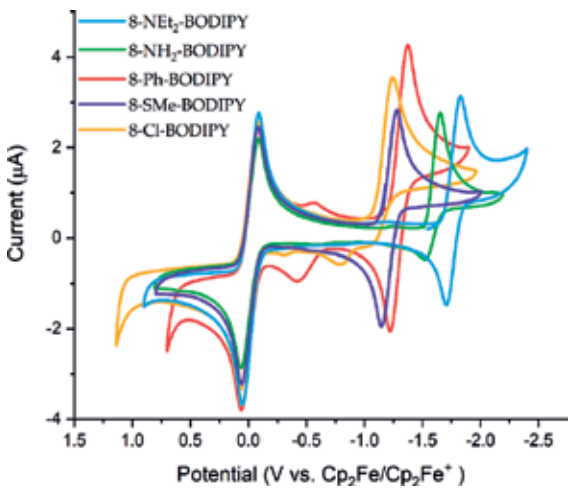

Figure 4. Stacked cyclic voltammograms of 8-SMe-BODIPY, 8-Cl-BODIPY, 8-Ph-BODIPY, 8-NH_2-BODIPY, and 8-NEt_2-BODIPY in dichloromethane. Scan rate = 100 mV/s and electrolyte = Bu_4NPF_6. The wave at 0 V is attributed to the ferrocene internal standard.

from the reduction of a BODIPY or azaBODIPY core (more reversible reduction waves) [5]. Bard and coworkers have shown that the inductive electron-withdrawing effect of a cyanide substituent in the 8-position results in an easier reduction by about 300 mV, when compared to a methylated-BODIPY. However, introduction of a more electron-donating group, such as diethylamine, results in the opposite effect [6]. Lack of the substitution in the 8-position causes for a reduced BODIPY core to be a more reactive/less stable radical anion [5]. Substitution at the 8-position of a BODIPY core can stabilize a radical anion, but substituents bearing an acidic proton residing near the 8-position, such as carboxylic acids, can result in electrophilic attack on the radical center by the acidic proton upon reduction [5].

Although no unpaired spin density resides on the boron or fluorine atoms in the reduced BODIPY or azaBODIPY dyes, substitution at the boron center also influences the reduction potential of a BODIPY core. Substituting one or both fluorine atoms with fused benzene rings, catecholate groups, or alkynyl moieties does not affect the stability of the radical anion or cation [5]. However, substitution at the boron center introduces more electron density into the system as the electron-withdrawing fluorine's are removed, disfavoring reduction of the BODIPY core. Substitution on the boron center increases the energy of both the HOMO and the LUMO, with a larger change occurring for the LUMO, resulting in a larger separation between reduction and oxidation waves when compared to the respective BF_2-containing BODIPY dyes.

Heiden and coworkers have recently described the redox properties of diamines containing one and two BODIPY molecules [4]. The redox-active behavior of the BODIPY fluorophores is showcased with the presence of quasi-reversible and irreversible redox events, in relation to the free diamines. All of the BODIPY-containing diamines exhibit either quasi-reversible or irreversible reductions between the range of −0.82 V to −1.95 V (**Table 1**). The incorporation of two BODIPY fragments into the diamine scaffold resulted in two separate reduction events, with a separation of about 100 mV. BODIPY-appended diamines derived from electron deficient diamines (e.g. ortho-phenylenediamine) resulted in milder reduction potentials than more electron rich diamines (e.g. trans-1,2-diaminocyclohexane or ethylenediamine).

Diamine	E° potential (V)
One BODIPY	
Ethylenediamine	−1.89
Phenylenediamine	−1.70
Diaminocyclohexane	−1.86
Diphenylethylenediamine	−1.80
Two BODIPYs	
Ethylenediamine	−1.85, −1.95
Phenylenediamine	0.82, −1.26, −1.35
Diaminocyclohexane	−1.74, −1.89
Diphenylethylenediamine	−1.67, −1.80

Table 1. Redox potentials for BODIPY-appended diamines.

http://dx.doi.org/10.5772/intechopen.79704

Although there are several examples of reductions of BODIPY molecules, the reductions are often undertaken *in situ*, without isolation of the reduction product. A reduced BODIPY molecule with an appended 1,1,3,3-tetramethylguanidine fragment (BoTMG) has been recently reported by Heiden and coworkers [7]. Electrochemical analysis of acetonitrile solutions of BoTMG revealed a reversible reduction at −1.86 V vs. Cp_2Fe/Cp_2Fe^+. The reduced BoTMG was isolated by reducing BoTMG with 1.5 equivalents KC_8 in the presence of one equivalent 18-crown-6. 18-crown-6 was employed to coordinate the potassium cation to aid in solubility of the reduced BoTMG. Although the resulting red solution/solid exhibited a 15 nm hypsochromic shift when compared with the absorbance spectrum of BoTMG, the solution did not fluoresce under UV light. The presence of an unpaired electron was verified by EPR spectroscopy (g value = 2.00289; **Figure 5**). Crystallographic analysis of the reduction of BoTMG revealed the presence of an anionic BoTMG molecule with the fluorine atoms of the BODIPY residing 2.627(1) and 3.181(1) Å away from the potassium ion (**Figure 5**). The potassium ion resided within the 18-crown-6 and also exhibited a coordinated THF molecule 2.816(1) Å away (**Figure 5**), yielding an overall formula of [K(18-crown-6)(THF)][BoTMG]. The $[BoTMG]^-$ fragment showed a lengthening of the C(2)—C(3) and the C(7)—C(8) bonds by about 0.03 Å, suggesting a greater degree of single-bond character, when compared to the neutral BoTMG. The N(3)—C(5) bond length increased by about 0.09 Å and the N(3)—C(10) shortened by about 0.06 Å upon reduction of BoTMG. From the bond distances and the unpaired spin density plot of $[BoTMG]^-$ (**Figure 5**), the free electron resides primarily on C(5). The reduced BoTMG was reported to be stable in acetonitrile, THF, benzene, and fluorobenzene, reacting with halogenated and protic solvents.

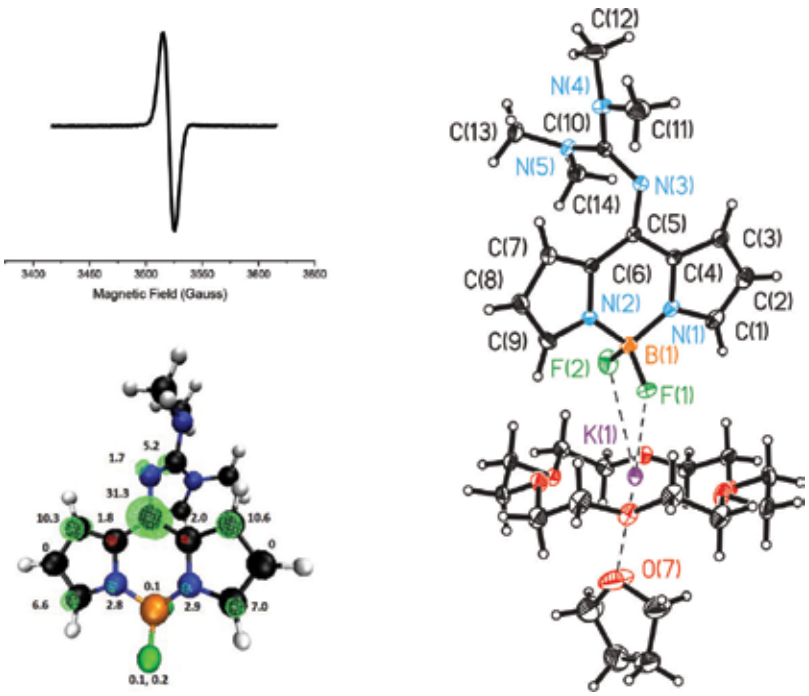

Figure 5. (top left) EPR spectrum of [K(THF)(18-crown-6)][BoTMG], (bottom left) unpaired spin density plot (isovalue = 0.01 e^-/a.u.) for $[BoTMG]^-$, and (right) molecular structure of [K(THF)(18-crown-6)][BoTMG]. Thermal ellipsoids are drawn at 50% probability.

Other redox agents have been appended to BODIPY cores. Cosa and coworkers have incorporated an ubiquinone fragment into a BODIPY core at the 3-position, resulting in +50 and +430 mV shifts in the reduction potential of the ubiquinone fragment, respectively [8]. The more positive shift of the second reduction is proposed to be stabilized via resonance through the BODIPY core. In a related study, Misra and coworkers have described the influence of appending a BODIPY core to each of the nitrogen centers of phenylenediamine and to each of the oxygen centers of phenylenediols [9]. Appending two BODIPYs to para-phenylenediol resulted in a slightly more favorable reduction than the meta- or ortho-substituted phenylenediol, respectively. In the case of two BODIPY cores appended to a phenylenediamine, the meta-substituted complex exhibited the mildest reduction potentials, followed by the para- and ortho-substituted phenylenediamine, respectively.

3. Oxidation of BODIPY and azaBODIPY dyes

Although BODIPY dyes are prone to reductions, many also are capable of undergoing oxidations. The oxidation potential of a BODIPY core can be manipulated by about 1.3 V, ranging from a potential as high as 1.55 V to a potential as low as 0.18 V vs. Cp_2Fe/Cp_2Fe^+. Although the oxidation potentials can vary a large potential range, depending on the substitution of the BODIPY core, the average reduction potential of a BODIPY core resides at 610 mV vs. Cp_2Fe/Cp_2Fe^+, with about 2/3 of the reported BODIPY molecules exhibiting a reduction potential about 330 mV from the average value.

An unpaired spin density plot of an oxidized parent-BODIPY molecule (**Figure 6**) revealed 18% of the electron density resided on the 8a-positions. About 13% of the electron density resided in each of the 3,5-positions, and about 12% of the electron density resided in the 8-position. Only about 6% of the unpaired spin density resided in each of the 2,6-positions of the BODIPY dye. About 4% of the unpaired spin density resided in each of the nitrogen centers (4a-position). As seen with the unpaired spin density plots for the reduced parent-BODIPY dye, the most electronegative atoms, boron and fluorine, contained negligible spin density

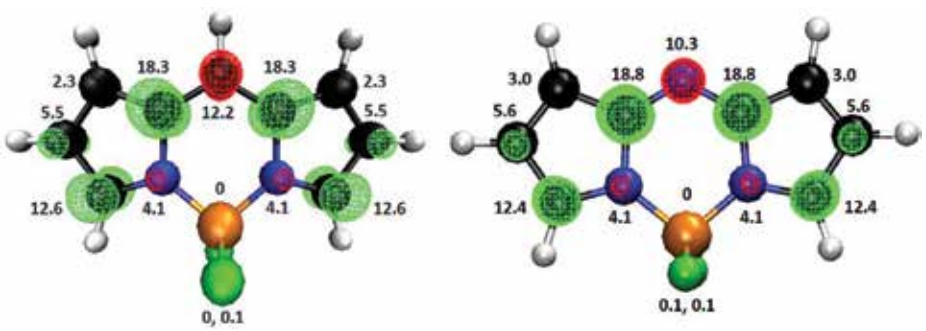

Figure 6. Unpaired spin density plots of the oxidized (left) parent BODIPY and (right) parent-azaBODIPY dyes. Isovalue = 0.01 e^-/a.u. The numbers indicate the percent of unpaired spin density present on each atom.

in the oxidized parent-BODIPY dye. Whereas there were measureable differences between the unpaired spin densities for the reduced parent-BODIPY dye and the reduced parent-aza-BODIPY, the unpaired spin densities observed for the oxidized parent-azaBODIPY dye were almost identical to the unpaired spin densities for the oxidized parent-BODIPY dye (**Figure 6**).

Analysis of the bond distance and bond order changes of a BODIPY and an azaBODIPY core revealed a decrease in aromaticity upon oxidation (**Figure 7**). Upon oxidation, contractions of the bonds between the 1,7- and 2,6-positions, the 8- and 8a-positions, and the 3,5- and 4a-positions resulted. Lengthening of the bonds between the 1,7 and 8a-positions and the 2,6 and 3,5-positions also occurred upon oxidation. Using Mulliken charge analysis, the location of the greatest positive charge of the oxidized parent-BODIPY and parent-azaBODIPY dyes resided on the carbon atoms in the 1,7-positions.

Analysis of the oxidation potentials of substituted azaBODIPY and BODIPY dyes revealed that the oxidation potential of azaBODIPY dyes were on average about 20 mV easier to oxidize (more negative potentials) than the respective BODIPY dyes [10]. The small difference in oxidation potentials between azaBODIPY and BODIPY dyes is attributed to the similarity in changes in aromaticity upon oxidation. A NICS(0) calculation of the parent-azaBODIPY and BODIPY dyes showed almost an identical change in aromaticity upon oxidation, with the azaBODIPY dye exhibiting a slightly smaller change in aromaticity upon oxidation. The slightly reduced change in aromaticity of the azaBODIPY dye is attributed to its ability to be oxidized slightly more readily than the parent-BODIPY dye. Molecular orbital analysis also revealed a linear correlation between the HOMO energy and the oxidation potential of the BODIPY and azaBODIPY dye. The slightly more favorable oxidation of an azaBODIPY is also attributed to the HOMO energy of the azaBODIPY dye being on average 2.8 kcal lower (more easily oxidized) than the respective BODIPY dye.

Substitution of the BODIPY or azaBODIPY core can also influence the oxidation potential. Substitution in the 2-position of a BODIPY and azaBODIPY dye resulted in a large difference in unpaired spin density for the oxidized BODIPY. In the case of phenyl substitution in the

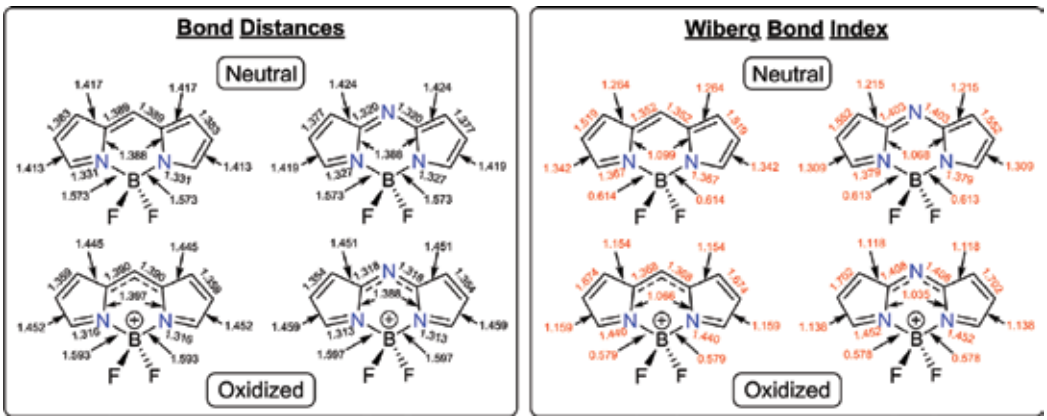

Figure 7. Lists of computed bond distances (black, Å) and Wiberg bond indices (red) for the (top) parent-BODIPY and parent-azaBODIPY cores and the (bottom) oxidized parent-BODIPY and parent-azaBODIPY core.

2-position or 3-position, a 10% difference in unpaired spin density was observed between the 2- and 6-positions and the 3- and 5-positions of the oxidized BODIPY core. A similar result was observed for methyl and chloride substitution at the 2- or 3-positions, but to a lesser extent (3–4% instead of 10%). Substitution at the 3-position resulted in the least positive oxidation potential, followed by the 2-, 1-, and 8-positions. Similar results were obtained for the oxidation of a substituted azaBODIPY dye. Where substitution in the 3-postion resulted in the most positive oxidation potential, the highest energy HOMO was also observed. A direct correlation between the energy of the HOMO and oxidation potential resulted. Substituents consisting of electron-withdrawing groups resulted in lower energy HOMO energies and higher (more positive) oxidation potentials. The opposite trend is observed for substitution of a BODIPY and azaBODIPY core with electron-donating groups.

Further verifying the computational results, Cosa and coworkers have shown that the introduction of a cyanide group in the 2-position of a BODIPY dye results in a more difficult oxidation by 400 mV, with no influence on the reversibility of the reduction. The addition of a second cyanide, in the 6-position, shifts the oxidation potential to a more positive value by an additional +200 mV (more difficult to oxidize), but the reduction of the BODIPY dye is no longer reversible [11]. Whereas the incorporation of a cyanide in the 2,6-positions of the BODIPY core can shift the oxidation potential by +400 and +200 mV, the incorporation of a chloride in the 2,6-positions increases the oxidation potential by +200 mV (more difficult to oxidize) with each substitution.

An additional method to generate a BODIPY dye capable of undergoing an oxidation is to incorporate a ferrocene fragment. Li and coworkers have incorporated two ferrocenyl fragments in the 3,5-positions through a vinyl linker [12]. The resulting ferrocenyl BODIPY complex exhibits a reversible reduction at −1.49 V and a reversible oxidation at 0.51 V that are BODIPY-based. The ferrocene-based oxidations occur at −0.01 V, where a single two electron oxidation is observed for scan rates greater than 50 mV/s. Bulk electrolysis at 0.21 V resulted in a color change from blue to purple. The color change is attributed to the oxidation of both of the ferrocenyl fragments, as evidenced by the adsorption band of the BODIPY core remaining unchanged and the loss of the adsorption at 700 nm and growth of the adsorption at 600 nm. Ravikanth and coworkers have examined the influence of placing a ferrocene and an ethynyl-ferrocene fragment in different locations on a BODIPY-core [13]. Introduction of a ferrocenyl fragment generated reversible ferrocene-based oxidations 230–360 mV more positive than free ferrocene, irreversible BODIPY-based oxidations 990–1190 mV more positive than free ferrocene, and reversible BODIPY-based reductions 1010–1110 mV more negative than free ferrocene. Similar results have been observed by several other groups that have incorporated ferrocene fragments into BODIPY cores [14–18]. Although incorporation of a ferrocenyl fragment into a BODIPY dye can introduce an additional oxidation wave, the reduction of the BODIPY dye is nearly unaffected by the presence of ferrocene moieties, which is primarily due to the added electron residing on the BODIPY core [19]. The separation of the oxidation potentials of multiple ferrocene-appended BODIPY dyes largely depends on the interactions between the two ferrocene moieties. Non-interacting redox centers normally display a difference of 35 mV between their redox potentials [20]. If a small splitting is observed between the two oxidation waves associated with the ferrocene oxidations, then the difference in oxidation potentials is attributed to electrostatic effects [18]. Although small separations between the ferrocene oxidations are

often observed, Kovtun and coworkers have shown that the implementation of a non-coordinating electrolyte did not change the reversibility of redox processes, but increased the separation between the first and second ferrocene oxidation waves from 250 mV ($[Bu_4N][ClO_4]$) to 340 mV($[Bu_4N][B(C_6F_5)_4]$) [21]. Examination of the influence of peripheral electron-donating or electron-withdrawing groups on a BODIPY core on the oxidation potential of an appended ferrocene fragment is quite small, often only shifting the potential by 30–60 mV. Although substitution of the BODIPY core weakly influences the oxidation potential of an appended ferrocene moiety, exposure to Lewis acidic cations can have a greater effect. Kaur and coworkers have shown that a +130 mV shift in the oxidation of the appended ferrocene and +80 mV shift in the BODIPY reduction results when a ferrocenyl-appended BODIPY is exposed to Hg^{2+} ions [22].

Plenio and coworkers have incorporated the BODIPY core into N-heterocyclic carbene scaffolds coordinated to iridium and rhodium centers for use in carbon monoxide detection. Plenio and coworkers have incorporated two different BODIPY cores into a N-heterocyclic carbene scaffold, where each of the BODIPY cores are connected to the carbene through a five carbon linker [23]. With the free BODIPY dyes having oxidation potentials of 0.90 and 1.01 V, coordination to an IrCl(COD) fragment, where COD = cis-cyclooctadiene, shifts the oxidation potentials to 0.92 and 1.02 V, respectively. Whereas coordination to an iridium center resulted in slightly more difficult oxidations of the BODIPY dyes, coordination to a RhCl(COD) fragment resulted in BODIPY dyes that were slightly easier to oxidize (0.89 and 1.00 V). As expected, the large distance between the appended-BODIPY dyes and metal centers results in very little influence of the metal center on the electrochemistry of the BODIPY dye.

4. Manipulating the redox chemistry of BODIPY dyes

The redox chemistry of a BODIPY and azaBODIPY core can be influenced through substitution of the BODIPY core. Computational analysis of the influence of substitution on the redox potential of the BODIPY fragment revealed that substitution in the 3,5-positions resulted in the highest energy HOMO and LUMO, but the smallest HOMO-LUMO gap. Substitution in the 3,5-positions of a BODIPY core resulted in the most negative reduction potentials. Complete alkylation of a BODIPY core exhibits one reversible one-electron oxidation and one reversible one-electron reduction, indicating the generation of stable radical ions. In aprotic solvents, radical stability correlates with electrochemical reversibility [2]. Absence of substitution in the 2-, 3-, 5-, or 6-positions destabilizes the radical cation produced upon oxidation. A similar destabilization is observed in the absence of substitution in the 1-, 3-, 5-, 7-, or 8-positions upon generation of a radical anion from a reduction.

Lack of substitution in the 3,5-positions of a BODIPY core results in a radical cation that is vulnerable to nucleophilic attack and is capable of dimerization. The rapid dimerization of radical BODIPY cations lacking substitution in 3,5-positions result in irreversible anodic waves in the cyclic voltammogram [5]. The presence of sterically bulky substituents at the 3,5-positions protect the radical cation from nucleophilic attack by a neutral BODIPY dye, leading to dimerization, or attack by surrounding solvent molecules, such as acetonitrile. Electron withdrawing substituents in the 3,5-positions may also induce a partial positive charge on the 2,6-positions, increasing the susceptibility for dimerization

at the 2,6-positions. When BODIPY cores lacking substitution in the 2,6-positions dimerize, the dimerized BODIPY dyes are often easier to oxidize than the original BODIPY dye. The increased ability to oxidize the BODIPY dimer over the original BODIPY dye can lead to the generation of oligomers of the BODIPY dye. Although dimerization of BODIPY dyes often occurs at BODIPY dyes lacking substitution, Heiland and coworkers have shown that 2,6-substituted BODIPY dyes are still prone to dimerization upon oxidation through the loss of a substituent [5]. The possibility of dimerization of a BODIPY dye can be investigated through the analysis of the reversibility of the oxidation wave as a function of scan rate. At faster scan rates, the oxidation processes exhibit increased reversibility due to the suppression of rate of dimer formation. Functionalization at the 1-, 7-, or 8-positions of a BODIPY dye do not influence the stability of the radical cation.

5. Use of redox to manipulate basicity of appended bases

The fact that BODIPY molecules are susceptible to reductions suggests that the BODIPY fragment can act as an electron-withdrawing group. Heiden and coworkers have found that the addition of an amine center to the BODIPY molecule in the 8-position does not result in Lewis acid-base adduct formation with strong Lewis acids (e.g. $B(C_6F_5)_3$). Further verifying this result, Akkaya and coworkers were able to show that a 1,7-bis(2-pyridyl)-2,5-diphenyl-azaBODIPY can be used as a near-IR sensor for Hg^{2+} ions [24]. Although this azaBODIPY can be utilized as a chemical sensor, 20 equivalents of the heavy metal is needed to see a response. Similar results have been observed by other research groups, where excess heavy metal ions are needed to show a fluorescent response [25–29]. The requirement of large amounts of Lewis acid to see a fluorescent response, suggests that azaBODIPY- and BODIPY-derived sensors act as a poor ligands for coordination to metal ions.

To counteract the strong electron-withdrawing nature of the BODIPY dye, Heiden and coworkers have shown that appending a 1,1,3,3-tetramethylguanidine fragment to a BODIPY molecule in the 8-position (BoTMG) results in a decrease of the basicity of the tetramethyl-guanidine fragment by 15 pK_a units. Protonation of the guanidinylated BODIPY, generating $[BoTMGH]^+$, resulted in a bathochromic shift by about 100 nm (45 nm in the emission) and a slight decrease in the quantum yield, from 0.17 to 0.13. In addition to influencing the photophysical properties, a shift of 870 mV to a more positive value was observed in the reduction peak upon protonation of the guanidine fragment. Further analysis of the electrochemical reactions, revealed the presence of an irreversible reduction peak at −0.99 V and a quasireversible reduction at −1.86 V. These results were attributed to the reduction of $[BoTMGH]^+$ at −0.99 V, which undergoes an electrochemical, followed by a chemical reaction leading to the unstable complex ([BoTMGH]), which decays into BoTMG through the transfer of H-atoms (H•). Although H_2 generation from the coupling of two H• was exergonic by 19.3 kcal/mol, no H_2 was observed experimentally. The absence of H_2 was further verified by electrochemical experiments, where the addition of 1, 2, 5, 10, and 20 equivalents of trifluoroacetic acid resulted in an increase in current at a potential of −1.19 V, but no current increase was observed after 20 equivalents of acid (**Figure 8**). To further investigate the influence of an added electron

http://dx.doi.org/10.5772/intechopen.79704

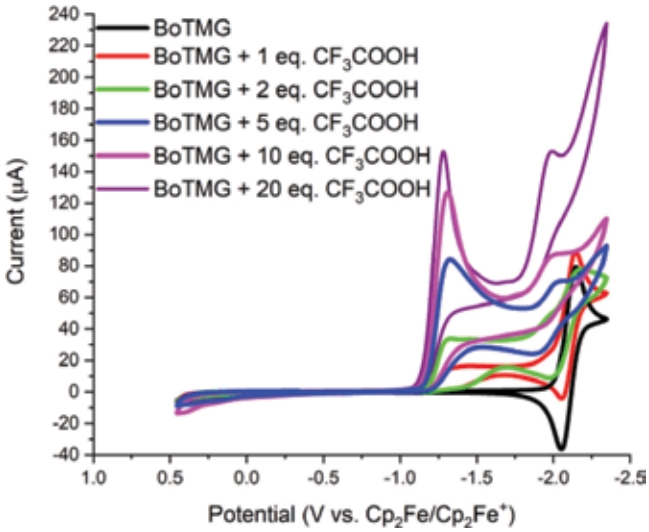

Figure 8. Cyclic voltammogram of an acetonitrile solution of BoTMG in the presence of 0–20 equivalents of trifluoroacetic acid (CF_3COOH). Electrolyte = Bu_4NPF_6 and scan rate = 50 mV/s.

to a BODIPY core on the basicity of the appended guanidine, the acidity of [BoTMGH] was measured experimentally to be 23.4 in MeCN. This result shows that by reducing the BODIPY core, the basicity of an appended amine can be increased by about 14 pK_a units.

6. Electrochemical chemiluminescence of BODIPY dyes

Recent investigations into the electrochemistry of BODIPY dyes has shown that many BODIPY dyes exhibit electrogenerated chemiluminescence (ECL). ECL occurs when radical anions and cations generated in an electrochemical experiment combine to generate an excited state, which emits light upon relaxation to the ground state (Eqs. (1)–(4)) [2]. ECL is a function of radical stability, where stable and long-lived singlet or triplet radicals, with high photoluminescent quantum yields, tend to produce bright ECL. BODIPY singlet lifetimes are in the nanosecond range, while triplet lifetimes are in the microsecond range. BODIPY cores lacking substitution in the 2,6-positions result in unstable radical cations, leading to low annihilation intensity upon reduction. Long wavelength ECL, above 700 nm, can be generated by the formation and annihilation of dimerized BODIPY cores [2, 30].

$$\text{BODIPY} + e^- \rightarrow \text{BODIPY}^{\bullet -} \quad (1)$$

$$\text{BODIPY} - e^- \rightarrow \text{BODIPY}^{\bullet +} \quad (2)$$

$$\text{BODIPY}^{\bullet -} + \text{BODIPY}^{\bullet +} \rightarrow 2\,\text{BODIPY}^{*} \quad (3)$$

$$\text{BODIPY}^{*} \rightarrow \text{BODIPY} + h\nu \quad (4)$$

ECL can be enhanced through the substitution of the BODIPY core. For example, Hesari and coworkers have successfully enhanced ECL in a BODIPY dye by appending an electron donating biphenyl carboxylic acid in the 8-position, and two styryl groups containing long alkyl chains in the 3,5-positions of the BODIPY core [31]. The biphenyl and styryl substituents increased intermolecular π-interactions, providing a feasible route for energy transfer. The 1,7-positions were substituted with methyl groups, to increase the stability of the electrogenerated radicals, and discourage dimerization. An ECL efficiency as high as 100% relative to $[Ru(bipyridine)_3]^{2+}$, where bpy = bipyridine, was observed [31]. In addition to a single BODIPY dye exhibiting ECL, bipyridine and thiolate-separated BODIPY dimers can produce ECL signals corresponding to the simultaneous transfer of two electrons to non-interacting BODIPY groups. The bipyridine and thiolate-separated BODIPY dimers exhibit substitution in the 2-, 3-, 5-, and 6-positions to increase radical stability [2]. BODIPY dyes lacking substitution in critical locations are vulnerable to dimerization, leading to multiple ECL signals. As reported by Bard and coworkers, upon comparison of two poly(ethylene glycol)-substituted BODIPY dyes, the BODIPY that did not exhibit enough steric bulk in the 3,5-positions resulted in two ECL signals while the other BODIPY resulted in only one ECL signal [6].

7. Photoredox chemistry with BODIPY dyes

The implementation of light to promote the conversion of difficult organic transformations has received increased interest from the organic community. The illumination of organic reactions utilizing a photoredox catalyst, a light-sensitive compound that mediates the transfer of electrons (via single-electron transfer events) between chemical compounds when illuminated, can promote reactions that progress slowly or not at all. Dye molecules are attractive photoredox catalyst motifs due to their strong light absorbing capabilities [32–35].

Photocatalysis often involves the excitation of a photocatalyst from a singlet ground state to a singlet excited state upon illumination. The higher energy excited state results in a catalyst molecule that acts as a stronger reductant due to the presence of an electron in a high-energy state. Similarly, the photoexcited catalyst molecule also acts as a stronger oxidant than the ground state molecule due to the presence of a low energy singly occupied orbital which is capable of accepting an electron. Functionalized BODIPY dyes can act as good photocatalyst candidates as they can have long lived triplet excited states, in the microsecond range, as well as tunable redox potentials. To achieve long-lived triplet states, the incorporation of heavy atoms (e.g. iodide) into the BODIPY core can promote intersystem crossing from a singlet excited state to a triplet excited state. BODIPY dyes capable of intersystem crossing events exhibit triplet excited state lifetimes (μs) about 1000 times longer than a singlet excited state (ns) [36].

BODIPY photocatalysts have recently been used to oxidize 1,4-dihydropyridines [37]. A key characteristic of the BODIPY photocatalysts is the presence of methyl groups in the 1,7-positions of the BODIPY core to prevent rotation of the phenyl group in the 8-position, which reduces non-radiative decay of the excited state. The presence of iodide in the 2,6-positions increases the likelihood of intersystem crossing through the heavy atom effect, which increases the lifetime of the excited state. The incorporation of a single styryl phenyl group with a para-alkylamine in the 3,5-positions lengthens the conjugated π-system, providing enough electron donation

http://dx.doi.org/10.5772/intechopen.79704

from the dimethylamine fragment to stabilize the radical anion without hindering catalytic reactivity. A BODIPY photocatalyst, **Figure 9**, generated 98% of the pyridine product in 28 min. Without the presence of a styryl amino substituent in the 3,5-positions on the BODIPY core, the reaction conversion slightly decreased by 3%. The yield decreased an additional 1% with the addition of an electron-withdrawing cyanide group into the styryl substituent at the 3,5 positions. The oxidation reaction was more drastically effected by the addition of an electron-withdrawing nitro group onto the para-position of the phenyl group located at the 8-position of the BODIPY photocatalyst, resulting in a 30% reduction in product conversion. The decrease in catalytic activity is attributed to the increased stabilization of the radical anion, which reduces the reactivity of the radical anion, preventing the loss of H^+ (**Figure 9**). When a styryl group with a para-alkylamine is added to the 3,5-position on the nitro-containing BODIPY, the reaction yield decreased further, to 11.9%, as both of the substitutions stabilize BODIPY radical anions.

BODIPY cores containing iodide substituents have also been utilized in aerobic oxidation reactions through the photocatalytic generation of singlet oxygen ($^1O_2$). For example, Zhao and coworkers have described the aerobic oxidative coupling of amines and the photooxidation of dihydroxylnaphthalenes, via C—H functionalization of 1,4-naphthoquinone, to produce *N*-aryl-2-amino-1,4-naphthoquinones. All of the iodide-containing BODIPY dyes tested outperformed the traditional [Ir(2-phenylpyridine)(bpy)]$^+$ (37% conversion) and [Ru(bpy)$_3$]$^{2+}$ (58% conversion) photocatalysts with 100% conversion in 1 h. Rose Bengal, another traditional photocatalyst, exhibited only an 81% conversion in 1 h [38]. Cozzi and coworkers have showed iodide-containing BODIPY dyes are able to photocatalytically promote the Atom-Transfer Radical Addition (ATRA) reaction between brominated alkanes and alkenes using sodium ascorbate as a sacrificial reductant. The proposed reaction mechanism utilizes a BODIPY-based long-lived triplet excited state to generate an organic radical from the brominated alkane. The photocatalytic reaction generated yields greater than 50% for all 20 substrates described, utilizing only 1 mol% of the BODIPY dye [39].

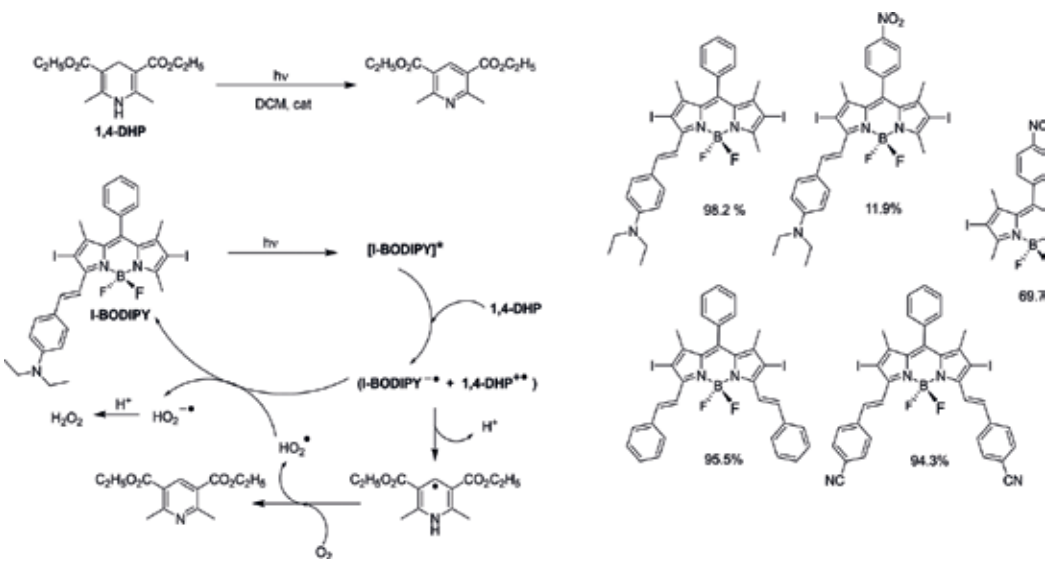

Figure 9. Reaction scheme (top left) and mechanism (bottom left) of the catalytic oxidation of 1,4-dihydropyridines with various BODIPY photocatalysts (right). The numbers shown below the BODIPY photocatalysts indicate product yields after 60 min.

BODIPY dyes have also been utilized as heterogeneous photoredox catalysts. Zhao and coworkers have affixed a BODIPY dye containing iodide substituents in the 2,6-positions to porous silica. The heterogeneous photocatalyst was employed in tandem oxidation and [3 + 2]-cycloaddition reactions of tetrahydroisoquinoline with *N*-phenylmaleimides to generate pyrrolo[2,1-a] isoquinoline in 82% isolated yield after 1 h [40]. BODIPY cores affixed via aza-linkers to fullerene molecules have also shown some catalytic ability, specifically for the tandem oxidation/[3 + 2] cycloaddition of tetrahydroisoquinoline with *N*-phenylmaleimide to produce pyrrolo[2,1-a] isoquinolines [41]. A C_{60}-appended BODIPY dye has been shown to perform oxidative [3 + 2] cyclizations on varying phenylmaleimides, generating product yields greater than 80% in an hour, which was twice as much product as $Ru(bpy)_3Cl_2$ promoted over 4 h [41].

8. Conclusions

BODIPY and azaBODIPY dyes are capable redox reagents, which can act as electron reservoirs in electron transfer reactions. The reduction potential of a BODIPY core can be manipulated by almost 1.4 V, ranging from a potential as reducing as −2.4 V to a potential as moderate as −0.35 V vs. Cp_2Fe/Cp_2Fe^+. The respective azaBODIPY dyes are on average about 600 mV easier to reduce (more positive potentials) than the respective BODIPY dyes. In addition to reductions, the oxidation potential of a BODIPY core can be manipulated by about 1.3 V, ranging from a potential as high as 1.55 V to a potential as low as 0.18 V vs. the Cp_2Fe/Cp_2Fe^+ couple. Although a large shift between the reduction potentials of a BODIPY and azaBODIPY-core result, the difference in oxidation potentials is less profound (about 20 mV). Reduction at a BODIPY or azaBODIPY core results in an increase of aromaticity of the BODIPY or azaBODIPY core. The opposite trend occurs upon oxidation of a BODIPY or azaBODIPY core. The redox nature of a BODIPY core can be utilized to modulate the basicity of an appended amine center by 14 pK_a units, exhibit electrochemically generated chemiluminescence, and promote photoredox reactions. The redox behavior of the BODIPY and azaBODIPY cores opens up the possibility of implementing these dye molecules in many exciting future electron transfer applications, such as redox flow batteries [5] and switchable catalysis [42].

Acknowledgements

We would like to thank Washington State University and the Washington State University Seed Grant Program for funding this research. This work is supported in part by the Biological Electron Transfer and Catalysis (BETCy) EFRC, an Energy Frontier Research Center funded by the U.S. Department of Energy, Office of Science (DE-SC0012518).

Author details

Brena L. Thompson and Zachariah Heiden*

*Address all correspondence to: zachariah.heiden@wsu.edu

Washington State University, Pullman, WA, United States

References

[1] Gerischer H, Willig F. Reaction of excited dye molecules at electrodes. Topics in Current Chemistry. 1976;**61**:31-84

[2] Nepomnyashchii AB, Bard AJ. Electrochemistry and electrogenerated chemiluminescence of BODIPY dyes. Accounts of Chemical Research. 2012;**45**:1844-1853. DOI: 10.1021/ar200278b

[3] Loudet A, Burgess K. BODIPY dyes and their derivatives: Syntheses and spectroscopic properties. Chemical Reviews. 2007;**107**:4891-4932

[4] Treich NR, Wimpenny JD, Kieffer IA, Heiden ZM. Synthesis and characterization of chiral and achiral diamines containing one or two BODIPY molecules. New Journal of Chemistry. 2017;**41**:14370-14378. DOI: 10.1039/C7NJ02670F

[5] Heiland N, Cidarer C, Rohr C, Piescheck M, Ahrens J, Bröring M, Schröder U. Design and evaluation of a boron dipyrrin electrophore for redox flow batteries. ChemSusChem. 2017;**10**:4215-4222. DOI: 10.1002/cssc.201701109

[6] Suk J, Omer KM, Bura T, Ziessel R, Bard AJ. Electrochemistry and electrogenerated chemiluminescence of some BODIPY derivatives. Journal of Physical Chemistry C. 2011;**115**: 15361-15368. DOI: 10.1021/jp201844s

[7] Kieffer IA, Allen RJ, Fernandez JL, Deobald JL, Thompson BL, Wimpenny JD, Heiden ZM. Utilization of a fluorescent dye molecule as a proton and electron reservoir. Angewandte Chemie, International Edition. 2018;**57**:3377-3380. DOI: 10.1002/anie.201713174

[8] Greene LE, Godin R, Cosa G. Fluorogenic ubiquinone analogue for monitoring chemical and biological redox processes. Journal of the American Chemical Society. 2016;**138**:11327-11334. DOI: 10.1021/jacs.6b06899

[9] Misra R, Dhokale B, Jadhav T, Mobin SM. Meso-aryloxy and meso-arylaza linked BODIPY dimers: Synthesis, structures and properties. New Journal of Chemistry. 2014;**38**:3579-3585. DOI: 10.1039/C4NJ00354C

[10] Gut A, Lapok L, Jamroz D, Gorski A, Solarski J, Nowakowska M. Photophysics and redox properties of aza-BODIPY dyes with electron-withdrawing groups. New Journal of Chemistry. 2017;**41**:12110-12122. DOI: 10.1039/C7NJ02757E

[11] Lincoln R, Greene LE, Krumova K, Ding Z, Cosa G. Electronic excited state redox properties for BODIPY dyes predicted from Hammett constants: Estimating the driving force of photoinduced electron transfer. The Journal of Physical Chemistry. A. 2014;**118**:10622-10630. DOI: 10.1021/jp5059148

[12] Yin X, Li Y, Li Y, Zhu Y, Tang X, Zheng H, Zhu D. Electrochromism based on the charge transfer process in a ferrocene–BODIPY molecule. Tetrahedron. 2009;**65**:8373-8377. DOI: 10.1016/j.tet.2009.08.008

[13] Rao MR, Kumar KVP, Ravikanth M. Synthesis of boron-dipyrromethene–ferrocene conjugates. Journal of Organometallic Chemistry. 2010;**695**:863-869. DOI: 10.1016/j.jorganchem.2010.01.009

[14] Liu JY, El-Khouly ME, Fukuzumi S, Ng DKP. Photoinduced electron transfer in a ferrocene–distyryl BODIPY dyad and a ferrocene–distyryl BODIPY–C_{60} triad. Chemphyschem. 2012;**13**:2030-2036. DOI: 10.1002/cphc.201200167

[15] Maligaspe E, Pundsack TJ, Albert LM, Zatsikha YV, Solntsev PV, Blank DA, Nemykin VN. Synthesis and charge-transfer dynamics in a ferrocene-containing organoboryl aza-BODIPY donor–acceptor triad with boron as the hub. Inorganic Chemistry. 2015;**54**:4167-4174. DOI: 10.1021/acs.inorgchem.5b00494

[16] Didukh NO, Zatsikha YV, Rohde GT, Blesener TS, Yakubovskyi VP, Kovtun YP, Nemykin VN. NIR absorbing diferrocene-containing meso-cyano-BODIPY with a UV-Vis-NIR spectrum remarkably close to that of magnesium tetracyanotetraferrocenyltetraazaporphyrin. Chemical Communications. 2016;**52**:11563-11566. DOI: 10.1039/C6CC06344F

[17] Kaur N, Van Steerteghem N, Singla P, Kaur P, Clays K, Singh K. Second-order nonlinear polarizability of ferrocene-BODIPY donor-acceptor adducts. Quantifying charge redistribution in the excited state. Dalton Transactions. 2017;**46**:1124-1133. DOI: 10.1039/C6DT04455G

[18] Zatsikha YV, Didukh NO, Nemez D, Schlachter AC, Karsenti P-L, Kovtun YP, Harvey PD, Nemykin VN. Ferrocene-BODIPY merocyanine dyads: New NIR absorbing platforms with optical properties susceptible to protonation. Chemical Communications. 2017;**53**:7612-7615. DOI: 10.1039/C7CC03332J

[19] Galangau O, Fabre-Francke I, Munteanu S, Dumas-Verdes C, Clavier G, Méallet-Renault R, Pansu RB, Hartl F, Miomandre F. Electrochromic and electrofluorochromic properties of a new boron dipyrromethene–ferrocene conjugate. Electrochimica Acta. 2013;**87**:809-815. DOI: 10.1016/j.electacta.2012.09.048

[20] Bard AJ, Faulkner LR. Electrochemical Methods: Fundamentals and Applications. 2nd ed. New York: John Wiley & Sons, Inc; 2001

[21] Zatsikha YV, Maligaspe E, Purchel AA, Didukh NO, Wang Y, Kovtun YP, Blank DA, Nemykin VN. Tuning electronic structure, redox, and photophysical properties in asymmetric NIR-absorbing organometallic BODIPYs. Inorganic Chemistry. 2015;**54**:7915-7928. DOI: 10.1021/acs.inorgchem.5b00992

[22] Kaur N, Kaur P, Singh K. Ferrocene-BODIPY push–pull dyad: A common platform for the sensing of Hg^{2+} and Cr^{3+}. Sensors and Actuators, B: Chemical. 2016;**229**:499-505. DOI: 10.1016/j.snb.2016.01.134

[23] Halter O, Fernandez I, Plenio H. Fine-tuning the fluorescence gain of fret-type (BODIPY)(bBODIPY')-NHC-iridium complexes for CO detection with a large virtual stokes shift. Chemistry: A European Journal. 2017;**23**:711-719. DOI: 10.1002/chem.201604757

[24] Coskun A, Yilmaz MD, Akkaya EU. Bis(2-pyridyl)-substituted boratriazaindacene as an NIR-emitting chemosensor for Hg(II). Organic Letters. 2007;**9**:607-609. DOI: 10.1021/ol062867t

[25] Peng X, Du J, Fan J, Wang J, Wu Y, Zhao J, Sun S, Xu T. A selective fluorescent sensor for imaging Cd^{2+} in living cells. Journal of the American Chemical Society. 2007;**129**:1500-1501. DOI: 10.1021/ja0643319

[26] Lu H, Xiong L, Liu H, Yu M, Shen Z, Li F, You X. A highly selective and sensitive fluorescent turn-on sensor for Hg^{2+} and its application in live cell imaging. Organic & Biomolecular Chemistry. 2009;**7**:2554-2558. DOI: 10.1039/b902912e

[27] Atilgan S, Kutuk I, Ozdemir T. A near IR di-styryl BODIPY-based ratiometric fluorescent chemosensor for Hg(II). Tetrahedron Letters. 2010;**51**:892-894. DOI: 10.1016/j.tetlet.2009.12.025

[28] Jeong Y, Yoon J. Recent progress on fluorescent chemosensors for metal ions. Inorganica Chimica Acta. 2012;**381**:2-14. DOI: 10.1016/j.ica.2011.09.011

[29] Wagner S, Broedner K, Coombs BA, Bunz UHF. Pyridine-substituted BODIPY as fluorescent probe for Hg^{2+}. European Journal of Organic Chemistry. 2012;**2012**:2237-2242. DOI: 10.1002/ejoc.201101839

[30] Richter MM. Electrochemiluminescence (ecl). Chemical Reviews. 2004;**104**:3003-3036. DOI: 10.1021/cr020373d

[31] Hesari M, Lu J-s, Wang S, Ding Z. Efficient electrochemiluminescence of a boron-dipyrromethene (BODIPY) dye. Chemical Communications. 2015;**51**:1081-1084. DOI: 10.1039/C4CC08671F

[32] Hattori S, Ohkubo K, Urano Y, Sunahara H, Nagano T, Wada Y, Tkachenko NV, Lemmetyinen H, Fukuzumi S. Charge separation in a nonfluorescent donor−acceptor dyad derived from boron dipyrromethene dye, leading to photocurrent generation. The Journal of Physical Chemistry. B. 2005;**109**:15368-15375. DOI: 10.1021/jp050952x

[33] Hu L, Paul-Ludovic K, Pierre DH. Azophenine as central core for efficient light harvesting devices. Chemphyschem. 2018;**19**:596-611. DOI: 10.1002/cphc.201701183

[34] Yeo H, Tanaka K, Chujo Y. Effective light-harvesting antennae based on BODIPY-tethered cardo polyfluorenes via rapid energy transferring and low concentration quenching. Macromolecules. 2013;**46**:2599-2605. DOI: 10.1021/ma400015d

[35] Bucher L, Desbois N, Harvey PD, Gros CP, Sharma GD. Porphyrin antenna-enriched BODIPY–thiophene copolymer for efficient solar cells. ACS Applied Materials & Interfaces. 2018;**10**:992-1004. DOI: 10.1021/acsami.7b16112

[36] Dong Y, Iagatti A, Foggi P, Zhao J, Mazzone G, Xu K, Ji W, Di Donato M, Russo N. BODIPY-squaraine triads: Preparation and study of the intramolecular energy transfer, charge separation and intersystem crossing. Dyes and Pigments. 2017;**147**:560-572. DOI: 10.1016/j.dyepig.2017.08.028

[37] Wang R, Geng Y, Zhang L, Wu W, Fan W, Li Z, Wang L, Zhan L, Wu X, Wu M. Intramolecular charge transfer-enhanced bodipy photosensitizer in photoinduced electron transfer and its application to photoxidation under mild condition. Chinese Journal of Chemistry. 2015;**33**:1251-1258. DOI: 10.1002/cjoc.201500494

[38] Huang L, Zhao J, Guo S, Zhang C, Ma J. BODIPY derivatives as organic triplet photosensitizers for aerobic photoorganocatalytic oxidative coupling of amines and photooxidation of dihydroxylnaphthalenes. The Journal of Organic Chemistry. 2013;**78**:5627-5637. DOI: 10.1021/jo400769u

[39] Magagnano G, Gualandi A, Marchini M, Mengozzi L, Ceroni P, Cozzi PG. Photocatalytic ATRA reaction promoted by iodo-BODIPY and sodium ascorbate. Chemical Communications. 2017;**53**:1591-1594. DOI: 10.1039/c6cc09387f

[40] Guo S, Zhang H, Huang L, Guo Z, Xiong G, Zhao J. Porous material-immobilized iodo-bodipy as an efficient photocatalyst for photoredox catalytic organic reaction to prepare pyrrolo[2,1-a]isoquinoline. Chemical Communications. 2013;**49**:8689-8691. DOI: 10.1039/C3CC44486D

[41] Huang L, Zhao J. C_{60}-BODIPY dyad triplet photosensitizers as organic photocatalysts for photocatalytic tandem oxidation/[3+2] cycloaddition reactions to prepare pyrrolo[2,1-a] isoquinoline. Chemical Communications. 2013;**49**:3751-3753. DOI: 10.1039/C3CC41494A

[42] Blanco V, Leigh DA, Marcos V. Artificial switchable catalysts. Chemical Society Reviews. 2015;**44**:5341-5370. DOI: 10.1039/C5CS00096C

Chapter 5

Decomposition Mechanisms of BODIPY Dyes

Yuriy S. Marfin, Sergey D. Usoltsev and
Evgeniy V. Rumyantsev

Additional information is available at the end of the chapter

http://dx.doi.org/10.5772/intechopen.80498

Abstract

The stability of metal complexes in both thermodynamic and kinetic aspects always was a matter of interest in the field of coordination chemistry. Practical implementation of a fluorophores in a field of molecular biology also is essentially constrained by their solvolytic and protolytic stability. The aforementioned emphasizes interest in a search for factors of quantitative stability-based discrimination on a row of BODIPY derivatives. This chapter shows that thermodynamic stability of a dipyrrinates varies to a large extent from a mostly undestructable solvolytically BODIPYs to a very volatile in the same aspect rare-earth element complexes.

Keywords: BODIPY, decomposition mechanisms, stability, acidic conditions, kinetic data, dissociation

1. Introduction

The stability of metal complexes in both thermodynamic and kinetic aspects always was a matter of interest in the field of coordination chemistry. Whereas the thermodynamical approach to investigation of coordination compound stability was well established back before the first half of the twentieth century [1, 2], there were very few, if any, attempts to systematize patterns of formation and destruction of complexes in a kinetical aspect.

A monograph published in 2007 [3] highlights the factors affecting kinetics of dissociation and mechanisms of this process for a vast range of coordination compounds. Both well-known 'Verner' complexes and the most contemporary porphyrinato and phthalocyaninato complexes are discussed therein. Remarkable contribution made to the topic by the authors was systematization of the factors, influencing both kinetic and thermodynamic stability of the

complex compounds. Due to the universal nature of the proposed models, they could be easily adapted to describe dissociation processes taking place for other complexes. High impact of both external (selected solvent and reagent) and internal (molecular structure) parameters on the dissociation process, showed in the monograph, emphasizes importance of the study for pure and applied chemistry of the dipyrrins.

The process of optimisation of physicochemical properties of the compounds essentially implies a search for the compromise between the photophysical efficiency and stability. The latter, in turn, includes resilience to solvolytic, protolytic and solvoprotolytic dissociation and photochemical, thermooxidative and some other destruction routes [4, 5]. Our research shows that thermodynamic stability of a dipyrrinate varies to a large extent from a mostly undestructable solvolytically BODIPYs to a very volatile in the same aspect rare-earth element complexes. Work of our colleagues from Tomsk [6–8] shows that immobilization of a BODIPY in a sol–gel silicon oxide involves specific interactions of a chromophore with a silanol moiety of a matrix. This drastically influences fluorescence quantum yield of the chromophore, decreasing it up to a factor of 100 and causing significant changes in the shape of both fluorescence and absorbance spectrum. Interestingly, a similar behaviour is observed for BODIPY upon interaction with protic solvents and Arrhenius acids. The common thing in both situations is that sol–gel technology involves usage of aggressive medium on the early stages of either acid-catalysed process or a base-catalysed one [9]. Research [10] shows decrease of pH to affect BODIPY photophysical parameters in an irreversible manner. Namely, HCl addition in ethanol causes BODIPY destruction via $[BF_2]^+$ elimination, leading to a protonated form of dipyrromethene. Further development of a practically important process of a composite material elaboration obviously requires a careful study of stability of a fluorophore in an acid and basic media. Practical implementation of a fluorophore in a field of molecular biology also is essentially constrained by their solvolytic and protolytic stability. The aforementioned emphasizes interest in a search for factors of quantitative stability-based discrimination in a row of BODIPY derivatives.

Our collaboration with the Institute of Solution Chemistry of the Russian Academy of Sciences pushed the limits in the field thanks to the huge amount of data and experience in the studies of such processes for porphyrins and phthalocyanines. Until the current review on dipyrrinate stability, our colleagues from ISC RAS have published [11, 12] kinetics of $Cu(II)$, $Ni(II)$, $Co(II)$ and $Hg(II)$ dissociation processes in a benzene solution of acetic acid. Surprisingly, $Hg(II)$ complexes do undergo dissociation even in acid-free benzene and chloroform solutions. Such a process involves formation of $Hg \cdot Solv$ adducts alongside with protonated dipyrromethene via the stage of a π-complex formation:

$$[Hg(dpm)_2 + C_6H_6 \leftrightarrow \left[Hg(dpm)_2\right] \cdot C_6H_6 \leftrightarrow [C_6H_6 \cdots Hg \cdots dpm]^+ dpm^- \rightarrow [C_6H_5 - Hg - dpm]$$
$$[C_6H_5 - Hg - dpm] + C_6H_6 \rightarrow [C_6H_5 - Hg - C_6H_5] + Hdpm \quad (1)$$

Analysis of dissociation kinetics of other stated dipyrrinates in acetic acid benzene solutions yields a row of descending stability to protolytic dissociation:

$$\left[Cu(dpm)_2\right] > \left[Co(dpm)_2\right] \approx \left[Zn(dpm)_2\right] \gg \left[Hg(dpm)_2\right] \gg \left[Ni(dpm)_2\right] \quad (2)$$

Whereas this row coincides roughly with a respective row for thermodynamic stability, it has absolutely nothing to do with the corresponding dependencies for complexes of a structurally flexible chelate and amines like ethylenediamine. Stability of the $Ni(II)$ complex for porphyrins and phthalocyanines also occupies different positions in a corresponding row. Moreover, somehow, comparable destruction rate in such a condition is only observed for yet the most labile macrocyclic complex [13] being samarium(II) octaphenyltetraazaporphyrinate—$[(Acac)SmOPTAP]$. This $[(Acac)SmOPTAP]$ in benzene with 0.2 M $AcOH$ (303.15 K) has a $k_{obs} = 1.6 \cdot 10^{-4} s^{-1}$. $\left[Co(dpm)_2\right]$ and $\left[Zn(dpm)_2\right]$ in a similar condition (benzene, 0.33 M $AcOH$, 303.15 K) exhibit k_{obs} below $1.1 \cdot 10^{-4} s^{-1}$.

To summarize, available data demonstrates lack of macrocyclic effect in dipyrrinates to negatively impact complexes stability. Influence of this structural disadvantage is exemplified for the $Ni(II)$ complexes as stated above. At the same time, spatial rigidity as compared to diammines and similar chelates implies their distinct behaviour granting special interest in the field.

2. Protolytic dissociation of alkylated Zn (II) dipyrrinates

Here we review research on kinetics of $Zn(II)$ dipyrrinate $\left[Zn(dpm)_2\right]$ protolytic dissociation [14]. The structures discussed are presented below:

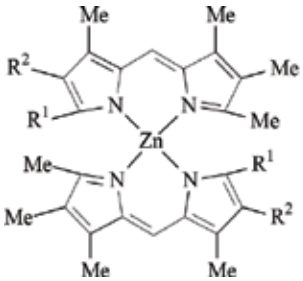

$$[Zn(dpm^1)_2]: R^1 = H, R^2 = Me$$
$$[Zn(dpm^2)_2]: R^1 = Me, R^2 = H$$
$$[Zn(dpm^3)_2]: R^1 = Me, R^2 = Et$$

$Zn(II)$ dipyrromethene complexes were shown to be quite perspective among other d-metal complexes, because due to fully occupied d-electron shell, no ligand fluorescence quenching occurs. It was found earlier [15] that $\left[Zn(dpm)_2\right]$ complexes are exposed to protolytic dissociation in C_6H_6–CH_3COOH solutions, so such a mixture was also used to study protolytic dissociation in this case.

Electronic absorption and fluorescence spectroscopy was used for examination of dissociation kinetics at 298, 308, 318 and 328 K temperature points. Observed rate constant (k_{obs}), activation energy (E_a) and entropy ($\Delta S^{\neq}$) were calculated as follows:

$$k_{obs} = \frac{1}{\tau} \cdot ln\left(\frac{A_0 - A_\infty}{A_\tau - A_\infty}\right) \quad (3)$$

where A_0, A_∞ and A_τ are absorbance in the first, intermediate and the last point, respectively.

$$E_a = 19.1 \cdot \frac{T_1 T_2}{T_2 - T_1} \cdot lg \frac{k^{T_2}}{k^{T_1}}, \qquad \Delta S^{\neq} = 19.1 \cdot lgk^T + E_a/T - 19.1 \cdot lgT - 205 \tag{4}$$

Electronic absorption spectra of the compounds exhibit bright characteristic absorption band at 500 nm corresponding to $S_0 \rightarrow S_1$ electronic transition and charge-transfer band at ~370 nm. Fluorescent bands are single-peak mirror images of the main absorption band.

It was shown, that addition of acetic acid in benzene provokes decrease of the long-wavelength absorption maximum (λ_{abs} = 497–506 nm) with a simultaneous increase pro rata in the 485–488 nm peak, corresponding to the protonated ligand form (H_2dpm^+). On the other side, a decrease in the main fluorescence band of the compound was not accompanied by any other changes which was in the good agreement with the fact that protonated dipyrromethene is not fluorescent (**Figure 1**).

It is reasonable to state, therefore, that $\left[Zn(dpm)_2\right]$ protolytic dissociation yields protonated ligand form—H_2dpm^+.

Even the smallest acid amounts provoked immediate $\left[Zn\left(dpm^1\right)_2\right]$ dissociation all the way to the equilibrium state. Data obtained from the experiments allowed us to measure protolytic dissociation equilibrium constant corresponding to the following scheme:

$$\left[Zn\left(dpm^1\right)_2\right] + 4HAcO = Zn(AcO)_2 + 2\left[H_2\left(dpm^1\right)^+ \cdots AcO^-\right] \tag{5}$$

Measured to be $5 \cdot 10^{-6} l^2/mol^2$, this constant is in the good agreement with existing data on thermodynamic stability of a similar complex [16].

Linearization of kinetic data for the $\left[Zn\left(dpm^3\right)_2\right]$ in the semi-logarithmic scale indicates first-order reaction relative to complex concentration (**Figure 2**). Dependence of the observable rate constant from the HAcO concentration could be written as

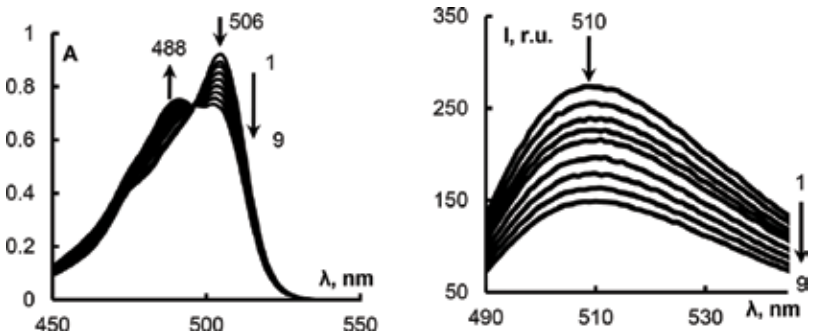

Figure 1. Left: changes in EAS of benzene [$Zn(dpm^3)_2$] solution upon *AcOH* addition (C = 0.78 *M*) (1—0 *min*; 9—30 *min*); and right: changes in [$Zn(dpm^2)_2$] benzene solution fluorescence upon *AcOH* addition (C = 0.7 *M*) (1—0 *min*; 9—30 *min*).

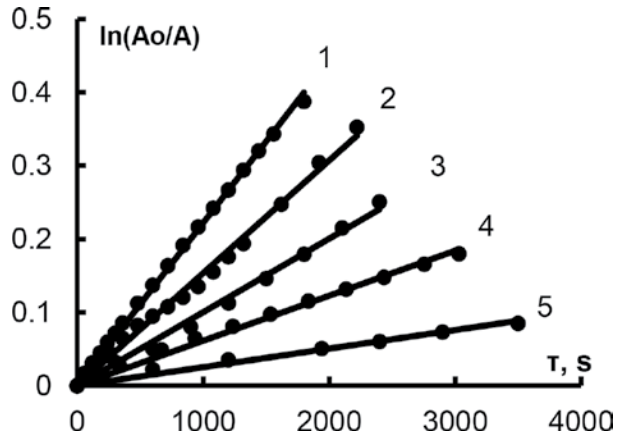

Figure 2. Kinetics of the $[Zn(dpm^3)_2]$ dissociation upon different *AcOH* concentrations (1—0.78 *M*; 2—0.67 *M*; 3—0.54 *M*; 4—0.39 *M*; and 5—0.21 *M*).

$$k_{obs} = kC_{HAcO}^2 \tag{6}$$

According to the literature data [17–19], Gammet's acidity function is in direct ratio with acid concentration in the range used (0.21–0.78 M); thus activity could be safely substituted with the concentration.

Protolytic dissociation, therefore, proceeds the same way as protonated ligand formation and could be described by the third-order kinetic equation:

$$-\frac{dC_{[Zn(dpm)_2]}}{d\tau} = k_{obs}C_{[Zn(dpm)_2]}C_{AcOH}^2 \tag{7}$$

Data obtained is in good agreement with the literature and justifies participation of two acid molecules in the limiting stage of the reaction. Analogous mechanism takes place in the protolytic dissociation of metalloporphyrins [20, 21], possessing similar structure of the coordination centre. Kinetic constant values k^T at different temperatures and corresponding activation parameters are presented below:

T, K	*k*, $l^2/(mol^2 \cdot s)$	E_a, kJ/mol	$\Delta S^{\neq}$, J/(mol·K)	$\Delta H^{\neq}$, kJ/mol
$[Zn(dpm^2)_2]$				
298	0.0001	61.2 ± 2.3	−119.6 ± 10.3	58.7 ± 2.2
308	0.0002			
318	0.0005			
$[Zn(dpm^3)_2]$				
298	0.0003	52.3 ± 3.2	−141.1 ± 12.4	49.8 ± 3.2
308	0.0005			
318	0.0007			

T, K	k, $l^2/(mol^2 \cdot s)$	E_a, kJ/mol	$\Delta S^{\neq}$, J/(mol·K)	$\Delta H^{\neq}$, kJ/mol
Zn(II) bis(4,4′-dibutyl-3,3′,5,5′-tetramethyl-2,2′-dipyrrinate)				
298	0.0006	51.4	−142.3	48.9
303	0.00099			
313	0.00171			
318	0.00232			

Formation of a protonated ligand form H_2L^+ and derived above third-order kinetic equations allows us to represent protolytic dissociation as the three-stage process of a consequent pyrrolic nitrogen protonation:

$$\begin{gathered}\left[Zn(dpm)_2\right] + 2HAcO \leftrightarrow \left\{\left[Zn(dpm)_2 \cdot 2H\right]^{2+} \cdots 2AcO^-\right\} \quad k_1, slow \\ \left\{\left[Zn(dpm)_2 \cdot 2H\right]^{2+} \cdots 2AcO^-\right\} \rightarrow 2Hdpm + Zn(AcO)_2 \quad k_2, fast \\ Hdpm + HAcO \rightarrow [H_2dpm^+ \cdots AcO^-] \quad k_3, fast\end{gathered} \tag{8}$$

With the quasi-steady-state assumption, the equation for $\left[Zn(dpm)_2\right]$ could be rewritten as:

$$-\frac{dC_{\left[Zn(dpm)_2\right]}}{d\tau} = \left(\frac{k_1 k_2}{k_{-1} + k_2}\right) C_{\left[Zn(dpm)_2\right]} C_{HAcO}^2 \tag{9}$$

which coincides with the experimentally derived equation. Further simplification is possible with the assumption of kinetic insignificance of k_{-1} due to low inverse reaction rate:

$$-\frac{dC_{\left[Zn(dpm)_2\right]}}{d\tau} = k_1 C_{\left[Zn(dpm)_2\right]} C_{HAcO}^2 \tag{10}$$

The rate-determining step is, therefore, the first stage. Activation parameters obtained serve as the further approval for the conclusions stated above. Namely, increase in ordering due to formation of $\left\{\left[Zn(dpm)_2 \cdot 2H\right]^{2+} \cdots 2AcO^-\right\}$ intermediate is described by the negative values of activation entropy.

Data presented allows us to identify the effects of dipyrrolic ligand alkyl substitution to the kinetic stability of the corresponding complexes for the first time. Whereas the α-free complex was shown to be of the highest lability, it is obvious to assume the high impact of +I effect existing therein to be the most important stabilizing factor. This assumption is supported by the proposed mechanism: $\left\{\left[Zn(dpm)_2 \cdot 2H\right]^{2+} \cdots 2AcO^-\right\}$ stability is determined solely by the strength of N-H hydrogen bonds. Decrease in +I effect impact along with fast emergence of steric difficulties leads to severe weakening of those bonds upon alkyl chain elongation (literature data for dibutyl-substituted dipyrromethene [15] was also used for comparison). Methyl group, in turn, provides the highest inductive impact as compared to related sterical

difficulties—such a combination granting the lowest activation energy qualitatively represented by instant hydrolysis.

In our other paper [14], the search for analogies in photochemical and protolytic stability was performed.

Photochemical destruction processes of $\left[Zn\left(dpm^1\right)_2\right]$, $\left[Zn\left(dpm^2\right)_2\right]$ and $\left[Zn\left(dpm^3\right)_2\right]$ along with free dipyrromethene ligand and dipyrromethene hydrofluoride in ethanol were studied. OUFB-04 (180–275 nm, 11.4 W/m^2) was used, and observable destruction constants were evaluated from spectral changes at different time points (**Figure 3**). ^{1}H NMR spectra of the compounds were acquired using Bruker AVANCE-500 (Germany) spectrometer.

From the data obtained, we state the main role of oxidative hydroxylation of alkyl moieties and μ-carbon in the destruction process, yielding monopyrrolic products. Nuclear magnetic resonance spectroscopy data after irradiation indicates peaks, associated with $HO-CH_2-Pyr$ and alike moieties: ^{1}H NMR (500 MHz, $CDCl_3$) δ, ppm—1.25, 3.74, 7.39, 7.49 and 8.01.

Observable constants were measured to be $(8\pm3)\cdot10^{-2}$, $(3.4\pm0.5)\cdot10^{-2}$ and $(10\pm3)\cdot10^{-2}$, respectively. Photolysis speed, therefore, grows in direct proportion with 'alkylation degree', and β-substituent affects this process much more intensively than the α one. Observable constants for free dipyrromethene and dipyrromethene hydrofluoride were measured to be $(16.7\pm0.9)\cdot10^{-2}$ and $(8\pm2)\cdot10^{-2}$, respectively. As it was expected, free of any acid–base and coordinational interactions, dipyrrin structure becomes way more labile to photodestruction due to high electron density allocated at the π-conjugated system.

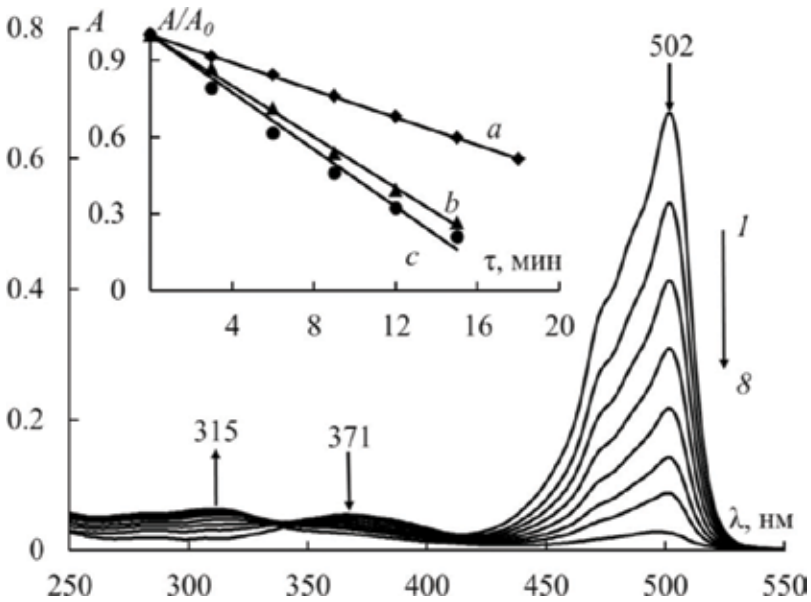

Figure 3. Changes in $[Zn(dpm^3)_2]$ ethanol solution EAS upon irradiation (1—0 *min*; 8—24 *min*); inset—relative optical density of the compounds upon irradiation (*a*—$[Zn(dpm^2)_2]$; b—$[Zn(dpm^1)_2]$; c—$[Zn(dpm^3)_2]$).

3. Protolytic dissociation of Pd(II) dipyrrinates and bis-dipyrrinates

Dipyrromethene ligands are known to possess flat molecular shape and mobile π-electron system. Such properties essentially suggest high interest in research concerning their DNA intercalating activity for anticancer purposes. The most promising complexes in this area are $Pt(II)$ and $Pd(II)$ organic coordination compounds, due to their flat square coordination polyhedra, perfect for fitting the molecule between nitrogenous bases. Unlike 3d-metal dipyrrinates, there are very few investigations carried out on their 4d analogues. There is also a high fundamental interest in comparative studies of the physicochemical properties for compounds with similar coordination environment but different ligand structures. Differences between dipyrrin and billadiene complexes are interesting object for the investigation; the latter possess additional chelating cycle, which provokes emergence of the differential polychelating effect [22].

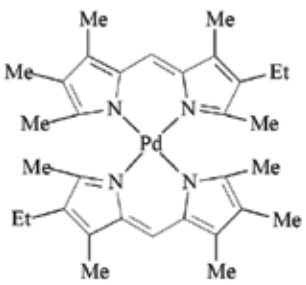

[Pd(dpm)$_2$]

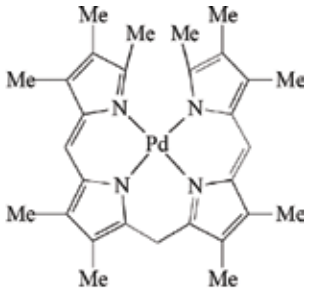

[Pd(bd)]

Here we review our research on $Pd(II)$ complexes with alkylated dipyrromethene (*Hdpm*) and billadiene-a,c (H_2bd).

Preliminary examination revealed absolute insusceptibility of the studied complexes to protolysis in C_6H_6–*AcOH* solution. $Pd(II)$ complexes are, therefore, way more stable to protolytic dissociation than the 3d-metal dipyrrinates. Trichloroacetic acid benzene solution showed measurable reaction rate at 298 K and therefore was used for further kinetic investigations. Emergence and gradual growth of 485 nm peak in electronic absorption spectra indicated formation of protonated ligand form upon complex destruction (**Figure 4**).

Linear dependencies obtained for data plotted in semi-logarithmic coordinates indicate first-order reaction relative to complex concentration. Observable rate constants, at the same time, suggest second-order reaction relative to CCl_3COOH concentration:

$$k_{obs} = kC^2_{CCl_3COOH} \tag{11}$$

Protolytic dissociation therefore could be described by the third-order equation, in a similar way as the ligand protonation process:

$$-\frac{dC_{[Pd(dpm)_2]}}{d\tau} = kC_{[Pd(dpm)_2]}C^2_{CCl_3COOH} \tag{12}$$

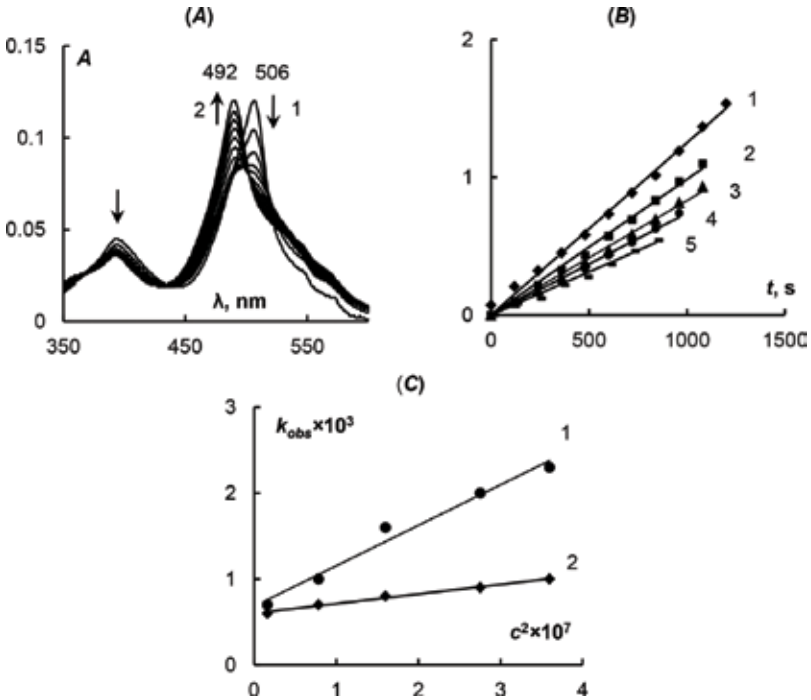

Figure 4. (A) Changes in [*Pd*(*bd*)] EAS upon protolytic dissociation 298.15 K; τ (s): 1—0 (s); 2—2820 (s); (B) kinetics of [*Pd*(*bd*)] dissociation at 298 K; $C^2_{CCl_3COOH} \cdot 10^4$; M: 6 (1), 5.3 (2), 4 (3), 2.8 (4), 1.3 (5); (C) dependence of k_{obs} from $C^2_{CCl_3COOH}$ (T = 298 K) for [*Pd*(*bd*)] (1) и [*Pd*(*dpm*)$_2$] (2).

$$-\frac{dC_{[Pd(bd)]}}{d\tau} = kC_{[Pd(bd)]}C^2_{CCl_3COOH} \tag{13}$$

Kinetical and activation parameters for the $Pd(II)$ complexes are listed below:

T, K	*k*	E_a, kJ/mol	$\Delta S^{\neq}$, J/(mol·K)	$\Delta H^{\neq}$, kJ/mol
[*Pd*(*dpm*)$_2$]				
298	4700 ± 200	52.4 ± 2.3	−6.0 ± 0.3	44.8 ± 2.2
308	7320 ± 360			
318	18,788 ± 393			
[*Pd*(*bd*)]				
298	1120 ± 50	65.8 ± 3.2	25.7 ± 0.5	65.3 ± 3.2
308	5210 ± 190			
318	5860 ± 280			

Formation of a protonated ligand form (H_2dpm^+ and H_4bd^{2+}) allows us to propose mechanism, analogical to the aforementioned bis-dipyrrinates dissociation scheme. Three-stage consequent nitrogen protonation reaction scheme is assumed:

$$\begin{gathered}\left[Pd(dpm)_2\right] + 2H^+\cdots A^- \leftrightarrow \left\{\left[Pd(dpm)_2 \cdot 2H\right]^{2+}\cdots 2A^-\right\}, \quad k_1, slow \\ \left\{\left[Pd(dpm)_2 \cdot 2H\right]^{2+}\cdots 2A^-\right\} \rightarrow 2Hdpm + PdA_2, \quad k_2, fast \\ Hdpm + H^+\cdots A^- \rightarrow [H_2dpm^+\cdots A^-], \quad k_3, fast\end{gathered} \tag{14}$$

Quasi-steady-state assumption for this process allows us to describe this process with the equation:

$$-\frac{dC_{\left[Pd(dpm)_2\right]}}{d\tau} = \left(\frac{k_1k_2}{k_{-1}+k_2}\right)C_{\left[Pd(dpm)_2\right]}C^2_{H^+\cdots A^-}, \tag{15}$$

As it was done for $Zn(II)$ complexes before, simplification with the assumption of k_{-1} kinetical insignificance could be done to rewrite equation in a convenient form:

$$-\frac{dC_{\left[Pd(dpm)_2\right]}}{d\tau} = k_1C_{\left[Pd(dpm)_2\right]}C^2_{H^+\cdots A^-} \tag{16}$$

Thus, the obtained activation parameters describe the transition state formation (rate-determining step). Here we also assume the possibility of interaction between the acid anion and Pd(II) atom.

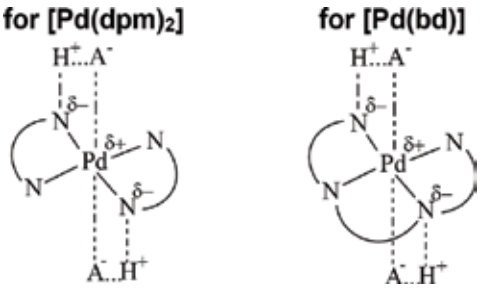

Comparison of the activation parameters for $\left[Pd(dpm)_2\right]$ and $[Pd(bd)]$ complexes suggests manifestation of differential polychelating effect, effectively screening coordination centre from external influence. Namely, observable dissociation rate constant is 4.2 times higher (T = 298 K) for bis-dipyrrinate than for billadiene complex, and activation energy of the limiting step is 1.3 times higher for the $[Pd(bd)]$.

It is worth mentioning here that in other researches, $Pt(III)$ billiverdine (natural billatriene) complex was found to be stable to protolysis in *DMSO-AcOH* solutions with up to 16.85 M acid concentration. At the same time, it dissociated instantly all the way to equilibrium state in $DMSO–H_2SO_4$ solutions. Data obtained for billiverdine and protoporphyrin IX complexes was used for evaluation of macrocyclic effect impact: kinetical stability increase measures 10^4 times for $Pt(III)$ protoporphyrinate. Macrocyclic effect was shown to significantly increase stability in the similar comparative study with the $Mn(III)$ complexes, where the stability increase was measured to be $1.73 \cdot 10^8$ times!

Both polychelating and macrocyclic effect should be therefore mentioned as the most important factors of coordination compound stabilization. The hallmark of these effects is a drastic decrease in dissociation rate constants upon switching from simply chelating ligands, to polychelating ones and, finally, to macrocyclic ligands.

4. Protolytic dissociation of Cu(II) and Ni(II) bis-dipyrrinates

$Cu(II)$ and $Ni(II)$ are known for their ability to form both biligand dipyrrinates $\left[M(dpm)_2\right]$ and a highly themodynamically stable heteroligand complexes $[Mdpm(X)]$. High stability of the latter (lg$K$ = 7–10) suggests formation of intermediate products with mixed coordination environment during protolytic dissociation process. This is indeed being the case for the $Cu(II)$ complex with butyl-substituted dipyrromethene [23, 24].

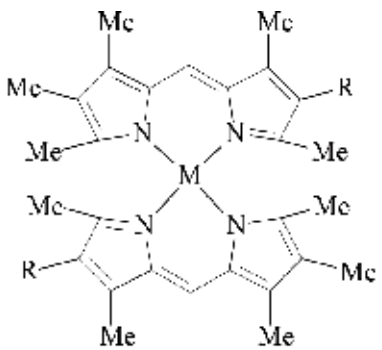

$$[Ni(dpm)_2]: M = Ni, R = Et$$
$$[Cu(dpm)_2]: M = Cu, R = Me$$

Investigation of $Cu(II)$ and $Ni(II)$ complexes protolytic dissociation was carried out to further understand influence of different factors on kinetic stability of dipyrrinates [15]. Benzolic $\left[Cu(dpm)_2\right]$ and $\left[Ni(dpm)_2\right]$ solutions possess three characteristic electronic absorption maxima: high-intensity one at 527–530 nm, second peak at 460–464 nm and the charge-transfer band in the near UV. The addition of a minimal AcOH amount was found to cause immediate intensity decrease for the main electronic absorption peak, accompanied by 488 nm peak emergence (**Figure 5**). Retaining of the spectral shape upon triethylamine addition approved this process to be reversible equilibrium. The thermodynamic equilibrium constant was obtained from the spectrophotometric titration data, assuming the process to be described with the equation below:

$$\left[Cu(dpm)_2\right] + 4AcOH = 2[H_2dpm](AcO) + Cu(AcO)_2 \tag{17}$$

Obtained thermodynamic constant value of $(7.55 \pm 0.4) \cdot 10^{-7} l^2/mol^2$ is in good agreement with the literature data on the $Cu(II)$ dipyrrinate stability. Unlike the butyl-dipyrromethene complexes [15], our objects were found to exhibit not the formation of heteroligand compounds even when the smallest acid amounts were used.

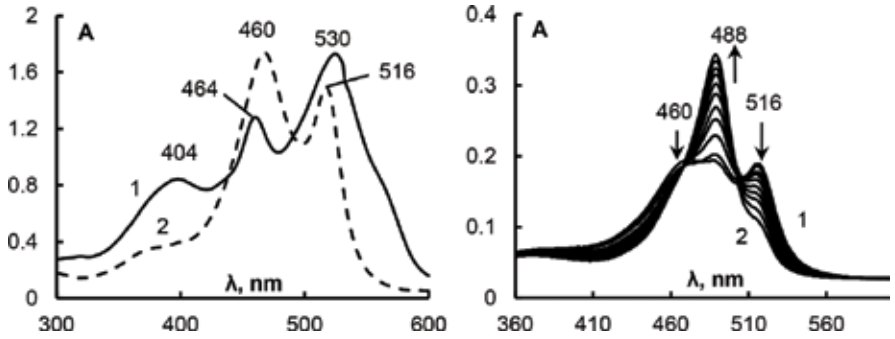

Figure 5. Left: [*Ni*(*dpm*)$_2$] (1) and [*Cu*(*dpm*)$_2$] (2) benzene solutions EAS; right: changes in [*Cu*(*dpm*)2] benzene solution EAS upon C_{AcOH} variation, M: 0.02 (1), 0.12 (2).

Unlike $\left[Cu(dpm)_2\right]$, the $\left[Ni(dpm)_2\right]$ formation is a kinetically controlled reaction which was found to take place with measurable rate in the acid concentrations range from $2.410 \cdot 10^{-4}$ to 0.2 M. Acid addition was found to provoke decrease in the 530 nm band with simultaneous increase in the H_2dpm^+ band at 493 nm (**Figure 6**). Whereas at the low acid concentrations ($\leq 2 \cdot 10^{-3}$), there were bands of heteroligand complex observable in the EAS, increase of the concentration led to a full dissociation lacking any complications.

Straight lines obtained in the semi-logarithmic coordinates suggest first-order reaction relative to complex concentration, described with the equation:

$$-\frac{dC_{\left[Ni(dpm)_2\right]}}{d\tau} = k_{obs} C_{\left[Ni(dpm)_2\right]} C^2_{AcOH} \tag{18}$$

Each of the two equilibria could be described, therefore, as the consequent protonation of the dipyrromethene ligand. For an equilibrium involving formation of heteroligand complex

$$\left[Ni(dpm)_2\right] + 2AcOH = [Ni(dpm)(AcO)] + [H_2dpm](AcO) \tag{19}$$

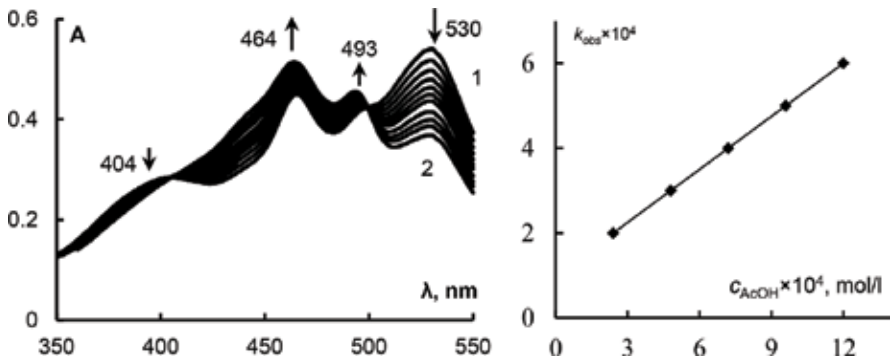

Figure 6. Left: changes in [*Ni*(*dpm*)$_2$] EAS upon acetic acid addition: 1—0 *min*; 2—reaction end; right: dependence of observable protolytic dissociation rate for [*Ni*(*dpm*)$_2$] relative to C_{AcOH}.

Kinetic scheme involves the following stages:

$$\begin{gathered}\left[Ni(dpm)_2\right] + AcOH \leftrightarrow \left\{Ni(dpm)_2(AcOH)\right\}^{\neq}, \quad k_1, slow \\ \left\{Ni(dpm)_2(AcOH)\right\}^{\neq} \rightarrow [Ni(dpm)(AcO)] + Hdpm, \quad k_2, fast \\ Hdpm + AcOH \rightarrow [H_2dpm](AcO), \quad k_3, fast\end{gathered} \tag{20}$$

For the heteroligand complex dissociation

$$[Ni(dpm)(AcO)] + 2AcOH = Ni(AcO)_2 + [H_2dpm](AcO) \tag{21}$$

And the kinetic scheme could be written as follows:

$$\begin{gathered}[Ni(dpm)(AcO)] + AcOH \leftrightarrow \{Ni(dpm)(AcO)(AcOH)\}^{\neq}, \quad k_1^*, slow \\ \{Ni(dpm)(AcO)(AcOH)\}^{\neq} \rightarrow Ni(AcO)_2 + Hdpm, \quad k_2^*, fast \\ Hdpm + AcOH \rightarrow [H_2dpm](AcO), \quad k_3, fast\end{gathered} \tag{22}$$

Observable second-order reaction relative to acid concentration suggests formation of the heteroligand complex to be the limiting stage of the process. Quasi-steady-state assumption along with concluded insignificance of heteroligand complex dissociation speed allows us to derive the equation:

$$-\frac{dC_{\left[Ni(dpm)_2\right]}}{d\tau} = \left(\frac{k_1k_2}{k_{-1}+k_2}\right) C_{\left[Ni(dpm)_2\right]} C_{AcOH}^2 \tag{23}$$

which is in good agreement with the experimentally derived equation:

$$k_{obs} = \frac{k_1k_2}{k_{-1}+k_2} \tag{24}$$

From the temperature variation experiments, activation parameters of the reaction were obtained.

T, K	k	E_a, kJ/mol	$\Delta S^{\neq}$, J/(mol·K)	$\Delta H^{\neq}$, kJ/mol
dpm^- = 3,3′,4,5,5′-pentamethyl-4′-ethyl-2,2′-dipyrromethene anion				
298	0.29 ± 0.02	43.9 ± 2.7	−115.2 ± 12.7	41.4 ± 2.5
318	0.42 ± 0.03			
328	0.83 ± 0.05			
dpm^- = 3,3′,5,5′-tetramethyl-4,4′-dibutyl-2,2′-dipyrromethene anion				
298	2279 ± 3	35 ± 3	−72.14 ± 13	32.5 ± 3.8
303	2660 ± 3			
313	4541 ± 5			
318	5272 ± 11			

Activation energy for the studied compound was found to be higher than that for the Ni(II) butyl-substituted dipyrrinate [15]. Strong inductive effect of alkyl moieties leads to higher electron-donating ability of the pyrrolic nitrogen and, therefore, increases kinetic stability of the compounds.

5. Patterns of BODIPY kinetic acid: Base dissociation

As it was mentioned before, understanding of a BODIPY behaviour in aggressive media is crucial within the scope of their practical application. The only data available to date was their higher solvolysis stability as compared to the d-metal dipyrrinates. Results reviewed below [25–28] thus are the first attempts of quantitative evaluation of a protolytic and solvoprotolytic resilience of a boron-dipyrromethenes.

6. Kinetical studies of BODIPY protolytic dissociation

Kinetic stability was evaluated for 4,4′-diethyl-3,3′,5,5′-tetramethyl-dipyrromethene ($Hdpm^1$), μ-phenyl-4,4′-diethyl-3,3′,5,5′-tetramethyl-dipyrromethene ($Hdpm^2$) and disodium 4,4′-disulpho-3,3′,5,5′-tetramethyl-dipyrromethene ($Hdpm^3$) difluoroborates. Studies were carried out in benzene, ethanol and water (both pure and mixed together) solutions. Acetic acid, trichloroacetic acid, trifluoroacetic acid, sulfuric acid and hydrogen chloride were used as protolysis agents.

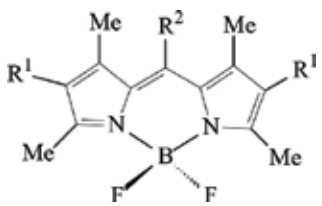

All of the compounds exhibited intense electronic absorption band at 528, 523 and 491 nm, respectively, and a charge-transfer band situated in a near UV region. Sulphonated complex exhibited hypsochromically shifted maximum due to the differences in electronic structure (**Figure 7**).

Electronic absorption and fluorescence spectroscopy data lacked any dissociation hallmarks for $\left[BF_2dpm^1\right]$ in benzolic and ethanolic solutions of acetic and trichloroacetic acid at 298 K. Neither did it in the pure corresponding acids. Heating followed by boiling for a time span of 20 to 30 minutes demonstrated absolute insusceptibility of a $\left[BF_2dpm^1\right]$ to acetic acid, whereas trichloroacetic acid evoked kinetically resolved decrease in the main absorption band at 528 nm with simultaneous raise of $[H_2L]^+$ characteristic band at 485 nm.

$\left[BF_2dpm^1\right]$ underwent dissociation in $EtOH\text{-}CF_3COOH$ and $EtOH\text{-}H_2SO_4$ solutions at 298 K with a speed sufficient for a ratiometric studies. $\left[BF_2dpm^2\right]$ showed itself to be way more volatile since dissociation was observed even in the $C_6H_6\text{-}CCl_3COOH$ solution at 298 K. Both

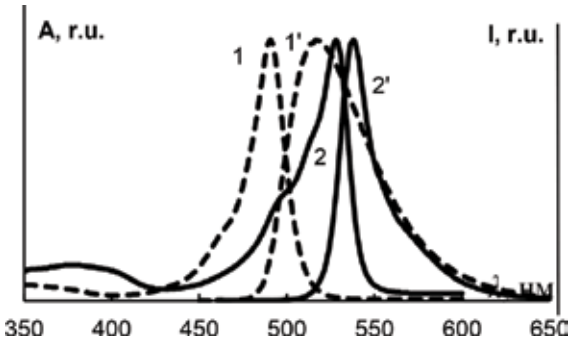

Figure 7. Electronic absorption (1, 2) and fluorescence (1′, 2′) spectra of $[BF_2dpm^2]$ and $[BF_2dpm^3]$ in EtOH and water.

protolytic and solvoprotolytic dissociation processes of the $\left[BF_2dpm^1\right]$ and $\left[BF_2dpm^2\right]$ complexes were found to yield the protonated form of the corresponding ligands $[H_2L]^+$. The water-soluble $\left[BF_2dpm^3\right]$ complex showed no hallmarks of dissociation in EAS in the 7–0 pH range (*HCl* aqueous). Overnight exposure to the lowest pH studied led to a very few, if any, changes in the electronic absorption spectrum of the compound. It was impossible to provoke $\left[BF_2dpm^3\right]$ kinetically resolved dissociation all the way up to the 2 M *HCl* concentration. The latter predictably yielded deprotonated form of the ligand $[H_2L]^+$.

To summarize, treatment of BODIPY with proton-donating agents leads to a fluorophore destruction down to a protonated ligand form. Protolytic or a solvoprotolytic destruction thus provokes significant changes in photophysical and spectral properties of the studied compounds due to destruction. Looking back to the technological aspects, irreversible changes in the dipyrrinates spectral characteristics after the sol-gel process should not have been erroneously described by the weak specific interactions [6, 7]. Instead, a way more pronounced dye destruction should have been taken into account.

Typical fluorescence and absorption changes observed during the dissociation process are presented below (**Figures 8** and **9**).

Formal kinetic analysis of a $\left[BF_2dpm^3\right]$ dissociation process reveals first order of the reaction relatively to the complex concentration. The observable rate constant, at the same time, is in a linear dependence from the H^+ ion activity:

$$k_{obs} = const \cdot a_{H^+} \tag{25}$$

Activities were calculated according to the literature data for an *HCl* aqueous solution [29, 30].

Kinetical equations of the second order are obviously applicable here:

$$-\frac{dC_{[BF_2dpm^{1,2}]}}{d\tau} = kC_{[BF_2dpm^{1,2}]}C_{HA} \qquad -\frac{dC_{[BF_2dpm^3]}}{d\tau} = kC_{[BF_2dpm^3]}C_{H^+} \tag{26}$$

Equations proposed along with the experimental data suggest one to assume the process to be the two-stage protonation of the complex as stated below:

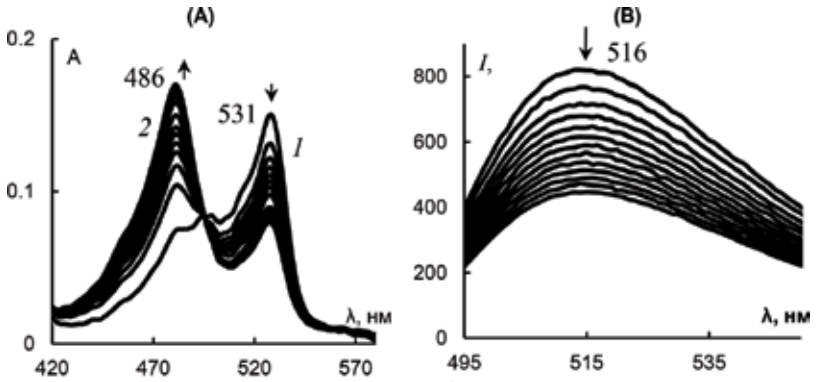

Figure 8. (A) Changes in EAS during [BF_2dpm^1] dissociation in *EtOH–*CF_3COOH binary mixture (C_{CF_3COOH} = 3.73 M at 298.15 K), t, s: 0 (1), 2700 (2); (B) decrease in fluorescence spectrum during [BF_2dpm^3] dissociation in *EtOH–*H_2SO_4 binary mixture.

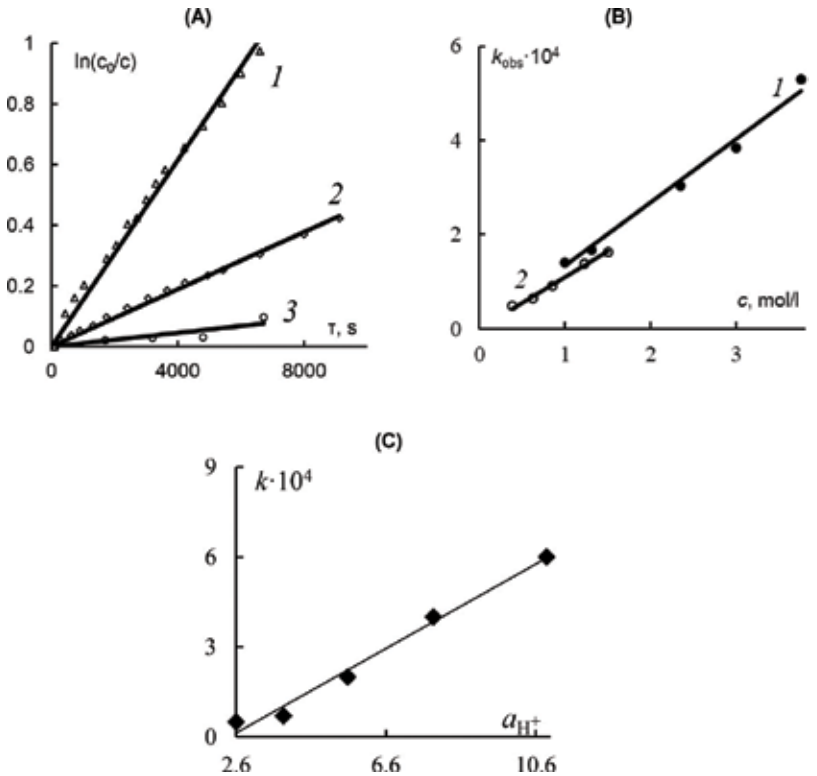

Figure 9. (A) Semi-logarithmic plot for the [BF_2dpm^1] dissociation in the *EtOH–*CF_3COOH binary mixture (T = 298.15 K), C_{CF_3COOH}, M: 0.384 (1), 0.62 (2), 1.23 (3); (B) changes in observable dissociation rate (k_{obs}) [BF_2dpm^1] relative to acid concentration in *EtOH*: 1, CF_3COOH; 2, H_2SO_4; (C) changes in observable dissociation rate (k_{obs}) [BF_2dpm^3] relatively to H^+ ion activity in aqueous *HCl*.

$$\begin{gathered}[BF_2dpm] + H^+\cdots A^- \leftrightarrow \left\{[BF_2dpm \cdot H]^+\cdots A^-\right\} \quad k_1, fast \\ \left\{[BF_2dpm \cdot H]^+\cdots A^-\right\} \rightarrow Hdpm + \left[BF_2^+\cdots A^-\right] \quad k_2, slow \\ Hdpm + H^+\cdots A^- \rightarrow [H_2dpm^+\cdots A^-] \quad k_3, fast\end{gathered} \tag{27}$$

Quasi-steady-state assumption (suggesting that step 2 is rate-determining) allows stating the kinetical equation for this process in a convenient form:

$$-\frac{dC_{[BF_2dpm]}}{d\tau} = \left(\frac{k_1k_2}{k_{-1}+k_2}\right)C_{[BF_2dpm]}C_{HA}, \tag{28}$$

which totally coincides with the experimentally derived equation stated before.

Kinetic and activation parameters for the studied reaction are listed in the table below.

BODIPY dissociation thus proceeds via the S_E2 route. Unlike the protolytic destruction of d-metal dipyrrinates process, rigorously mediated by attack of donating nitrogen atom, BODIPY destruction process was found to possibly involve interaction between fluorine and electrophilic agent. Since such an ambiguity was hard to resolve experimentally, quantum chemical examinations were carried out. Examination of potential energy surfaces for both possible reaction routes allowed us to state fluorine protonation followed by the subsequent HF elimination to be the first stage of the process.

This fact by itself, however, does not influence the kinetic model of the process proposed above.

Compound	T, K	$k \cdot 10^3$, l/(mol·s)	E_a, kJ/mol	$\Delta H^{\neq}$, kJ/mol	$\Delta S^{\neq}$, J/(mol·K)
EtOH–CF_3COOH					
[BF_2dpm^1]	298	0.20 ± 0.01	—	—	—
EtOH–H_2SO_4					
[BF_2dpm^1]	298 308 318	0.10 ± 0.01 0.40 ± 0.02 1.4 ± 0.1	104 ± 6	102 ± 6	20 ± 1
C_6H_6–CCl_3COOH					
[BF_2dpm^2]	298	0.50 ± 0.03	—	—	—
EtOH–H_2SO_4					
[BF_2dpm^2]	298 308 318	0.050 ± 0.003 0.090 ± 0.005 0.70 ± 0.004	103 ± 6	101 ± 5	12.0 ± 0.6
H_2O–HCl					
[BF_2dpm^3]	298	0.070 ± 0.004	—	—	—

Ultimately, obtained results allow us to state a set of patterns for kinetic BODIPY protolytic dissociation stability. Both $\left[BF_2dpm^1\right]$ and $\left[BF_2dpm^2\right]$ are only susceptible to dissociation in benzolic solutions upon heating. Temperature increase leads to the 'monomer ↔ dimer'

equilibrium shift for carboxylic acids and to the decrease of the solvated proton activity [31]. Interestingly, whereas the pure CF_3COOH does not provoke $[BF_2dpm^1]$ dissociation, the presence of $EtOH_2^+$ particles in ethanolic solutions leads to reasonable solvoprotolysis rates at 298 K. Dissociation rate is also affected positively by the solution acidity as can be seen from the comparison of $EtOH$-CF_3COOH and $EtOH$-H_2SO_4 systems above. The same pH solutions of $[BF_2dpm^1]$ and $[BF_2dpm^2]$ in $EtOH$-H_2SO_4 demonstrate the twice-reduced (for the latter) rate constant due to influence of the phenyl moiety on the nitrogen atom partial charge.

BODIPY, therefore, is unique in terms of kinetic stability towards protolytical and solvoprotolytical dissociation. Namely, different d-metal dipyrrinates in the C_6H_6–CH_3COOH solutions exhibit rate constants in the range from $0.6 \cdot 10^{-3}$ to $2.28 \cdot 10^3$ $l^2/(mol^2 \cdot s)$ or even demonstrate thermodynamically controlled equilibrium for the $Cu(II)$ complexes. Boron-dipyrromethenes, meanwhile, due to high B-N bond energy and pronounced chelating effect, are stable in similar conditions. As will be shown in the next section, BODIPYs also undergo the process of a protolytic dissociation by a mechanism, far different from the one occurring for dipyrrinates of d- and f-metals.

7. Quantum chemical modeling of protolytic dissociation mechanism

BODIPY, unlike d-metal dipyrrinates, has an ambiguity lying beneath the protolytic destruction mechanism due to specific coordination centre structure. In addition to the possibility of direct nucleophilic attack towards pyrrolic nitrogen, the phosphorus atom is also capable to interact with electrophilic agent with consequent HF elimination. Due to complexity of direct observation, quantum chemical investigation of potential energy surfaces for both of the possible protolytic dissociation mechanisms was performed.

Quantum chemical calculations were performed using GAUSSIAN03W and HyperChem 8.0.3 software. Semi-empirical PM6 method, which was verified basing on the experimental structural data for the bulky organic molecules, was used for rough geometry estimation and potential energy surface evaluation. Result refinement was performed using density functional theory approximation, with a B3LYP hybrid functional and a 6-31G(d,p) basis set.

The first studied mechanism involves direct nitrogen protonation with and consequent $B-N$ bond cleavage. On the other side, the second proposed mechanism involves formation of an $H-F$ hydrogen bond followed by HF elimination (**Figure 10**).

For potential energy surface cross sections, interatomic distance was chosen as an independent coordinate. Namely, those were $N-H$ bond length for the first mechanism and $F-H$ bond length for the second one.

Net Mulliken charges on the atoms show the favor for the second mechanism demonstrating fluorine to be more electron-rich than nitrogen. Optimized geometries for BODIPY and its single- and double-protonated forms are presented in **Figure 11**. Protonation of the atoms causes charge inversion on the fluorine atom and decrease of the partial positive charge on the pyrrolic nitrogen (**Table 1**).

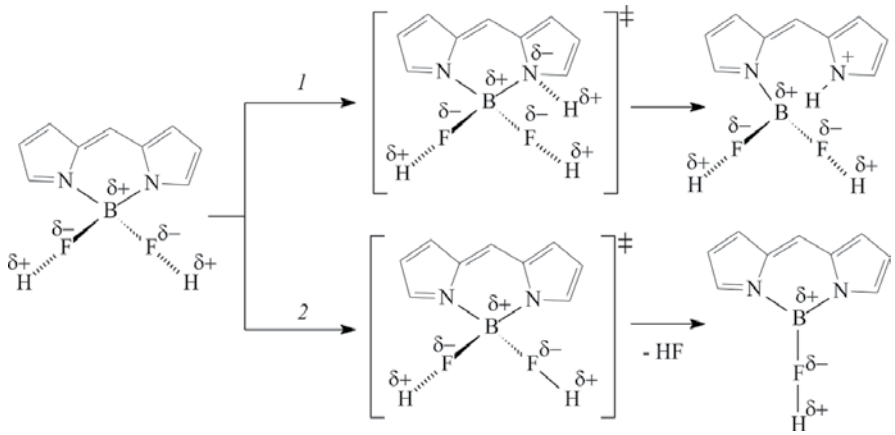

Figure 10. Proposed routes of BODIPY dissociation.

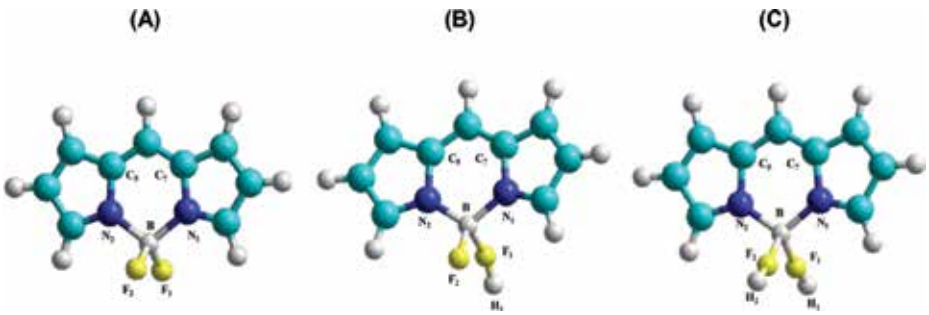

Figure 11. Optimized structures of BODIPY (A), single-protonated (B) and double-protonated (C) BODIPY forms.

Atom.	Structure		
	A	B	C
N_1	0.307	0.219	0.077
N_2	0.307	0.218	0.077
F_1	−0.21	0.052	0.072
F_2	−0.209	−0.158	0.071
B	0.06	0.13	0.021
H_1		0.307	0.323
H_2			0.323

Table 1. Net Mulliken atomic charges calculated using DF B3LYP/6-31G(d,p) approach.

$H-F$ bond length equilibrates near 0.957 Å with $B-F-H$ 155° bond angle. $B-F$ distance elongates upon interaction from 1.352 Å up to 1.521 Å with simultaneous $B-F$ order decrease from 0.97 down to 0.52. The latter explains ease of consequent destabilization and bond cleavage (**Figure 12**).

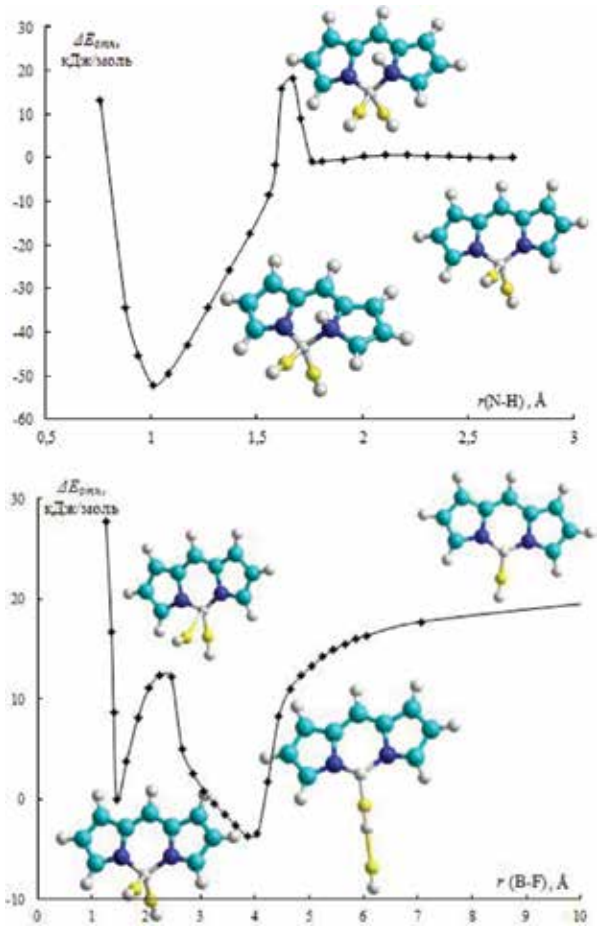

Figure 12. Potential energy surface cross sections for the first (top) and the second (bottom) mechanisms. ΔE (y axis) is calculated relatively to the stable BODIPY structure.

Activation energy for the nitrogen protonation corresponds to 18 kJ/mol. $N_1C_5C_7N_2$ dihedral angle increase from the fully planar ($\approx 0^\circ$) to a strongly twisted (15.6°) configuration occurs in this case.

For an *HF* elimination mechanism, there are two minima observed: the first one corresponds to the original BODIPY structure, whereas the second denotes trigonal coordination polyhedra of the complex as shown in the figure. Geometry of the transition state for this mechanism undergoes no pronounced changes except the obvious $B-F-H$ angle increase and $H-F$ bond tightening. The activation energy for this case estimates 12 kJ/mol mostly owing to the $B(III)$ coordination polyhedra change. Alas, the trigonal geometry is only possible in vacuo, since acid ligands will force back the tetrahedral shape in the condensed phase.

From the aforementioned we state that fluorine protonation with consequent *HF* elimination is the most probable mechanism of the first stage of BODIPY protolytic dissociation. This still corresponds to the kinetic model proposed above while nicely explaining outstanding stability of boron-dipyrromethenes to protolytic dissociation.

8. Hydrolysis and destruction of BODIPY in alkaline solutions

Resilience of BODIPY to the aggressive components of the reaction mixtures involved in the hybrid material formation is of high importance. Up to our first paper in the field [26], stability of boron-dipyrromethenes in the alkaline medium was never studied. Here we review kinetic stability of disodium 4,4′-disulpho-3,3′,5,5′-tetramethyl-dipyrromethene ($Hdpm^3$) difluoroborate $[BF_2dpm]$ in the aqueous *NaOH* solutions.

$[BF_2dpm]$ aqueous solutions exhibited intense absorption peak at 491 nm. There were very few, if any, changes in electronic absorption spectra upon pH increase from 7 up to 9, even after 24 h of exposure.

First, changes were observed at pH values ≥10—absorption maximum decrease was accompanied by the growth of 206 nm band, corresponding to the monopyrrolic products. Further, pH increase in the 10–12 range increased destruction rate dramatically (**Figure 13**).

Linearization using first-order reaction coordinates yields unity root mean square and approves the first-order reaction relative to the complex concentration. At the same time, dependence of k_{obs} from pOH suggests the second-order reaction relative to OH^- ion.

Acid (*HCl*) addition leads to full recovery of the photophysical characteristics, suggesting reversibility of the first stage of interaction studied. Thus, the first stage is the formation of unstable anionic ligand form, which consequently breaks down to yield monopyrrolic products. The suggested reaction scheme is presented below:

$$[BF_2dpm]^{2-} + 2OH^- \leftrightarrow \left[BF_2(OH)_2\right]^- + dpm^{3-} \quad k_1$$

$$dpm^{3-} \rightarrow colorless\ pyrroles \quad k_2 \tag{29}$$

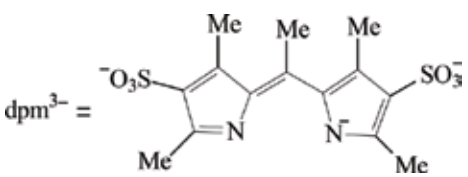

According to the scheme, the canonical kinetic equation could be written as

$$\frac{-dC_{BF_2dpm}}{d\tau} = k_{obs}C_{[BF_2dpm]} \tag{30}$$

Quasi-steady-state assumption for this reaction scheme allows stating the kinetical equation for this process in a form:

$$k_{obs} = \left(\frac{k_1k_2}{k_{-1}}\right)C^2_{(OH^-)} \tag{31}$$

which coincides with the experimentally obtained dependencies. Thus, total reaction rate equation could be written as

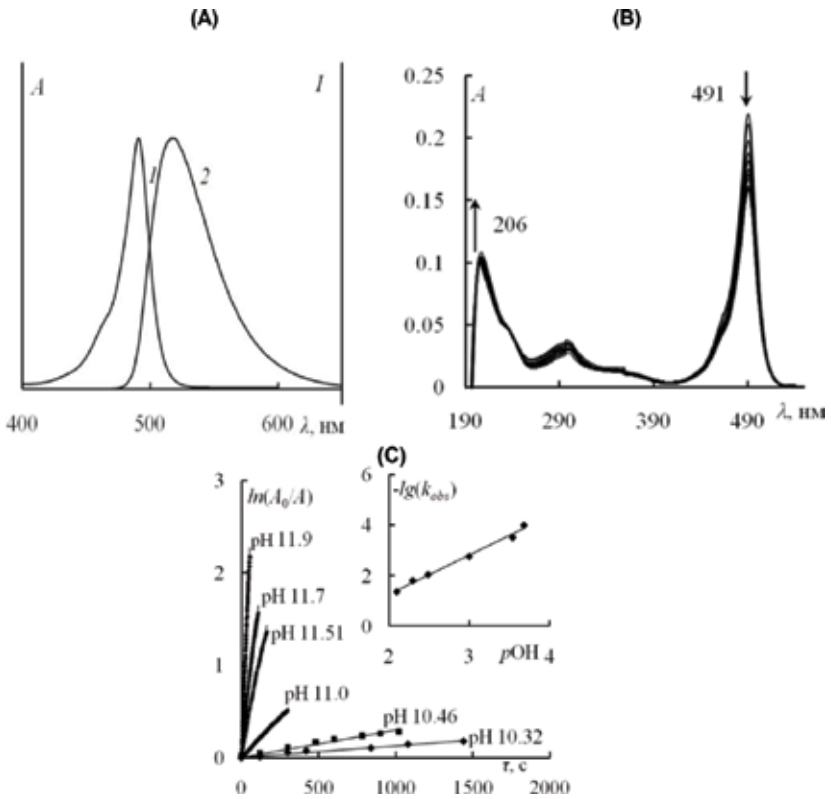

Figure 13. (A) Electronic absorption (1) and fluorescence (2) spectra of an aqueous [BF_2dpm] solution (pH 7.0); (B) changes in [BF_2dpm] EAS upon *NaOH* addition at 298 K; (C) kinetical data on [BF_2dpm] destruction at 298 K. (B inset) changes in solution absorbance relatively to the *pOH*.

$$\frac{-dC_{BF_2dpm}}{d\tau} = \left(\frac{k_1 k_2}{k_{-1}}\right) C_{[BF_2dpm]} C^2_{(OH^-)} \tag{32}$$

Ultimately, we can state high BODIPY stability towards alkaline medium, granting possibility of their usage in high pH range during hybrid materials synthesis. Proposed mechanism and data obtained for the hydrolytic BODIPY destruction in alkaline medium extends the frontiers of their practical applications, suggesting proper usage of acidic additives preventing boron-dipyrrin destruction.

9. Conclusions

Results reviewed in this chapter broaden the data on kinetic stability of dipyrrinates in acidic media. Introduction of the alkyl moiety to the ligand structure leads to an increase in the electron density near pyrrolic nitrogen atoms. Demonstrated results state decrease in stability

of intermediate complex upon alkyl chain length increase due to attenuation of +I effect impact. Kinetic stability of dipyrrinates is mainly affected by potency of interaction between electron-donating nitrogen atoms and acid molecules. This possibility, in turn, is highly susceptible to dipyrrin substituents amount, position and electron-donating behaviour. Central atom nature not just simply determines stability of the complex towards protolytic dissociation but fundamentally changes route of the process. Relative stability was stated for $Zn(II)$ and $Ni(II)$ dipyrrinates. The latter demonstrates formation of heteroligand complexes in the process of dissociation. $Pd(II)$ complexes have way higher stability and are only susceptible to dissociation in the trifluoroacetic acid solution. Outstanding stability is demonstrated by the boron difluoride dipyrromethenes, mostly due to the high $B-N$ bond energy and highly pronounced chelating effect. Quantum chemical investigations state that unlike that of d- and f-metal dipyrrinates, the first stage of BODIPY protolytic dissociation is fluorine protonation with consequent *HF* cleavage.

Investigation of the BODIPY destruction in aqueous alkaline medium suggests the first stage of the process to be the alkaline hydrolysis. Unstable intermediate anionic form of the ligand consequently decays yielding uncoloured monopyrrolic products. Analysis of the spectrophotometric data for the process is in good agreement with the reaction scheme proposed.

There is an ongoing research [32–36] on bis-dipyrrins protolytic dissociation stability. Generally, they are more labile, and benzene solutions of acetic acid are used for the investigation. Doubling the number of the electron-donating groups per molecule complicates the examination; however, with some assumptions made (such as synchronous protolysis) kinetical equations look quite similar with the ones derived in this chapter. It could be stated that lability of helicates (bis-dipyrrins binuclear complexes) in protolysis reactions also do increase if there are no any substituents in terminal pyrrole rings.

Author details

Yuriy S. Marfin*, Sergey D. Usoltsev and Evgeniy V. Rumyantsev

*Address all correspondence to: marfin@isuct.ru

Ivanovo State University of Chemistry and Technology, Ivanovo, Russian Federation

References

[1] Rumyancev EV, Marfin YS. Variacii struktury i supramolekulyarnogo okruzheniya kak sposoby vliyaniya na spektral'nye i fotofizicheskie harakteristiki kompleksov dipirrinov. In: XII Mezhdunarodnaya konferenciya «Spektroskopiya koordinacionnyh soedinenij». Tuapse; 2015. pp. 86-87 (Russian)

[2] Bersuker IB. Elektronnoe stroenie i svojstva koordinacionnyh soedinenij. In: Bersuker IB, editor. Vvedenie v teoriyu. 3-e izd, pererab. L.: Himiya; 1986. 287 p. (Russian)

[3] Berezin BD, Lomova TN. Reakcii dissociacii kompleksnyh soedinenij. M.: Nauka; 2007. 278 p (Russian)

[4] Grinberg AA. Vvedenie v himiyu kompleksnyh soedinenij. Izd. 3-e, pererab. i dop. M.: Himiya; 1966. 631 p (Russian)

[5] Kukushkin VY. Teoriya i praktika sinteza koordinacionnyh soedinenij. Akademii Nauk SSSR, Otd-nie fizikohimii i tehnologii neorgan. materialov. L.: Nauka; 1990. 260 p (Russian)

[6] Kukushkin YN. Himiya koordinacionnyh soedinenij. M.: Vyssh. shk.; 1985. 456 p (Russian)

[7] Kuznecova RT. Spektroskopicheskie i lazernye harakteristiki novyh effektivnyh lyuminoforov dlya shirokoj oblasti spektra na osnove kompleksov proizvodnyh dipirrolilmetena s diftorboratom. In: Kuznecova RT, Aksenova YV, Solodova TA, Bashkircev DE, Kopylova TN, Tel'minov EN, Majer i dr GV, editors. Optika i spektroskopiya. Vol. 115. No. 5. 2013. p. 797 (Russian)

[8] Aksenova YV. Fotonika i primenenie novyh lyuminoforov na osnove kompleksov dipirrolilmetenov. In: Aksenova YV, Kuznecova RT, Berezin MB, editors. Izvestiya Samarskogo nauchnogo centra Rossijskoj akademii nauk. Vol. 17. No. 2. 2015. pp. 56-59 (Russian)

[9] Aksenova YV. Spektroskopicheskoe izuchenie fotofizicheskih i fotohimicheskih svojstv koordinacionnyh kompleksov dipirrinov. In: Aksenova YV, Kuznecova RT, Berezin MB, Pavich TA, Arabej SM, editors. V knige: XXV S'ezd 304 po spektroskopii molodezhnaya nauchnaya shkola po optike i spektroskopii: sbornik tezisov. Moskva. 2016. pp. 66-67 (Russian)

[10] Marfin YS. Polimernye kompozicii, soderzhashchie bordipirrinovye lyuminofory. In: Marfin YS, Rumyancev EV, editors. V Vserossijskaya s mezhdunarodnym uchastiem konferenciya i shkola dlya molodyh uchenyh «Makromolekulyarnye nanoob'ekty i polimernye nanokompozity», g. Moskva; 2015. p. 89 (Russian)

[11] Banuelos J, Lopez Arbeloa F, Arbeloa T, Salleres S, Vilas JL, et al. Journal of Fluorescence. 2008;**18**(5):899

[12] Guseva GB. Vzaimodejstviya s rastvoritelyami linejnyh oligopirrol'nyh soedinenij i ih metallokompleksov. In: Guseva GB, Antina EV, Berezin MB, V'yugin AI, Balanceva EV, editors. ZHurn. fiz. himii. Vol. 76, No. 9. 2002. pp. 1595-1599 (Russian)

[13] Semejkin AS. Vzaimosvyaz' stroeniya i sol'vatacionnyh harakteristik alkilzameshchennyh dipirrolilmetenov, ih oksa- i tioanalogov. In: Semejkin AS, Berezin MB, CHernova OM, Antina EV, Syrbu SA, Lyubimova TV, Kutepov AM, editors. Izvestiya AN. Ser. him. No. 8. 2003. pp. 1712-1718 (Russian)

[14] Helevina OG. Kineticheskaya ustojchivost' kompleksov tuliya(III) i samariya(III) s oktafeniltetraazaporfirinom v sredah na osnove uksusnoj kisloty. In: Helevina OG, Miroshnichenko YS, Kabesheva EV, Kulinich VP, SHaposhnikov GP, editors. ZHurnal obshchej himii. Vol. 74. No. 12. 2004. pp. 1937-1941 (Russian)

[15] Rumyantsev EV, Marfin YS. Protolytic dissociation mechanisms and comparative acid. Stability of palladium(II), zinc(II), copper(II), and nickel(II) complexes of alkylated dipyrrins. Transition Metal Chemistry. 2014;**39**:699-704

[16] Guseva GB. Reakcionnaya sposobnost' α,α-dipirrolilmetena v reakciyah s nekotorymi kompleksami Co(II) i Cu(II). In: Guseva GB, Antina EV. Koord. Himiya; Vol. 32, No. 7. 2006. pp. 541-546 (Russian)

[17] Rumyancev EV. Kompleksy dipirrolilmetenov: faktory stabilizacii i fiziko-himicheskie svojstva. In: Rumyancev EV, Antina EV, Desoki A, editors. Sb.: Trudy XXIV Mezhdunarodnoj CHugaevskoj konferencii po koordinacionnoj himii i Molodezhnoj konferencii-shkoly «Fiziko-himicheskie metody v himii koordinacionnyh soedinenij». St. Peterburg. 2009. pp. 358-359 (Russian)

[18] Hammet LP, Deyrup AJ. Journal of the American Chemical Society. 1932;**54**:2721

[19] Stewart R, O'Donnell JP. Journal of the American Chemical Society. 1962;**84**:493-494

[20] Gammet L. Osnovy fizicheskoj organicheskoj himii. M.: Mir; 1972 (Russian)

[21] Olah A. Journal of Organic Chemistry. 2005;**70**:2413-2429

[22] Guseva GB. Termodinamika reakcij kompleksoobrazovaniya medi(II), cinka(II), kobal'ta (II), rtuti(II) I nikelya(II) S α,α-dipirrolilmetenom v dimetilformamide. In: Guseva GB, Antina EV, Berezin MB, V'yugin AI. Koordinacionnaya Himiya. Vol. 30, No. 1. 2004. pp. 32-35 (Russian)

[23] Klyueva ME. Proyavlenie makrociklicheskogo effekta v processe dissociacii kompleksov Zn2+ i Mn3+ s protoporfirinom: krat. soobshcheniya. In: Klyueva ME, Lomova TN, Berezin BD, editors. ZHurn. fiz. himii. Vol. 62, vyp. 12. 1988. pp. 3341-3344 (Russian)

[24] Klyueva ME. Vliyanie strukturnyh faktorov na kinetiku i mehanizm dissociacii marganec (III)tetrafeniloporfirinov v sernoj kislote. In: Klyueva ME, Lomova TN, Berezin BD. Tez. dokl. IV Vsesoyuz. soveshch. 305 «Probl. sol'vatacii i kompleksoobrazovaniya v rastvorah», Ivanovo, 6–8 iyunya 1989 g. Ivanovo, Ch. I. 1989. p. 44 (Russian)

[25] Pang W. Modulating the singlet oxygen generation property of meso-β directly linked BODIPY dimers. In: Pang W, Zhang X-F, Zhou J, Yu C, Hao E, et al. Chemical Communications, Cambridge, England. Vol. 48. 2012. pp. 5437-5439

[26] Rumyancev EV. Koordinacionnaya himiya dipirrolilmetenov i ih proizvodnyh: Fundamental'nye aspekty i prakticheskie prilozheniya. In: Rumyancev EV, Antina EV, editors. V sb. tezisov dokladov XXV Mezhdunarodnoj CHugaevskoj konferencii po koordinacionnoj himii i II Molodezhnoj konferencii-shkoly «Fiziko-himicheskie metody v himii koordinacionnyh soedinenij». 6–11 iyunya 2011. g., Suzdal'. pp. 31-32 (Russian)

[27] Rumyancev EV. Gidroliz i destrukciya borftoridnogo kompleksa dipirrolilmetena v shchelochnyh rastvorah. In: Rumyancev EV, Aleshin SN, editors. Izvestiya VUZov. Himiya i himicheskaya tehnologiya. Vol. 56, No. 2. 2013. pp. 67-70 (Russian)

[28] Rumyancev EV. Reakcii protoliticheskoj dissociacii dipirrolilmetenatov medi(II) i nikelya (II) v benzol'nyh rastvorah uksusnoj kisloty. In: Rumyancev EV, Aleshin SN, Antina EV, editors. ZHurnal obshchej himii. Vol. 83, No. 10. 2013. pp. 1738-1742 (Russian)

[29] Rumyantsev EV, Alyoshin SN, Marfin YS. Kinetic study of bodipy resistance to acids and alkalis: Stability ranges in aqueous and non-aqueous solutions. Inorganica Chimica Acta. 2013;**408**:181-185

[30] Rumyancev EV. Kvantovo-himicheskoe modelirovanie nachal'nyh stadij protoliticheskoj dissociacii borftoridnogo kompleksa dipirrolilmetena. In: Rumyancev EV, Marfin YS, Aleshin SN, editors. Izvestiya vysshih uchebnyh zavedenij. Seriya: Himiya i Himicheskaya Tehnologiya; Vol. 56, No. 9. 2013. pp. 18-22 (Russian)

[31] Robinson R, Stoks R. Rastvory elektrolitov. M.: 1963. 647 p (Russian)

[32] Guseva GB, Antina EV, Berezin MB. Kinetics of the dissociation of transition metal complexes with α,α-dipyrrolylmethene in acetic acid-benzene as a binary proton-donating solvent. Russian Journal of Coordination Chemistry. 2003;**29**(10):690-693

[33] Guseva GB, Antina EV, Ksenofontov AA, V'yugin AI. Kineticheskaya model' i mehanizm kislotnoj dissociacii bis(dipirrolilmetenatov) dmetallov. Kinetika i kataliz. 2014;**55**(4):411 (Russian)

[34] Antina LA, Guseva GB, V'yugin AI, Antina EV. Kineticheskaya ustojchivost' kompleksov ryada d-metallov s 3,3'-bis(dipirrolilmetenom) v binarnom protonodonornom rastvoritele uksusnaya kislota-benzol. ZHurnal obshchej himii. 2012;**82**(7):1195-1200 (Russian)

[35] Antina LA, Guseva GB, V'yugin AI, Antina EV. Kinetika reakcij dissociacii kompleksov cinka(II) s 3,3-bis(dipirrolilmetenami) v binarnom rastvoritele uksusnaya kislota-benzol. ZHurnal fizicheskoj himii. 2012;**86**(11):1759 (Russian)

[36] Stid DV, Etvud DL. Supramolekulyarnaya himiya. Vol. 2 t. M.: Akademkniga; 2007. 480 p (416 p, Russian)

Edited by Jorge Bañuelos-Prieto and Rebeca Sola Llano

Nowadays, dye chemistry is a booming area of research. In particular, BODIPY fluorophore dyes are in the spotlight since their chromophore allows the design of tailor-made molecules for specific (bio)technological purposes. *BODIPY Dyes: A Privilege Molecular Scaffold with Tunable Properties* aims to highlight such chemical versatility and modulable photophysical and electrochemical properties. The second and the third chapter deal with BODIPYs in chemosensing and as labels for bioimaging. The fourth chapter focuses on their electroluminescence and redox properties, and their role in photocatalysis. The fifth chapter provides deeper insight into the degradation mechanisms in acid and basic media. The book aims to overview the state of the art of BODIPYs and inspire readers involved in dye chemistry.

Published in London, UK

IntechOpen

ISBN 978-1-83881-816-6